

A Crash Course on Cooperative Wireless Networks

Mischa Dohler

22 October 2009

BUAA, Beijing

Mischa Dohler

Cooperative Communications

The Physical Layer



– UMTS & WiMAX Capacity & Coverage Extension –

The Opportunity Driven Multiple Access (ODMA) protocol [1] in 3GPP (discontinued with R'99) as well as the WiMAX standard facilitate relaying to enhance capacity and coverage. An extension to a distributed deployment will be shown to further boost capacity.

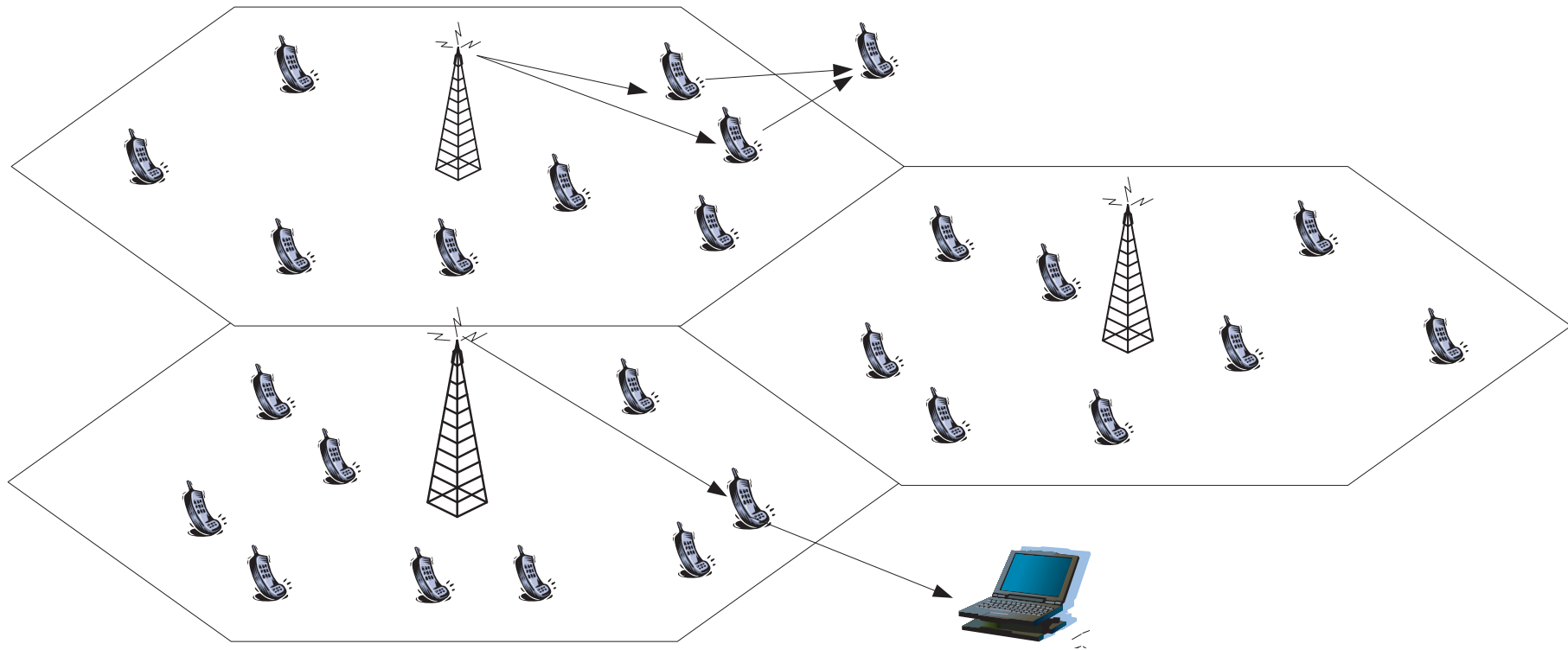


Figure 1: Traditional and distributed relaying in UMTS and WiMAX.

– WLAN Capacity & Coverage Extension –

Wireless Local Area Networks (WLANs) have sporadic hot-spot coverage in offices, cafes, train stations, etc [2]. Traditional and distributed relaying increases capacity at WLAN cell edges and closes coverage holes in sufficiently dense deployment areas (e.g. Orange's UNIK service).



Figure 2: Coverage extension of high-capacity indoor WLAN towards outdoor users.

– Sensor Networks –

Large scale sensor networks are only recently emerging with a vast gamut of applications [3]. Traditional and distributed relaying increases link reliability and - under some conditions - saves energy and hence increases the network's lifetime.

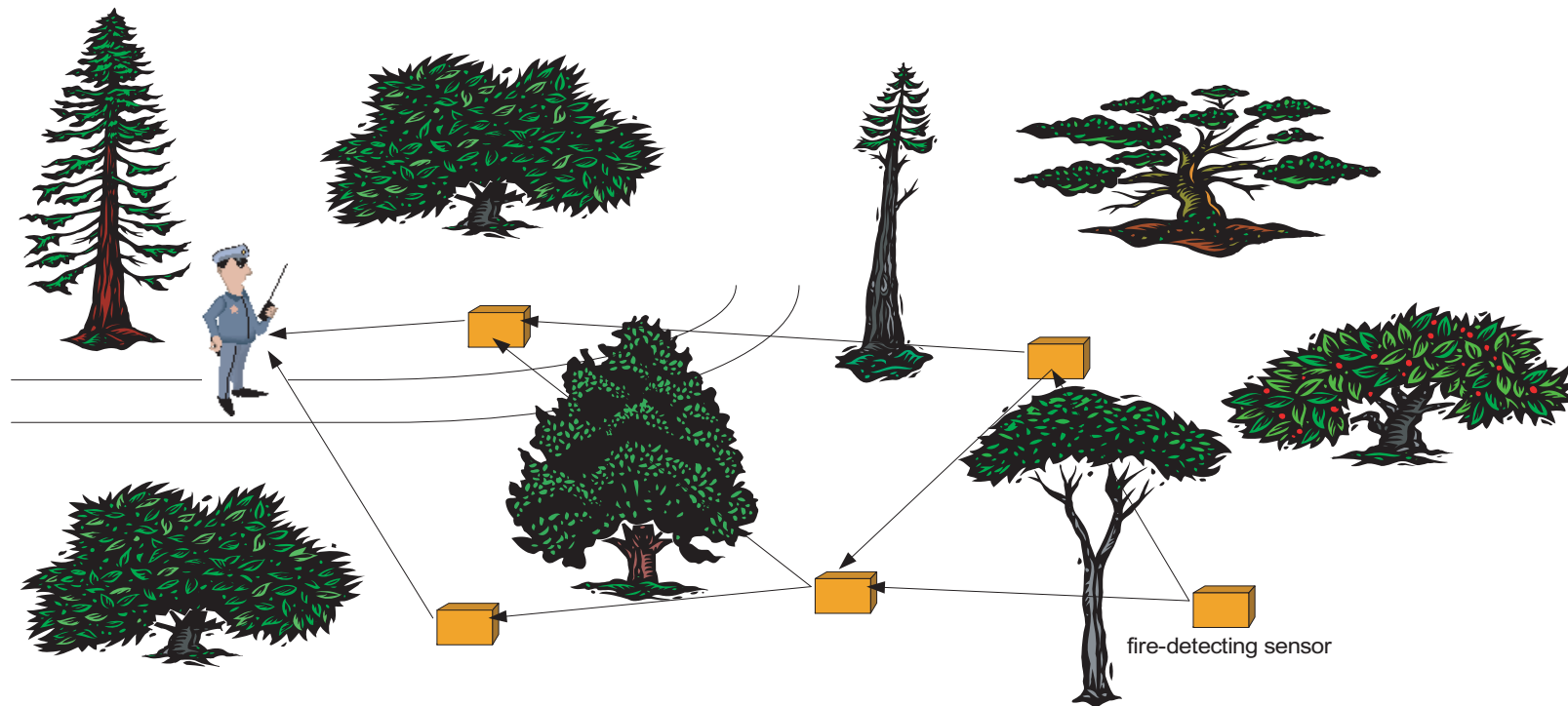


Figure 3: Distributed relaying sensor network for fire detection in forests.

– Pathloss Gains –

- **Pathloss Gain.** Due to the non-linear pathloss behavior, splitting the propagation path yields transmit power gains because the aggregate pathloss of the split path is less than the pathloss of the full path:
 - The pathloss, and hence the signal-to-noise ratio (SNR), is known to be inversely proportional to the propagation distance, i.e. $\text{SNR} \propto \frac{1}{x^n}$, where x is the distance between transmitter and receiver, and n is the pathloss exponent.
 - Splitting e.g. the communication path between source and destination in two equal distances and allocating to each part half of the power, the gain w.r.t. direct communication assuming a pathloss coefficient of $n = 4$ is quantified as

$$\frac{\frac{1/2}{(x/2)^4} + \frac{1/2}{(x/2)^4}}{\frac{1}{x^4}} = 16, \quad (1)$$

i.e. yielding a $10 \log_{10} 16 = 12$ dB power savings.

- This is a significant gain and one of the main incentive of using cooperative techniques.

– Tutorial Outline –

- 1. Preliminaries**
- 2. Capacity Bounds**
- 3. Hardware Realisation**
- 4. Channel Characterisation**
- 5. Transparent PHY Algorithms**
- 6. Regenerative PHY Algorithms**
- 7. MAC and Cross-Layer Design**
- 8. System Considerations**
- 9. The Road Ahead**
- 10. References**

PART 1

PRELIMINARIES

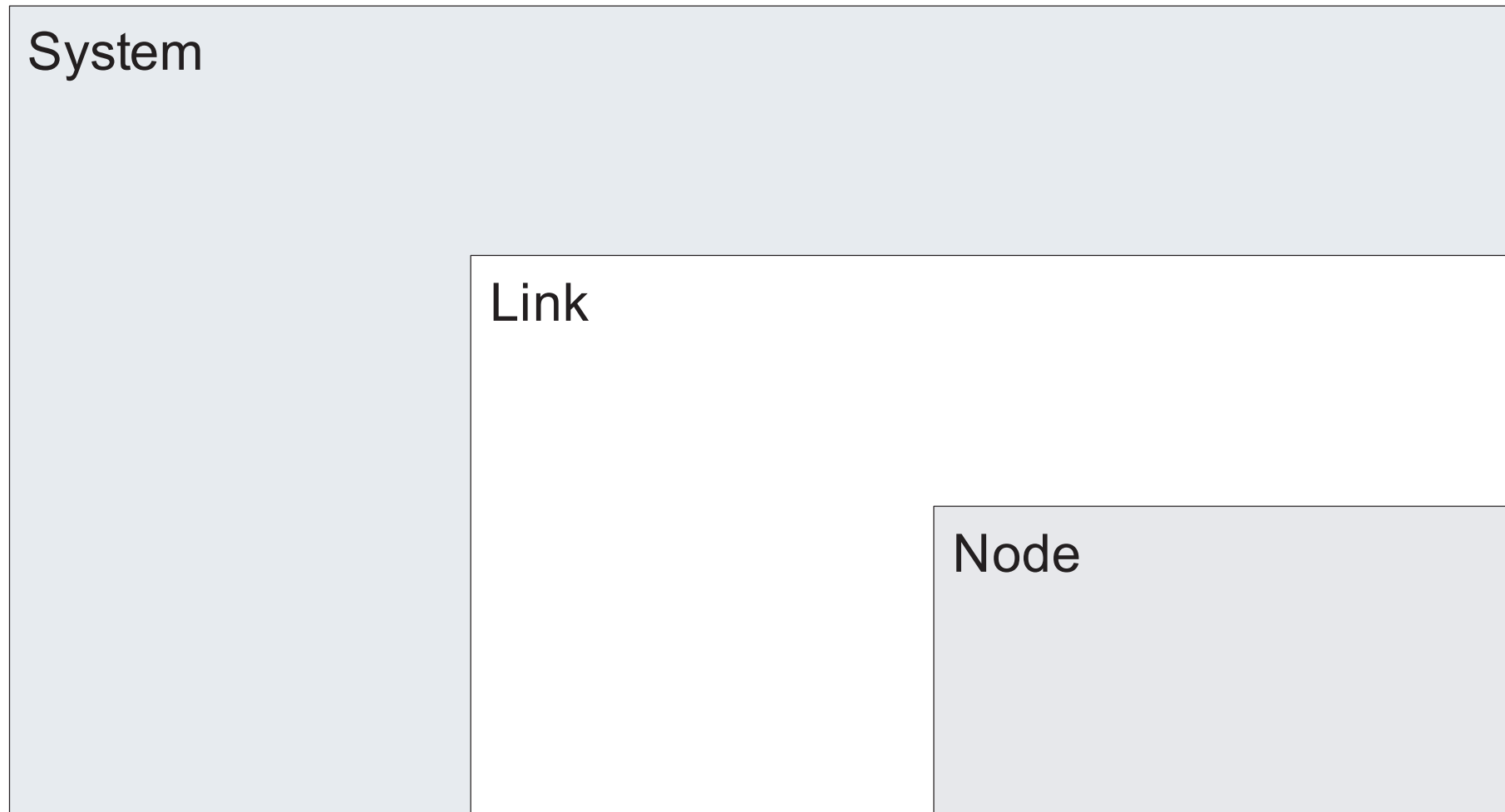
– Preliminary Note –

- Due to your differing background and also due to the large degrees of freedom of cooperative networks, a common understanding of the subject matter is pivotal.
- Such a common understanding is complicated by the fact that the same or similar concepts are given entirely different names; or, entirely different concepts, the same name.
- With the aim to harmonise at least some of the concepts, we will hence precede the tutorial with some important preliminaries, i.e.:
 1. useful definitions; and
 2. key milestones.

1.1 Useful Definitions

– Structure of Definitions –

- We will give some useful definitions as per below structure:

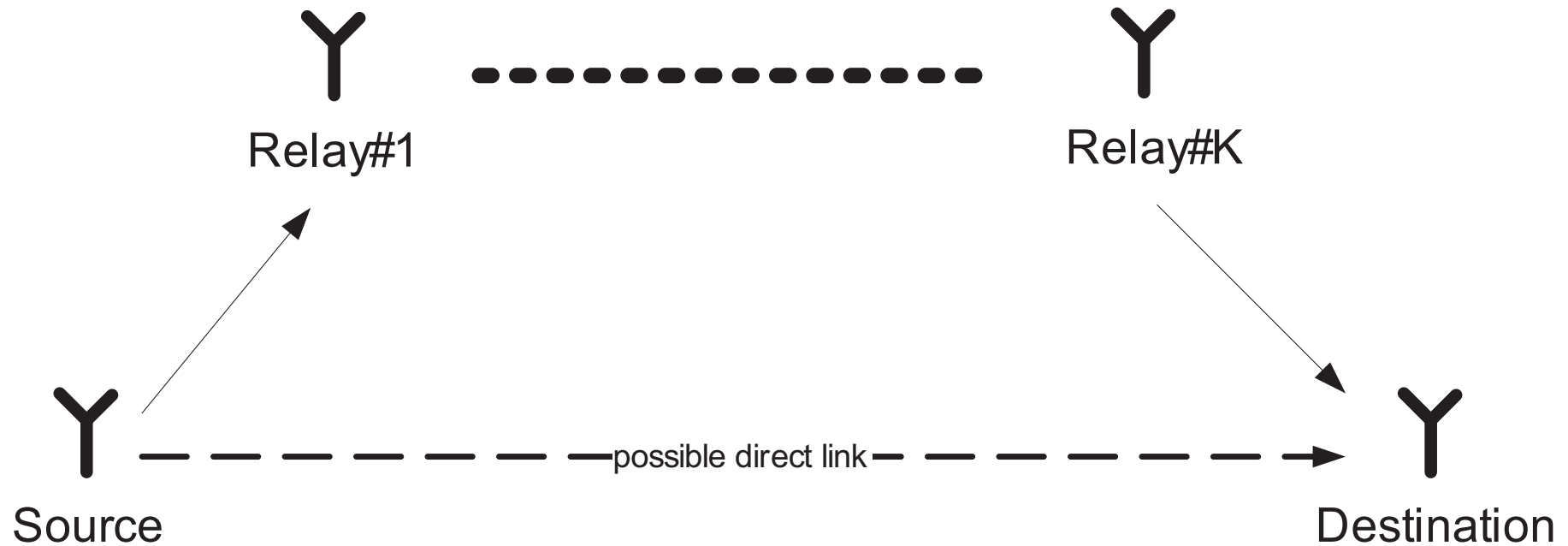


– System: Information Flow [1/5] –

- **From these canonical links, we can build different flows through network:**
 - direct link
 - serial relaying
 - parallel relaying
 - space-time relaying
 - and composites thereof
- **We differentiate further between flows:**
 - with/without interference between flows
 - with/without direct link between nodes which use relays

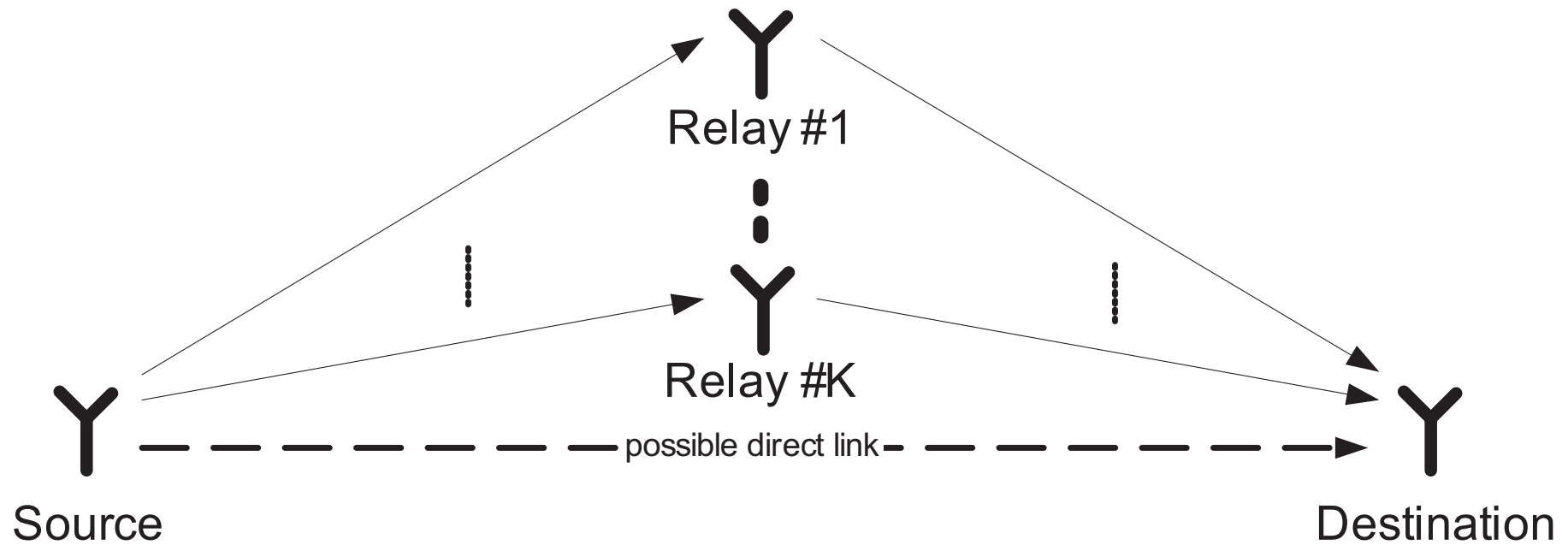
– System: Information Flow [2/5] –

- **Serial Relaying:**



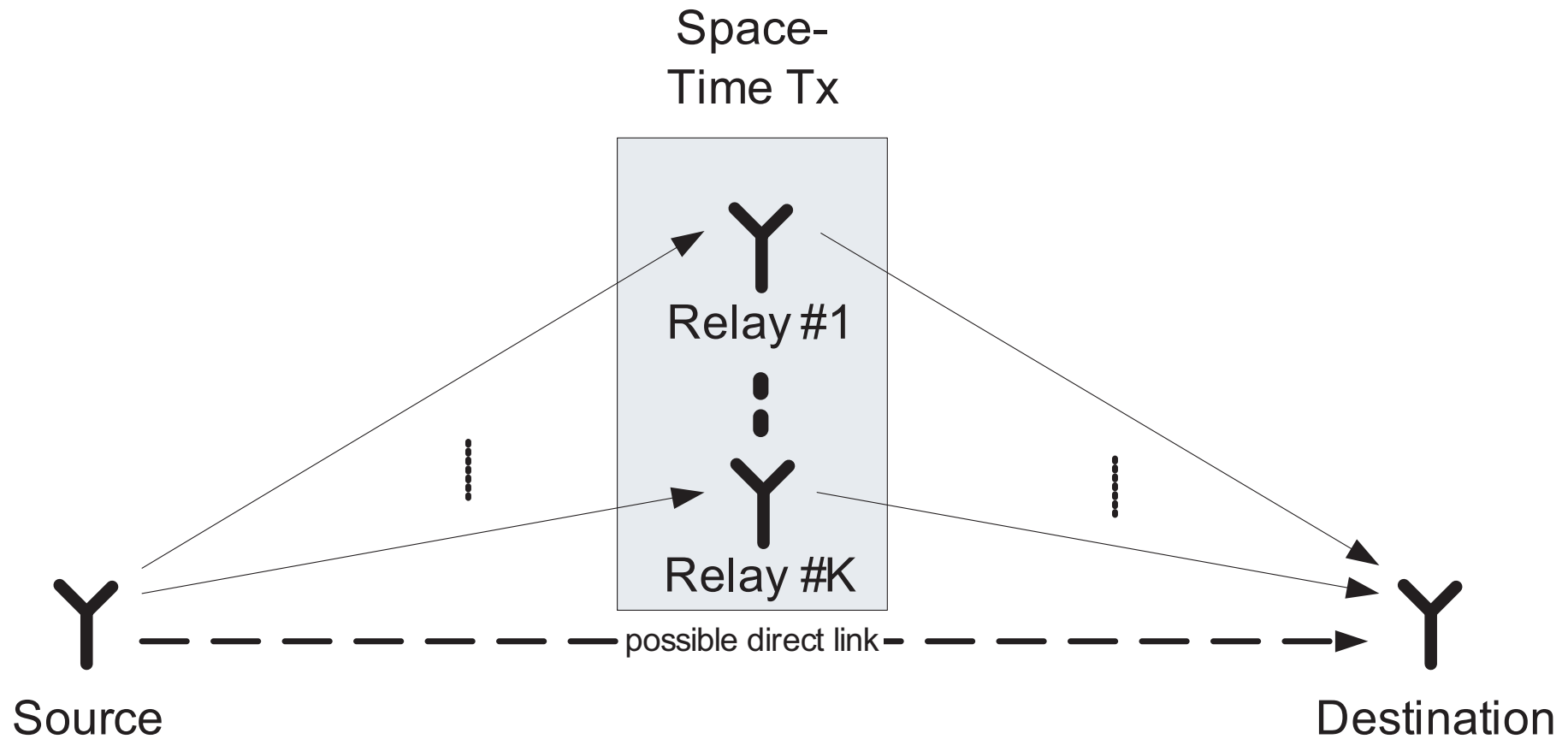
– System: Information Flow [3/5] –

- **Parallel Relaying:**



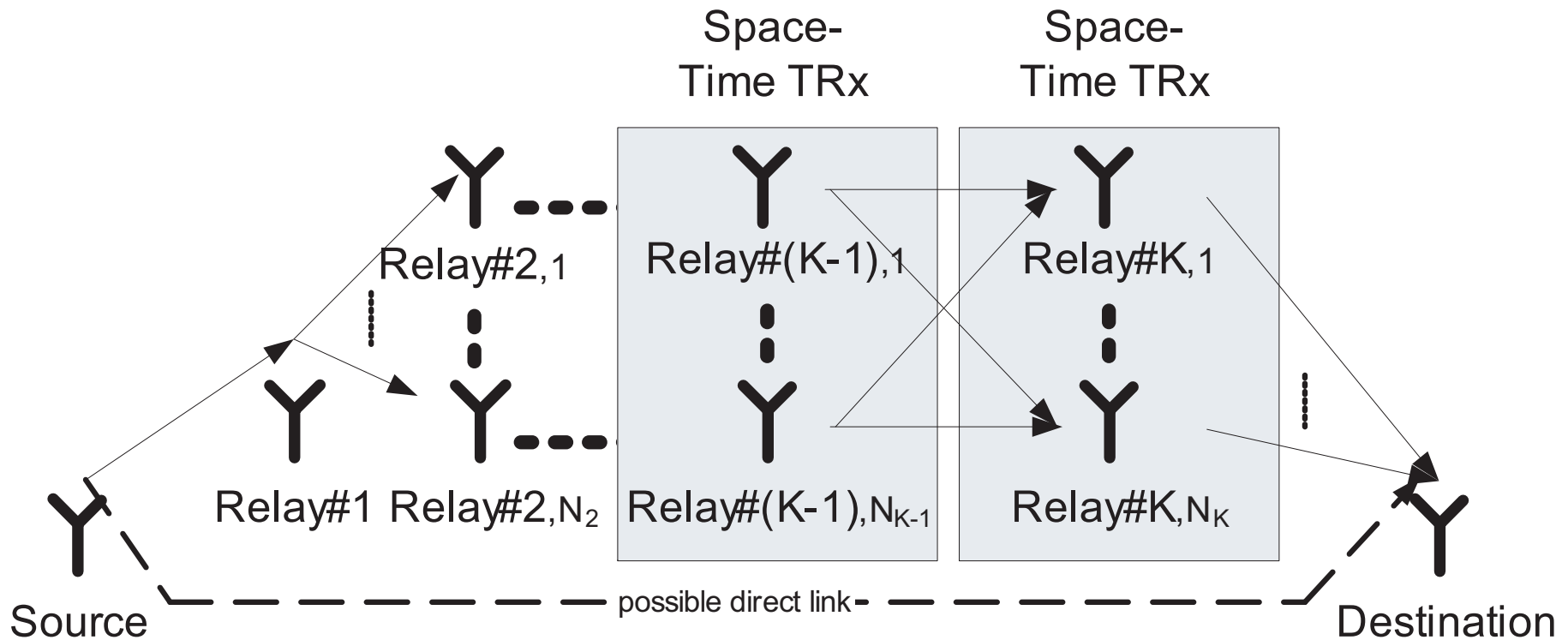
– System: Information Flow [4/5] –

- Space-Time Relaying:



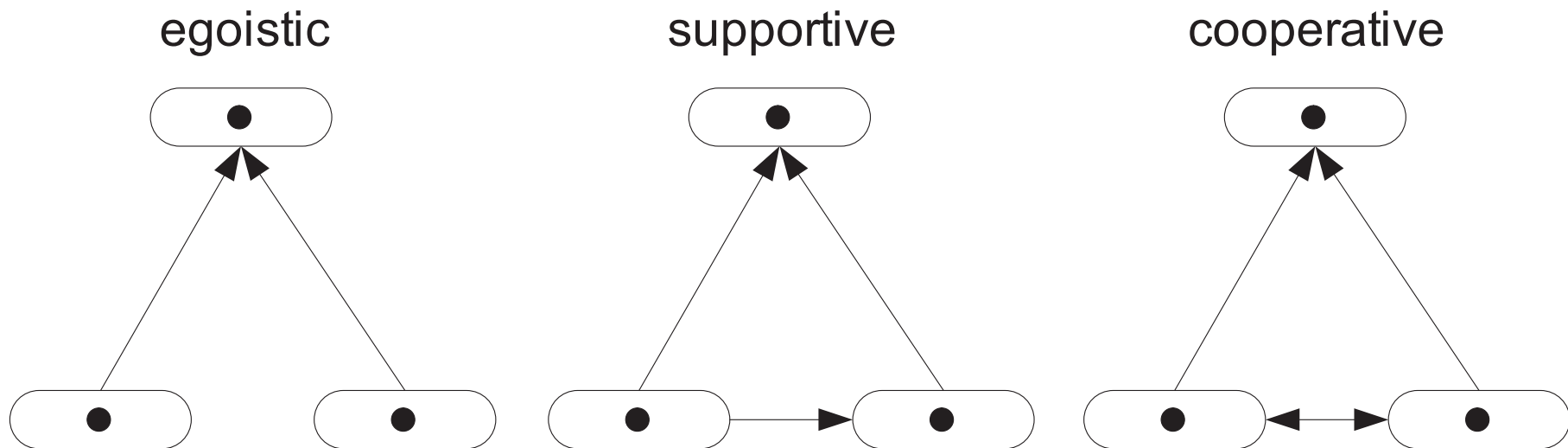
– System: Information Flow [5/5] –

- Composites Thereof:



– Node: Node Behaviour –

- The nodes in the network can have the following behaviour:
 - egoistic (no help)
 - supportive (unidirectional help)
 - cooperative (mutual help)



– Node: Relaying Methods –

- **Transparent Relaying:** neither information nor waveform are modified, allowing for simple power scaling and/or phase rotations; examples are:
 - Amplify and Forward (AF), i.e. amplification of analogue signal;
 - Linearly-Process and Forward (LF), i.e. phase-rotate and amplify signal;
 - Nonlinearly-Process and Forward (nLF), i.e. relay nonlinear soft information.
- **Regenerative Relaying:** information (bits) or waveform (samples) are modified, requiring more complex baseband operations; examples are:
 - Estimate and Forward (EF), i.e. detect and forward estimated signal;
 - Compress and Forward (CF), i.e. detect and compress estimated signal.
 - Decode and Forward (DF), i.e. detection, decoding and re-encoding;
 - Purge and Forward (PF), i.e. eliminate interference at relay;
 - Aggregate/Gather and Forward (GF), i.e. perform source coding and compression.

1.2 Key Milestones

– First Key Milestones –

- Early innovative contributions on supportive relaying as well as MIMO inspired the concept of cooperative relaying and distributed MIMO.
- Surprisingly, relaying systems had already been studied for almost four decades! Early key milestones are summarised on subsequent slides.

Supportive Relaying	1968 Meulen	1979 Cover & Gamal	1996 3GPP ODMA	1998 Nix <i>et al</i>	
Cooperative Relaying			1998 Sendonaris <i>et al</i>	2000 Laneman	
Distributed MIMO			2000 Dohler	2002 Laneman, Hunter	2003 Gupta, Stefanov
MIMO			1996 Foshini, Telatar	1998 Alamouti, Tarokh	

– My Pre-PhD Presentation Winter 1999/2000 –



Ph.D.: Past-Present-Future

Revolutionary Approach

KING'S
College
LONDON
Founded 1829

The Past

Azimuth Spectrum
Indoor Prediction

The Present

Evol. Approach

Space-Time P&C
User History
Resonance/Leakage

Revol. Approach.

Time-Frequency
Beat
Contr. Scrambling
Dyn. Frequ. Assign

Antenna Arrays

Quantum Theory

The Future

Artificially formed MS antenna arrays

- 3G Mobile Systems:

will have implemented Space-Time Processing and Coding assuming an antenna array at the BS to mitigate ISI and CCI while maximizing the spectrum efficiency. The Mobile Phone is assumed to have a single antenna, what clearly limits the opportunities of ST-Codes.

- Beyond:

Spectral problems usually occur in 'hot-spots', where the user density is very high. I suggest to investigate how adjacent mobiles could be used to form an multiple antenna array.

PART 3

HARDWARE REALISATION

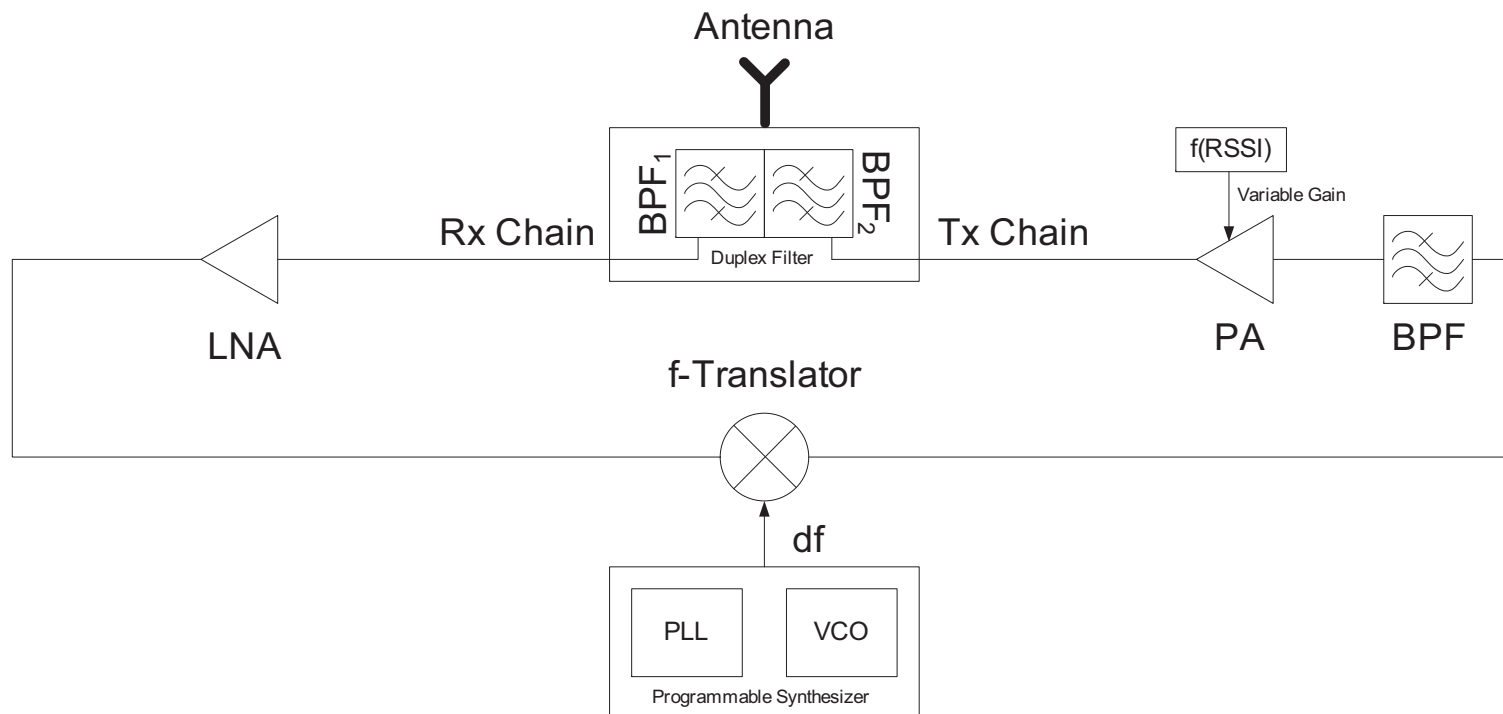
– Preliminary Note –

- In the end, it is the hardware which will facilitate as well as limit any implementation of cooperative relaying schemes.
- These limitations in hardware render the implementation of some of the recently proposed cooperative protocols infeasible.
- To understand what is really feasible, we will henceforth deal with the following topics:
 1. hardware architectures for transparent relaying transceivers;
 2. hardware architectures for regenerative relaying transceivers;
 3. comparison between these architectures;
 4. cost estimates of architectures.

3.1 Transparent Transceivers

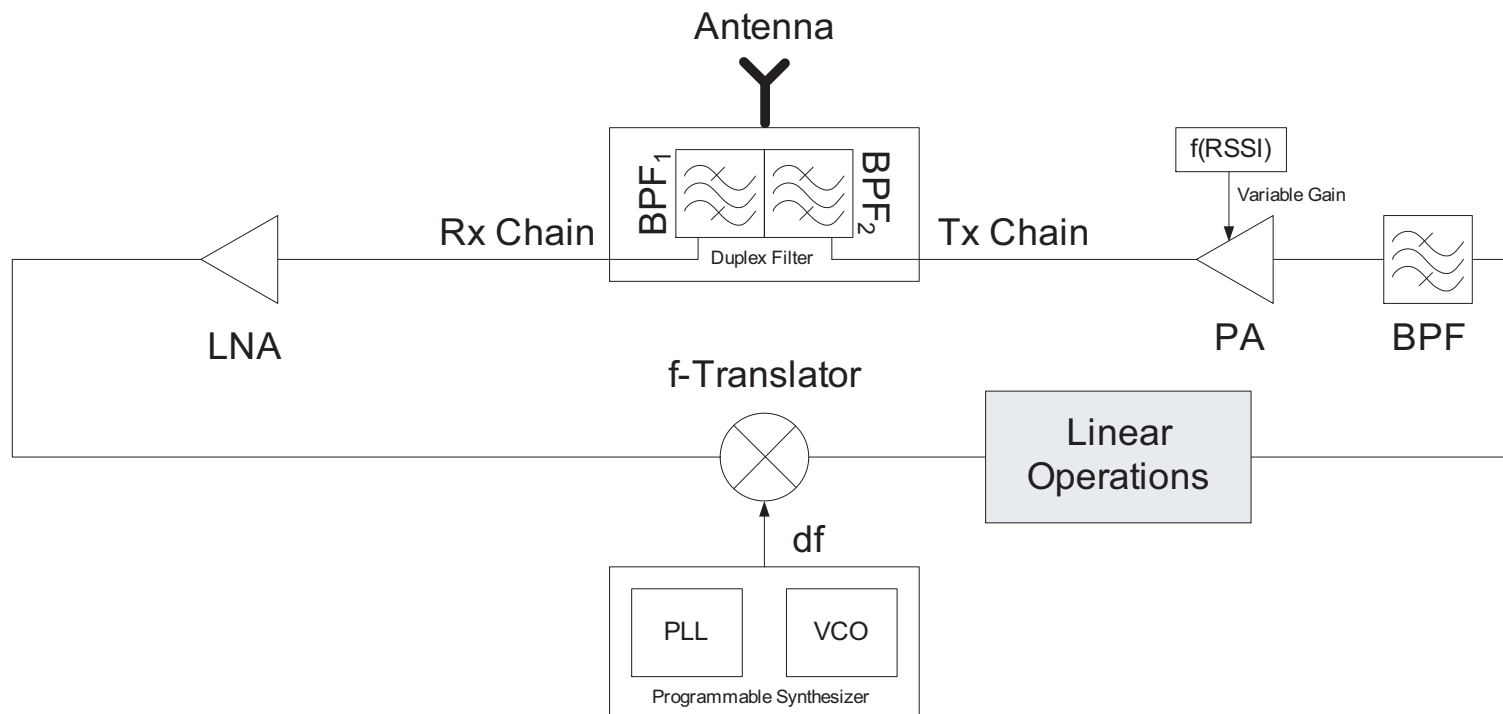
– Amplify & Forward Architecture –

- Important building blocks for the AF architecture:
 - frequency translator facilitating shift of df and variable gain power amplifier;
 - excellent duplex filters to avoid spillage (surface/bulk acoustic wave - SAW/BAW);
 - no storage of received signal, hence only (!) FDRA/FDMA protocols feasible.



– Linearly-Process & Forward Architecture –

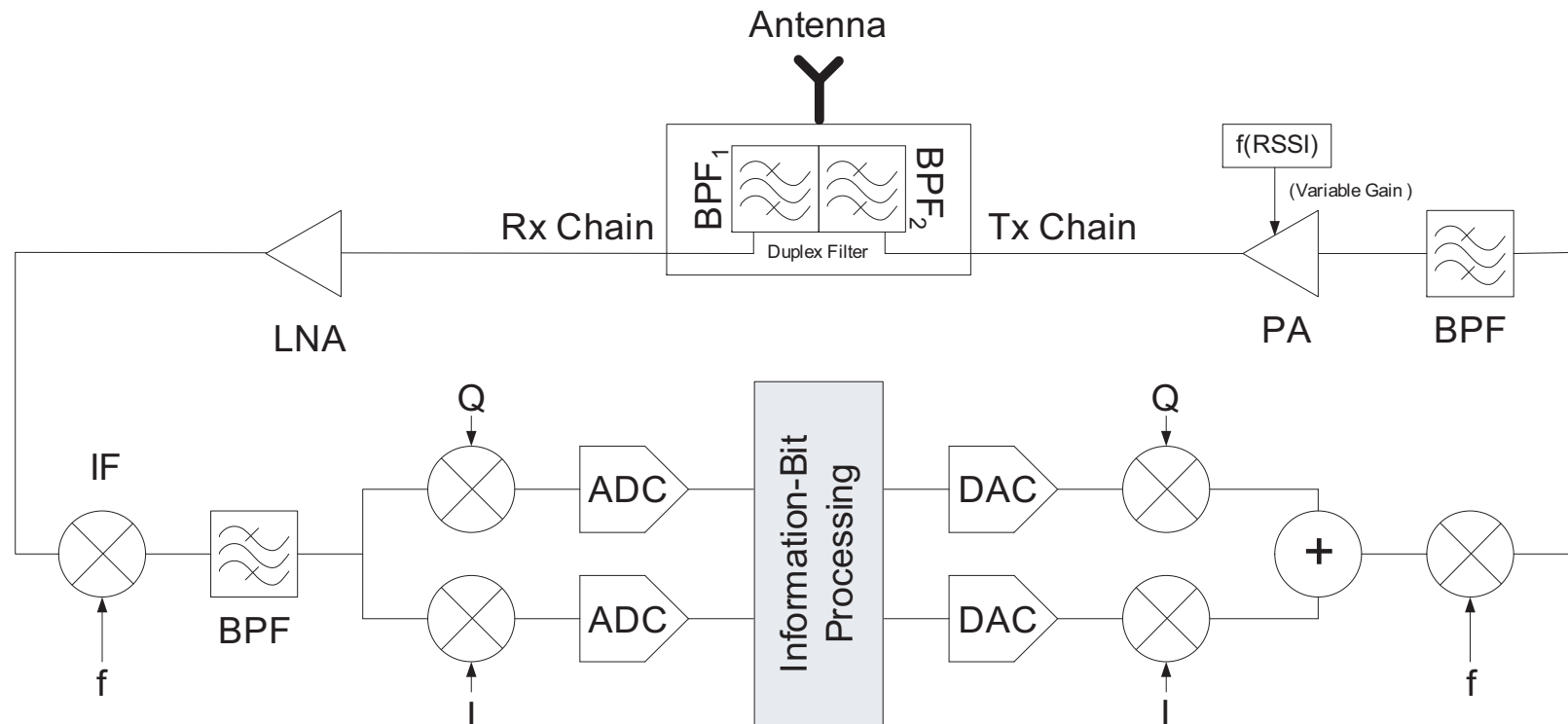
- Important building blocks for the LF architecture:
 - frequency translator df , good duplex filters, and variable gain power amplifier;
 - linear processing, such as phase rotation, etc;
 - no storage of received signal, hence only (!) FDRA/FDMA protocols feasible.



3.2 Regenerative Transceivers

– Information-Bit Processing Architectures –

- Important building blocks for the DF and PF architectures:
 - f-translators to baseband, synchronisation and ADC/DAC;
 - powerful baseband, including μ -controller, memory, data buses, etc;
 - processing of received signal, hence any type of protocol is feasible.



3.3 Architectural Comparisons

– Transceiver Complexity –

- using FMDA-like access requires very good filters to minimise spurious power spillage;
- information processing schemes are likely to be used with more sophisticated multi-carrier wideband access schemes, which require highly linear amplifiers;
- the complexity of non-transparent schemes is generally higher, where DF, PF and GF have highest complexity.

	AF	LF	nLF	EF	CF	DF	PF	GF
clock accuracy	+	+	+	+++	+++	+++	+++	+++
filter design	+++	+++	+++	++	++	++	++	++
power amplifier	+	+	+	+ / +++	+ / +++	+++	+++	+++
complexity	+	+	+	++	++	+++	+++	+++
memory				++	++	++	++	++

3.4 Cost Estimates

– Typical Cost of Transparent Architecture –

- The cost of the transparent architecture for the production of 1000 items at 900 MHz can be approximately estimated as per below table (values from Q3 2007).

List of Items	Approximate Cost in Euros
Bandpass Filter	2
Duplex Filter	6
Low Noise Amplifier	1
Programmable Synthesizer	8
Variable Gain Amplifier	5
Printed Circuit Board	5
Other Items	2
Total	27

– Typical Cost of Regenerative Architecture –

- The cost of the regenerative architecture for the production of 1000 items at 900 MHz can be approximately estimated as per below table.

List of Items	Approximate Cost in Euros
Transparent Architecture (minus Synthesizer)	19
Programmable Synthesizer	2×8
I&Q Brancher	2×5
ADCs/DACs	2×5
Signal Processing	15
Total	80

– Cost Trends [1/2] –

- Regenerative architecture is about 3 times more expensive than the transparent one.
- Every decade in produced items diminishes the cost by approximately 10 %.
- Going from 900 MHz to 2 GHz increases the price by approximately 5 %.
- Going from 900 MHz to 5 GHz increases the price by approximately 20 %.
- All estimates usually have a 10 % error margin.

– Cost Trends [2/2] –

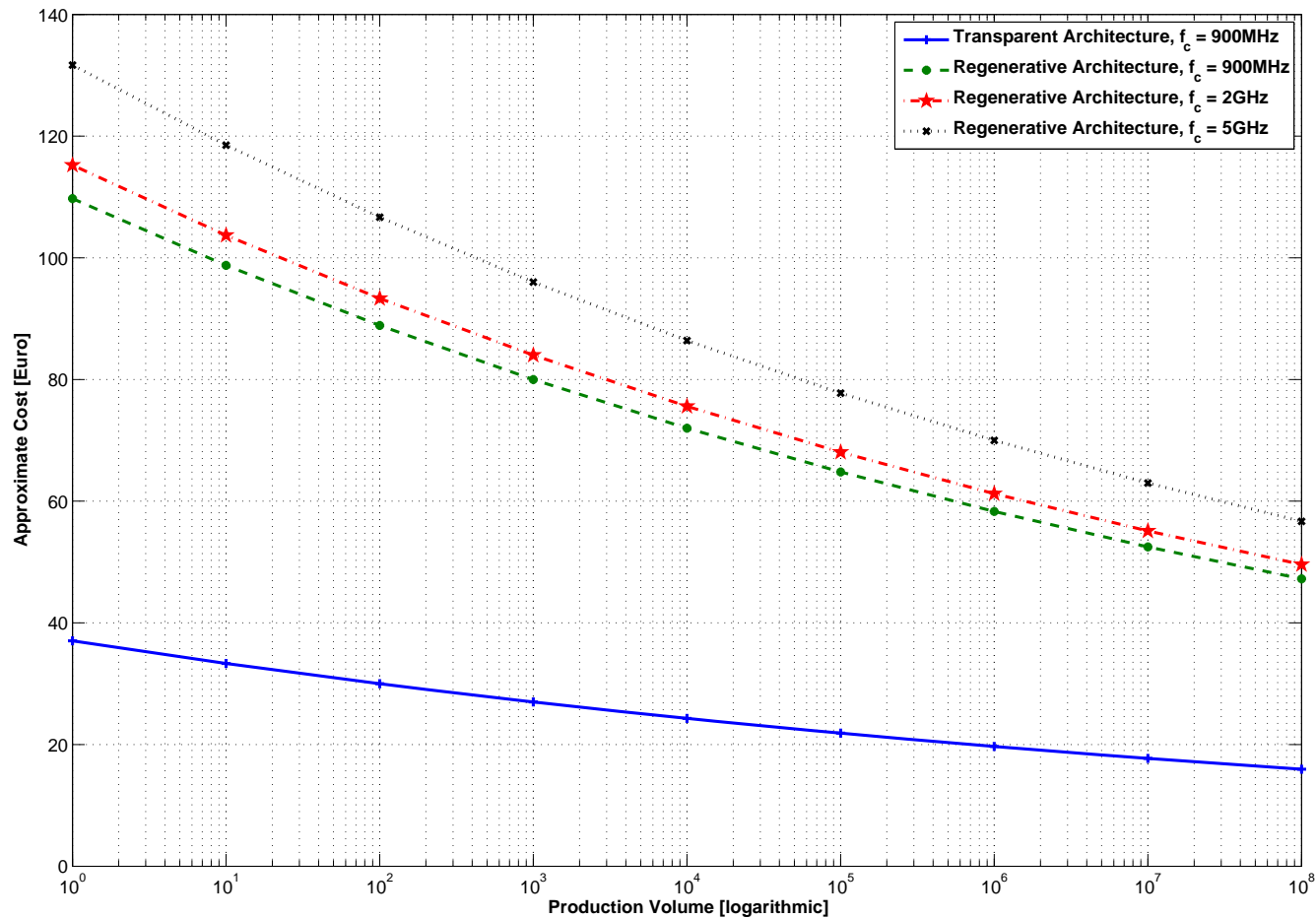
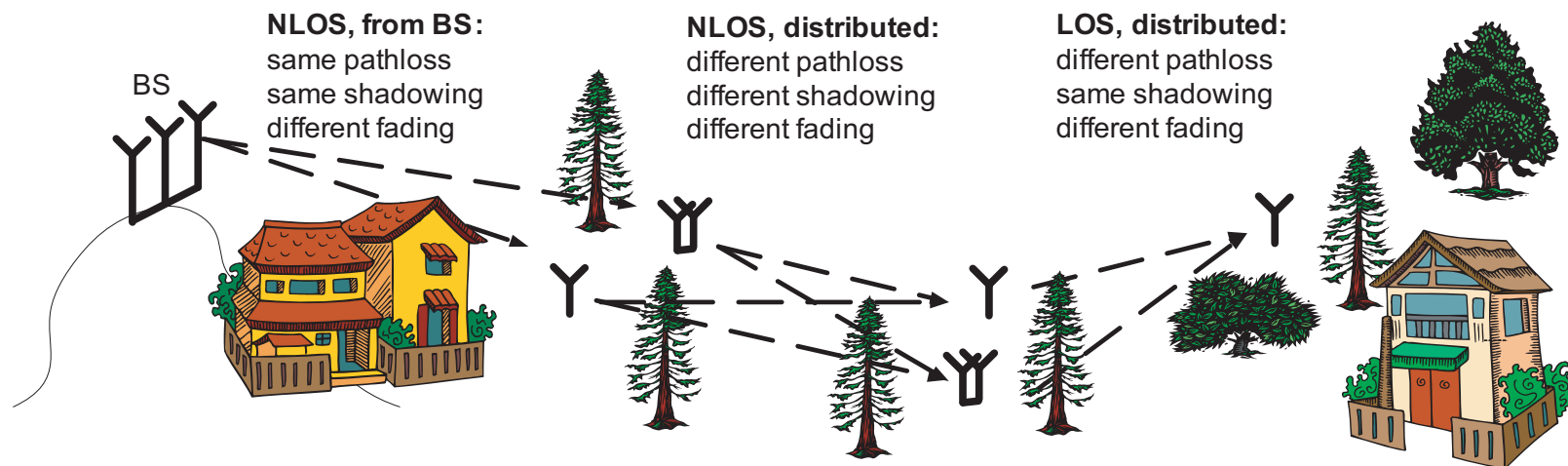


Figure 12: Transparent transceiver is significantly cheaper, whereas change in frequency has no major impact on costs.

PART 4
CHANNEL CHARACTERISATION

– Preliminary Note –

- In addition to physical channel, cooperative network becomes part of the channel [30].
- The cooperative relaying channel can be decomposed into the following cases:
 1. channel for regenerative relaying (BS-to-MT & MT-to-MT channel);
 2. channel for transparent relaying (cascaded channel);
 3. distributed MIMO channel behaviour.



4.1 Regenerative Relaying Channel

– Typical Regenerative Topology –

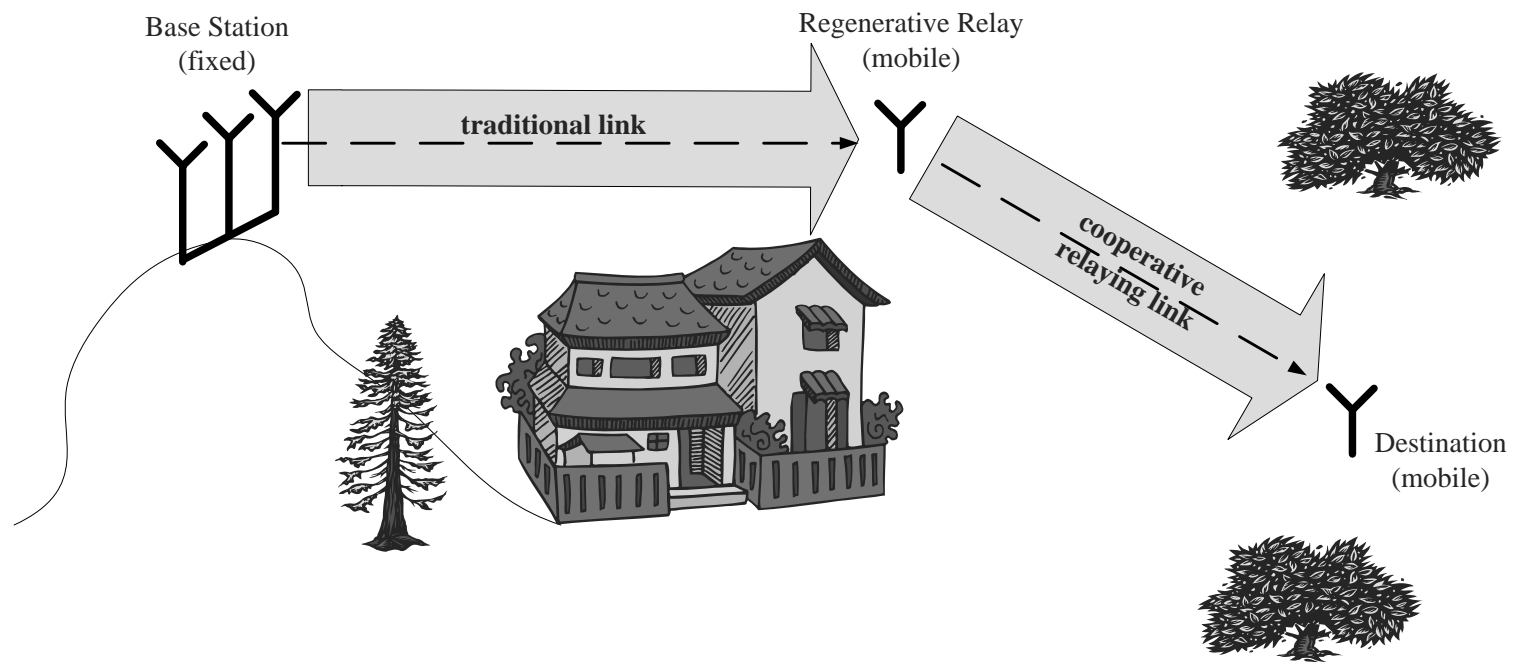


Figure 6: An example of a regenerative relaying channel.

– System Assumption –

- **Decoupling of Relay Stages.** The relay regenerates the signal which inherently decouples the fading channels before and after the relay.
- **Modeling Approach.** Unlike the transparent relay case, the channel of each segment can therefore be modeled separately which yields:

$$y_i = \sqrt{G_i} h_i x_i + n_i, \quad (3)$$

where x_i , y_i and n_i are respectively the transmitted signal, the received signal and the additive white Gaussian noise (AWGN) with power σ_i^2 experienced in the i –th relaying segment. Furthermore, $G_i = L_i \cdot S_i$ is the large-scale channel gain due to pathloss and shadowing and h_i is the generally complex channel coefficient due to fading.

- **Parametric Characterization.** The wireless regenerative relaying channel is hence characterized in each segment separately by L_i , S_i and h_i where the impact of each of these factors will be subsequently discussed.

– Impact on End-to-End Performance –

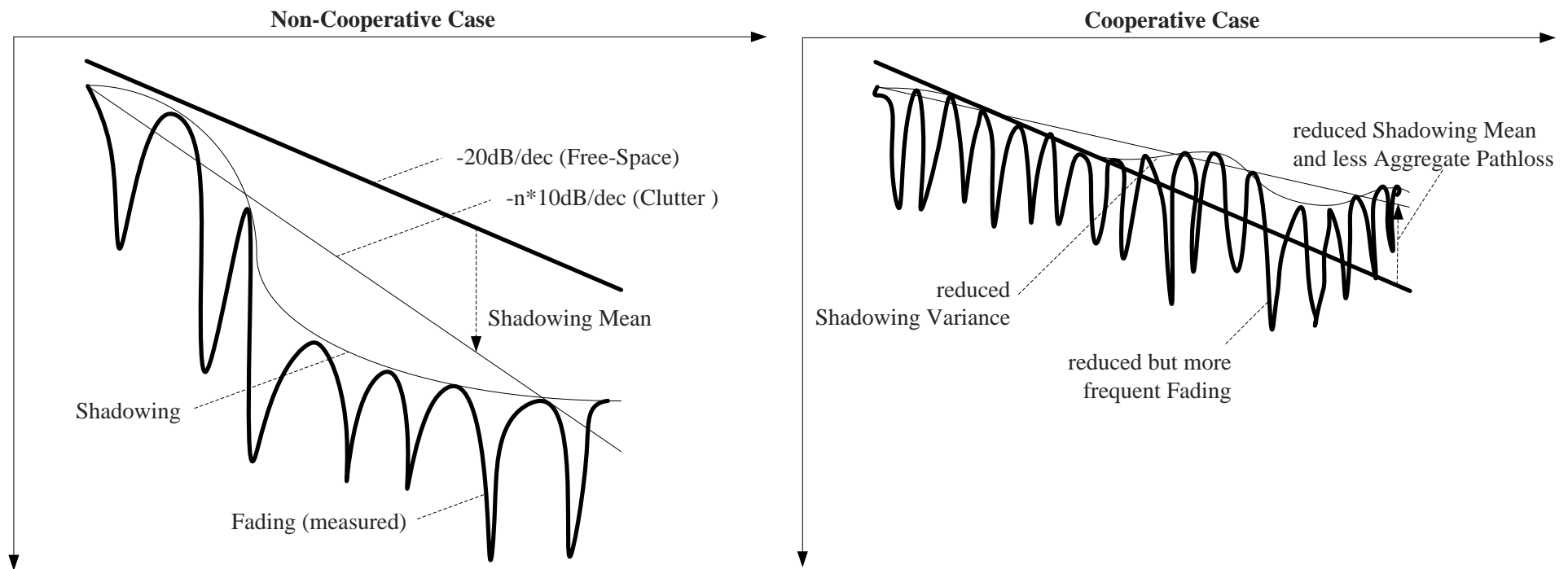


Figure 7: Regenerative cooperative communication impacts fading and shadowing and generally reduces pathloss.

– Change of Breakpoint Distance –

- **Traditional Breakpoint.** Most pathloss models exhibit a breakpoint behavior. The breakpoint distance can in some settings be approximately calculated as

$$d_{\text{bp}} \approx 4h_{\text{t}}h_{\text{r}}/\lambda,$$

where h_{t} and h_{r} are the transmitter and receiver heights respectively.

- **Reduced Breakpoint Distance.** Compared to BS-MS, reducing the antenna height of MS-MS by an order of magnitude (e.g. from 20m to 2m), the breakpoint distance is also reduced by an order of magnitude (e.g. from 100 m to 10 m).
- **System Impact.** Placing a relay between BS and some MS may advantageously move the traditional link from beyond the breakpoint to before the breakpoint but will likely cause the cooperative relaying link to be beyond breakpoint distance.

– Aggregate Pathloss Powergains [1/2] –

- **Nonlinear Pathloss Behavior.** Pathloss versus distance is highly non-linear, facilitating significant aggregate power gains. Therefore, placing relays in-between source and destination yields significant gains.
- **Example Topology.** Let us e.g. assume a system with the source and destination separated by d meters and relays placed at equidistance between them so that N relay segments occur. Assuming then an example pathloss model from [2], the pathloss in each relaying segment can be calculated in decibel as follows:

$$L = b + 10n \log_{10}(d/N), \quad (4)$$

where b is a constant and n the pathloss coefficient

– Aggregate Pathloss Powergains [2/2] –

- **Aggregate Pathloss Powergains.** The aggregate power gains due to this non-linear pathloss behavior, calculated as $10 \log_{10} N + L$, is summarized in Table 1 w.r.t. the case without relay in percent and in absolute dB values, assuming $d = 500$ m, $b = -62.01$ dB and $n = 5.86$.
- **General Trend.** These gains are significant which can be attributed to the large pathloss coefficient n . Furthermore, these gains even increase if a dual-slope pathloss model is assumed.

Relay Segments	1	2	3	4	5	6	7	8	9	10
Relative Gain [%]	0	18	32	44	55	65	75	84	93	102
Absolute Gain [dB]	0	15	23	29	34	38	41	44	46	49

Table 1: Absolute and relative aggregate pathloss gains with relays placed between source and destination separated by 500 m caused by the non-linear propagation model.

– Aggregate Shadowing Powergains [1/2] –

- **Decrease of Shadowing Variations.** In the case of serial relays with independent shadowing channels in each relaying hop, the performance is impacted by the weakest relaying segment. Therefore, the decrease in shadowing variation due to shorter communication distances significantly boosts performance of regenerative relaying systems.
- **Example Topology.** Let us again assume a system with the source and destination separated by d meters and relays placed at equidistance between them so that N relay segments occur. Using then e.g. the model of [2], the shadowing standard deviation in each relaying segment can be calculated in decibel as:

$$\sigma_{\text{dB}} = S_s \cdot \left(1 - e^{-\frac{d/N - d_0}{D_s}} \right), \quad (5)$$

where S_s , d_0 and D_s are some model specific constants.

– Aggregate Shadowing Powergains [2/2] –

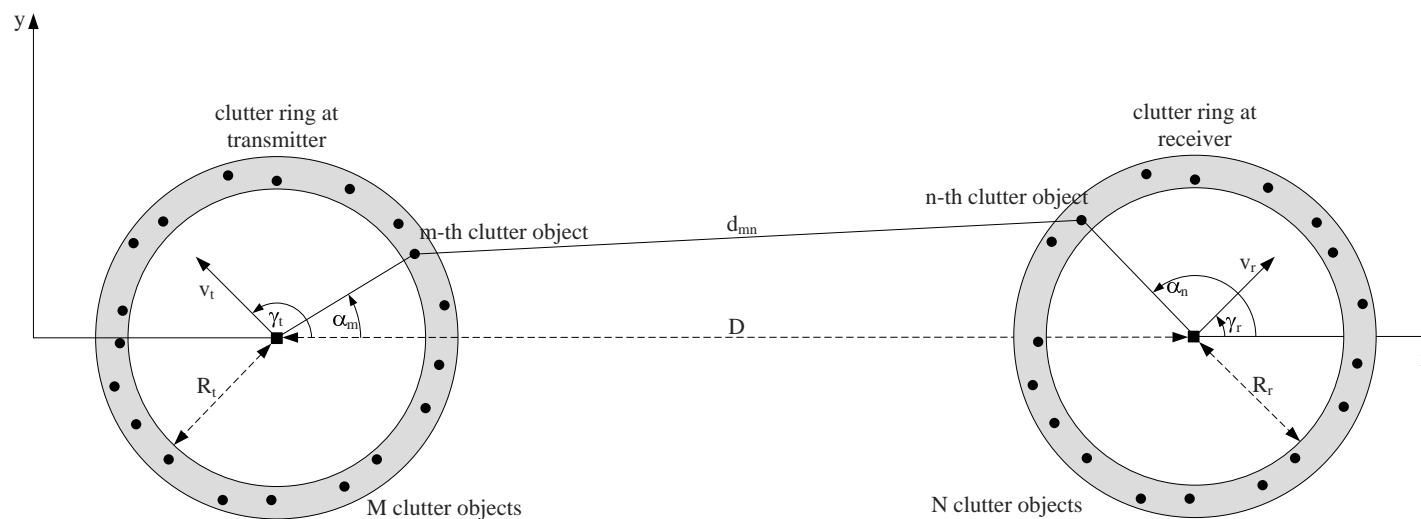
- Aggregate Shadowing Powergains.** Typically, the power margin due to shadowing is assumed to be about three times its standard deviation σ_{dB} . The aggregate power gains due to this non-linear shadowing behavior, calculated as $10 \log_{10} N + 3\sigma_{\text{dB}}$, is summarized in Table 4 w.r.t. the case without relay in percent and in absolute dB values, assuming $d = 500$ m, $S_s = 22.1$ dB, $d_0 = 10$ m and $D_s = 53$ m.
- General Trends.** These gains are fairly high for a large number of relays but turn into losses for a small number of relays, i.e. in the region of practical deployment. They are due to a small decrease in shadowing standard deviation for large distances and a strong decrease at very short distances.

Relay Segments	1	2	3	4	5	6	7	8	9	10
Relative Gain [%]	0	-3	-2	2	8	15	23	31	39	47
Absolute Gain [dB]	0	-2	-1	2	5	9	12	16	19	21

Table 2: Absolute and relative aggregate shadowing gains.

– Geometrical Model –

- **Geometrical Model.** Having originated in [5], this geometrical model is based on the following assumptions:
 - clutter is surrounding transmitter and receiver circularly and uniformly, forming a ring of scatterers;
 - waves which are reflected off several clutter surfaces as well as those which are further away are negligible because they suffer from increased pathloss;
 - the number of scatterers at either end is tending towards infinity, requiring that the power of each wave is negligible compared to the total mean power.



– Baseband Double-Bounced Model –

- **Baseband Model.** The baseband narrowband channel realization can be written as a superposition of any LOS, single bounced (SB) components which have only been bounced at the transmitter (SBT) and only bounced at the receiver (SBR), and the double bounced (DB) components.
- **Double Bounced Component.** Dealing here only with the double bounced component, it can be written as [6]:

$$h^{\text{DB}}(t) = \lim_{M,N \rightarrow \infty} \sum_{m=1}^M \sum_{n=1}^N a_{mn} \cdot e^{j(2\pi f_{mn}t - kd_{mn} + \phi_{mn})}, \quad (7)$$

where a_{mn} and ϕ_{mn} are the joint channel gain and phase shift caused by the interaction of m —th scatterers at the transmitter and n —th scatterer at the receiver; f_{mn} is the Doppler shift induced by moving Tx & Rx; kd_{mn} is the phase shift induced due to the wave traversing a distance d_{mn} whilst traveling from transmitter to receiver.

– Modeling Parameters [1/3] –

- **Modeling Parameters.** These variables are characterized as follows:

- **Amplitude** a_{mn} . The amplitude introduced by the m –th clutter at the transmitter is of the same relative magnitude but independent of the amplitude due to the n –th clutter at the receiver:

$$a_{mn} = a_m \cdot a_n = \frac{1}{\sqrt{MN}}, \quad (8)$$

where the last equation results from normalizing conditions which require that the power of (7) remains bounded and equal to one as $M, N \rightarrow \infty$.

- **Phase** ϕ_{mn} . The phase shift introduced by the m –th clutter at the transmitter is independent of the phase shift introduced by the n –th clutter at the receiver:

$$\phi_{mn} = \phi_m + \phi_n. \quad (9)$$

These phase shifts are random and, since the number of scatterers at either end is approaching infinit , these discrete random variables become continuous with PDFs $p_{\phi_t}(\phi_t)$ and $p_{\phi_r}(\phi_r)$, respectively. It can generally be assumed that they are uniformly distributed.

– Modeling Parameters [2/3] –

- **Modeling Parameters.** ... continued ...

- **Doppler Shift** f_{mn} . The Doppler shifts depend on the geometrical relation between direction of movement of transmitter or receiver and direction of departure or arrival of the wave. The Doppler shift introduced by the m –th clutter at the transmitter is generally independent of the Doppler shift introduced by the n –th clutter at the receiver:

$$f_{mn} = f_m + f_n \quad (10a)$$

$$f_m = \hat{f}_t \cdot \cos(\alpha_m - \gamma_t), \quad (10b)$$

$$f_n = \hat{f}_r \cdot \cos(\alpha_n - \gamma_r), \quad (10c)$$

where \hat{f}_t and \hat{f}_r are respectively the maximum Doppler shifts experienced at the transmitter and receiver and which are given as $\hat{f}_t = f_c \cdot v_t/c = v_t/\lambda$ and $\hat{f}_r = f_c \cdot v_r/c = v_r/\lambda$ with f_c being the carrier frequency and λ the wavelength. Since the location of the scatterers is not known a priori, the AOD α_m and AOA α_n are discrete random variables. However, since the number of scatterers at either end is approaching infinit , these discrete random variables become continuous with PDFs $p_{\alpha_t}(\alpha_t)$ and $p_{\alpha_r}(\alpha_r)$, respectively.

– Modeling Parameters [3/3] –

- **Modeling Parameters.** ... continued ...

- **Path Length** d_{mn} . The path length is impacted by the geometrical arrangement of clutter w.r.t. transmitter and receiver.

Case #1 – D is not significantly larger than $\max(R_t, R_r)$: This is typically encountered indoors and requires the exact expression for d_{mn} to be used:

$$d_{mn} = R_t + \sqrt{(R_t \sin \alpha_m - R_r \sin \alpha_n)^2 + (D - R_t \cos \alpha_m + R_r \cos \alpha_n)^2} + R_r, \quad (11)$$

which essentially prevents one from decoupling the two sums in (7) into two separate sums. Therefore, the CLT applies to the entire expression and the envelope $a = |h|$ is Rayleigh distributed.

Case #2 – $D \gg \max(R_t, R_r)$: It is typically encountered outdoors, leading to [6]:

$$d_{mn} \approx D + R_t \cdot (1 - \cos \alpha_m) + R_r \cdot (1 + \cos \alpha_n), \quad (12)$$

allowing to decouple the two sums in (7) into two separate sums, the resulting envelope being double-Rayleigh.

– Fading Distributions –

- **Unchanged Distributions.** With respect to non-cooperative systems, the statistical distributions of the complex channel, its envelope and power remain generally unchanged (unless there is a cascaded fading channel.)
- **Example Nakagami Distribution.** The PDFs of Nakagami- m envelope and power are:

$$p_a(a) = \frac{2m^m a^{2m-1}}{(\bar{g})^m \Gamma(m)} \exp\left(-\frac{ma^2}{\bar{g}}\right) \quad (13a)$$

$$p_g(g) = \frac{m^m (g)^{m-1}}{(\bar{g})^m \Gamma(m)} \exp\left(-\frac{mg}{\bar{g}}\right), \quad (13b)$$

where $\Gamma(\cdot)$ is the complete Gamma function and m is the Nakagami fading factor. Furthermore, a is the amplitude and g the power. This reduces to the Rayleigh fading case for $m = 1$ and a non-fading channel for $m \rightarrow \infty$. The Gamma distribution is well applicable to all MPCs which suffer from obstructed LOS or weak NLOS conditions.

– Temporal Autocorrelation Function [1/3] –

- **Importance.** The temporal ACF of the complex fading channel $h(t)$ is an important quantity since it allows to quantify the required pilot density and interleaver depths for coherent systems, the performance degradation for both coherent as well as non-coherent systems, etc.
- **Definition.** We will henceforth deal with the normalized ACF which is defined as

$$R(\Delta t) = \frac{\mathbb{E} \{h(t + \Delta t) \cdot h^*(t)\}}{\sqrt{\text{VAR} \{h(t + \Delta t)\} \cdot \text{VAR} \{h^*(t)\}}}, \quad (14)$$

where the expectation is taken w.r.t. the set of random variables which in our case are $\alpha_t, \alpha_r, \phi_t$ and ϕ_r . Furthermore, it is henceforth assumed that the average channel power $\text{VAR} \{h(t)\} = 1$ which allows us to drop it in subsequent derivations.

– Temporal Autocorrelation Function [2/3] –

- **ACF for M2M.** We can calculate the ACF as follows:

$$R(\Delta t) = \mathbb{E} \left\{ \lim_{M, N \rightarrow \infty} \sum_{m=1}^M \sum_{n=1}^N \frac{1}{\sqrt{MN}} \cdot e^{j(2\pi(f_m + f_n)(t + \Delta t) + kd_{mn} + \phi_m + \phi_n)} \times \right. \\ \left. \lim_{M, N \rightarrow \infty} \sum_{m'=1}^M \sum_{n'=1}^N \frac{1}{\sqrt{MN}} \cdot e^{-j(2\pi(f_{m'} + f_{n'})t + kd_{m'n'} + \phi_{m'} + \phi_{n'})} \right\} \quad (15a)$$

$$= \int_{-\pi}^{\pi} e^{j2\pi \hat{f}_t \cdot \cos(\alpha_t - \gamma_t) \Delta t} p_{\alpha_t}(\alpha_t) d\phi_t \times \\ \int_{-\pi}^{\pi} e^{j2\pi \hat{f}_r \cdot \cos(\alpha_r - \gamma_r) \Delta t} p_{\alpha_r}(\phi_r) d\phi_r \quad (15b)$$

$$= J_0 \left(2\pi \hat{f}_t \Delta t \right) \cdot J_0 \left(2\pi \hat{f}_r \Delta t \right), \quad (15c)$$

where $J_0(\cdot)$ is the zeroth order Bessel function of the first kind.

– Temporal Autocorrelation Function [3/3] –

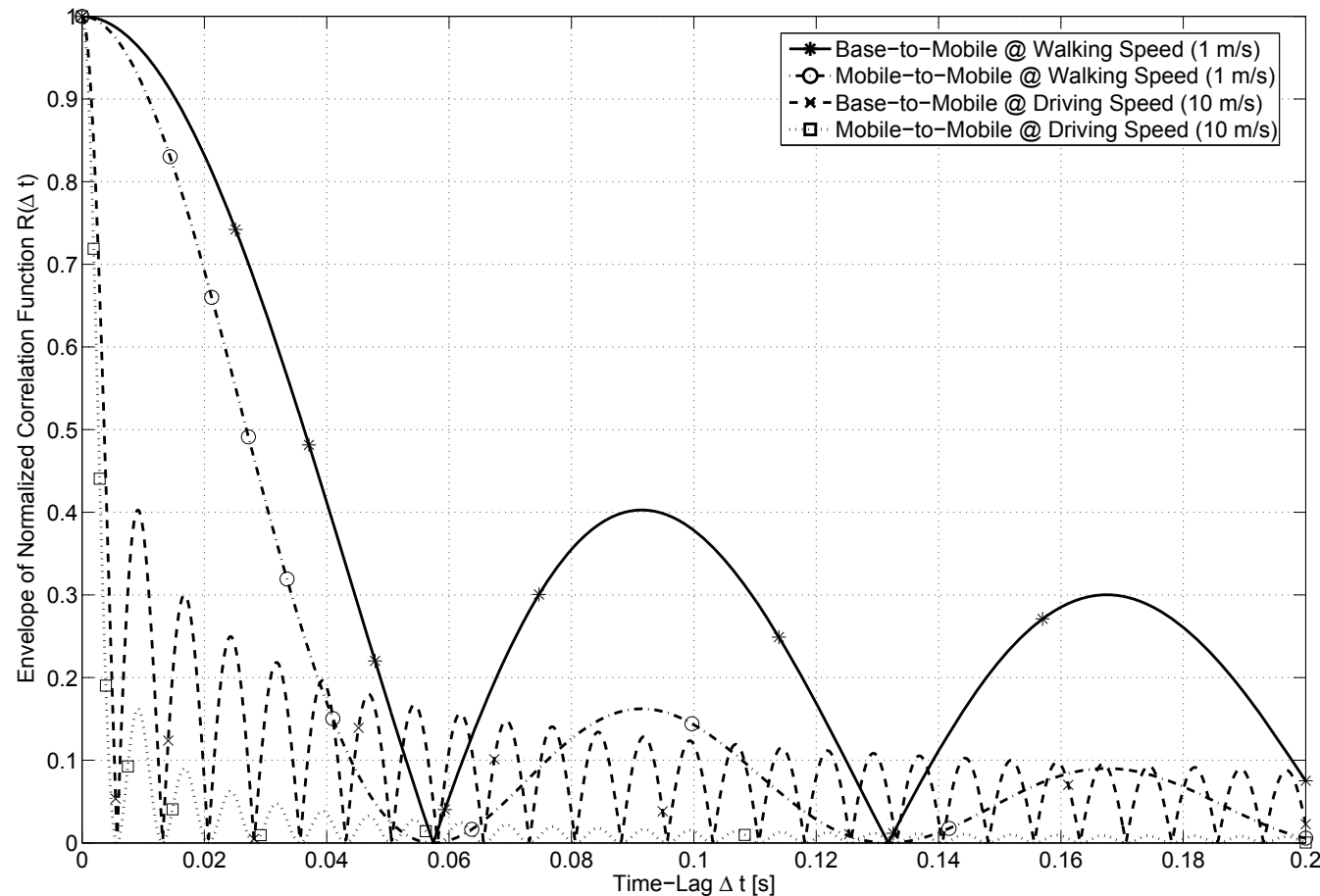


Figure 8: Absolute value of the temporal autocorrelation function of the complex fading channel for the base-to-mobile and mobile-to-mobile scenarios at $f_c = 2$ GHz. Observations: MS-to-MS channel decorrelates faster than BS-to-MS channel; good for code design, bad for channel estimation.

– Doppler Power Spectrum –

- **Definition.** The Doppler power spectrum of the complex channel $h(t)$ is determined from the Fourier transform of its temporal autocorrelation function $R(\Delta t)$, i.e.

$$\Psi(f) = \int_{-\infty}^{\infty} R(\Delta t) e^{-j2\pi f \Delta t} d\Delta t. \quad (16)$$

This transformation does clearly not yield any novel insights w.r.t. the already available autocorrelation function. However, it is of great value when simulating fading channels.

- **Doppler of M2M Channel.** Applying the Fourier transform to (15c) yields [7]:

$$\Psi(f) = \frac{1}{\pi^2 \sqrt{\hat{f}_t \hat{f}_r}} K \left[\sqrt{\frac{(\hat{f}_t + \hat{f}_r)^2 - f^2}{4\hat{f}_t \hat{f}_r}} \right], \quad (17)$$

where $K(\cdot)$ is the complete elliptic integral of the first kind. This function exhibits two peaks at $\pm(\hat{f}_t - \hat{f}_r)$ and is generally symmetric w.r.t. the motion of Tx/Rx.

– Level Crossing Rate –

- **Definition.** The level crossing rate of the channel's envelope represents the expected number of times per second the channel amplitude $a = |h|$ crosses level a_{thr} in the positive direction. It is an important notion for adaptive or opportunistic systems in that it quantifies the frequency the channel state changes and hence the frequency for need of adaptation or opportunity.
- **LCR of M2M Channel.** It can be calculated as [8]:

$$N(a_{\text{thr}}) = \sqrt{2\pi \left(\hat{f}_t^2 + \hat{f}_r^2 \right)} \cdot a_{\text{thr}} \cdot e^{-a_{\text{thr}}^2}, \quad (18)$$

assuming that $\mathbb{E} \{ |h|^2 \} = 1$. Generally, the MS-to-MS channel varies faster than BS-to-MS channel, which is advantageous since it creates opportunities more frequently but requires also more frequent adaptations, e.g. change of modulation and coding scheme.

– Average Fade Duration –

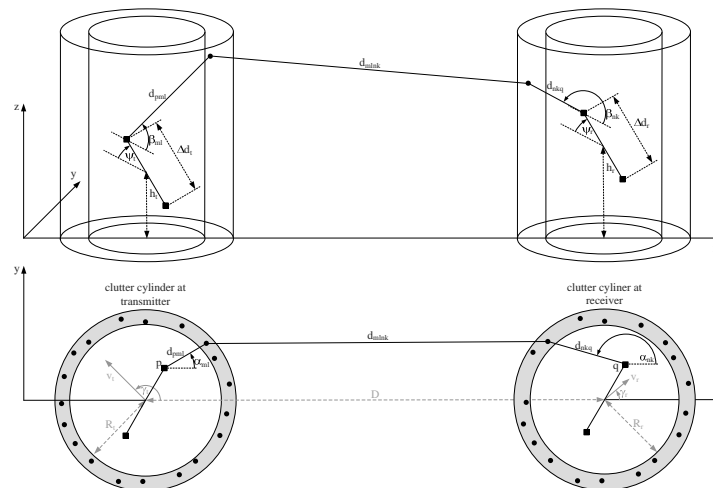
- **Definition.** It is the average duration of time the envelope spends below level a_{thr} . Again, it is an important notion for adaptive or opportunistic systems in that it quantifies the duration the system remains in the same state, e.g. same modulation order, etc.
- **AFD of M2M Channel.** It can be calculated as:

$$T(a_{\text{thr}}) = \frac{1}{\sqrt{2\pi (\hat{f}_t^2 + \hat{f}_r^2)}} \left(e^{a_{\text{thr}}^2} - 1 \right). \quad (19)$$

Again, the AFD of mobile-to-mobile channels is generally lower than of base-to-mobile channels due to the higher mobility at either end.

– Advanced Modeling –

- **Advanced Modeling.** Following exactly the same approach but with a little more involved mathematics, one can derive the temporal, spatial and spectral characteristics of the following cases:
 - Non-Isotropic Scattering Scenario
 - Ricean Fading Scenario
 - MIMO System
 - 3D Clutter Distribution
- **Spectral-Spatial-Temporal Characteristics.** An example model is:



4.2 Transparent Relaying Channel

– Typical Transparent Topology –

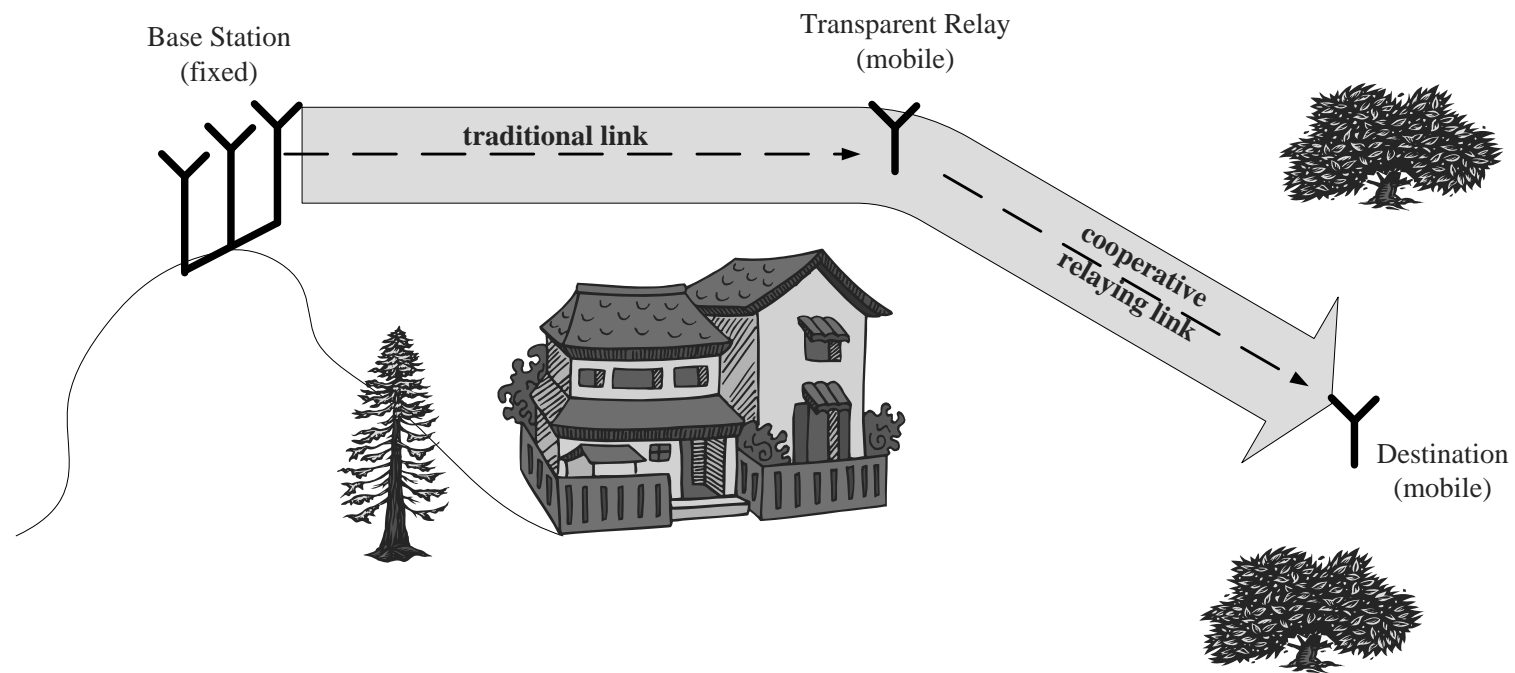


Figure 9: An example of a transparent relaying channel.

– System Assumption [1/2] –

- **Coupling of Relay Stages.** Transparent relaying couples the fading channels and the topology hence becomes part of the channel.
- **Modeling Approach.** In the example case of one relay leading to two relaying segments, the effective received signal is given as:

$$y_2 = \sqrt{G_2} \cdot h_2 \cdot A \cdot y_1 + n_2 \quad (20a)$$

$$y_1 = \sqrt{G_1} \cdot h_1 \cdot x_1 + n_1 \quad (20b)$$

which can be rewritten as

$$y_2 = A \cdot \sqrt{G_1 G_2} \cdot h_1 h_2 \cdot x_1 + A \cdot \sqrt{G_2} \cdot h_2 \cdot n_1 + n_2, \quad (21)$$

where the end-to-end wireless channel is characterized by $A \cdot \sqrt{G_1 G_2} h_1 h_2$ and the additive noise by $A \cdot \sqrt{G_2} \cdot h_2 \cdot n_1 + n_2$.

– System Assumption [2/2] –

- **Amplification Factor.** A is the amplification factor which can generally be variable, averaged or fixed:
 - **Variable Amplification Factor.** Relay has knowledge on the instantaneous fading conditions of the source to relay channel and the amplification factor counterweights deep fades:

$$A = \sqrt{\frac{P_2}{P_1 g_1 + \sigma_1^2}}, \quad (22)$$

where P_1 and P_2 are the respective average transmission powers of the sender and relay, g_1 is the instantaneous channel power in the first relaying segment and σ_1^2 is AWGN.

- **Average Amplification Factor.** The amplification in the relay injects in average the same power as the amplification given in (22), which yields the condition [9]:

$$A = \sqrt{\mathbb{E} \left\{ \frac{P_2}{P_1 g_1 + \sigma_1^2} \right\}}, \quad (23)$$

Different relaying channel statistics hence require very different amplification .

– Impact on End-to-End Performance –

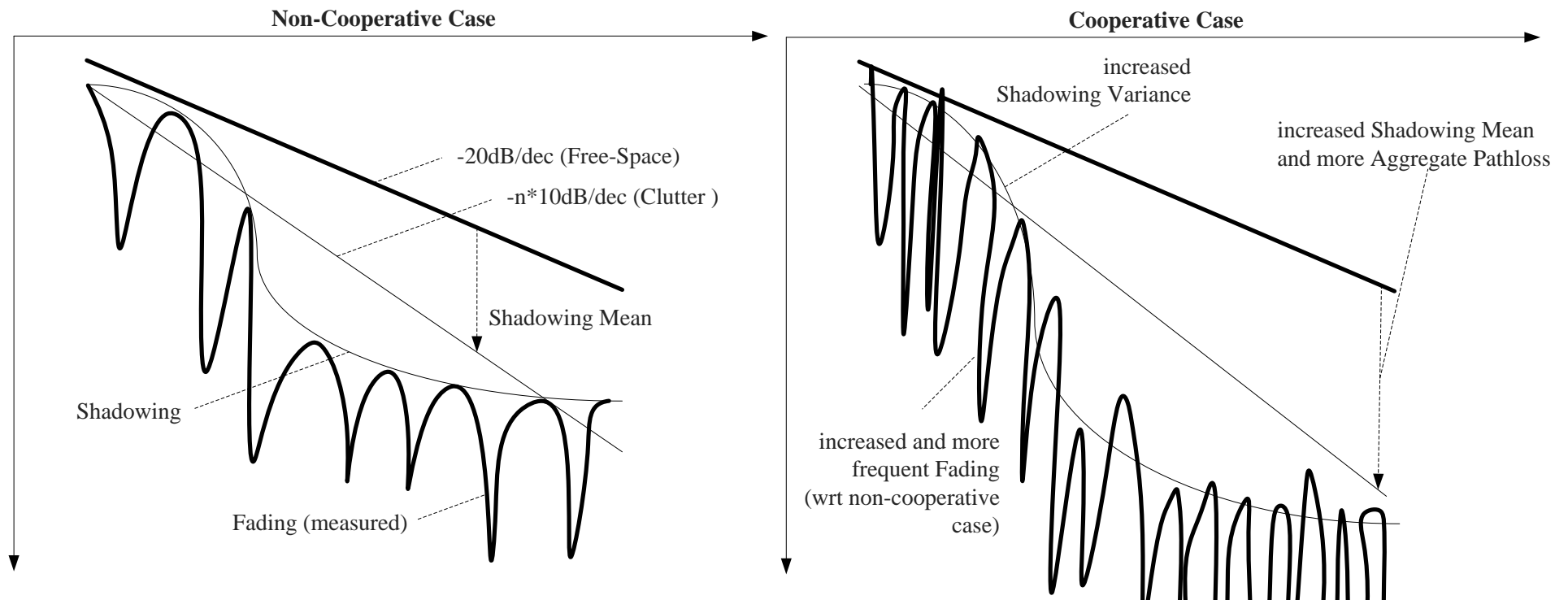
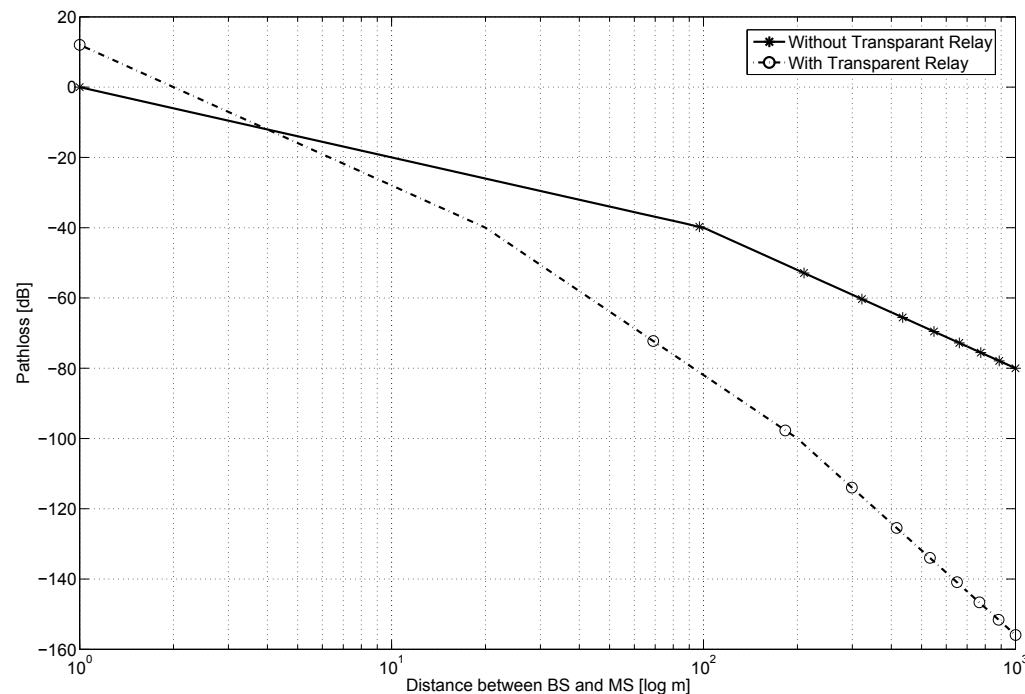


Figure 10: Transparent cooperative communication worsens fading behavior and also impacts shadowing and pathloss.

– Change of Breakpoint Behavior –

- **Change of Breakpoint Behavior.** The lower antenna heights together with the coupling of the relaying segments, yields fairly complex pathloss behaviors which can be quantified for a given pathloss model at hand.
- **Example Behavior.** Comparison between cases of no relay with fixed-gain relay placed exactly between transmitter and receiver.



– Increased Pathloss [1/2] –

- **Per-Stage Pathloss.** Let us assume for simplicity e.g. a fixed amplification factor and a single-slope pathloss model for both relaying stages. It is of the form

$L_i(d) = b_i + n_i \log_{10}(d)$, where b_i is some normalization constant and n_i the pathloss coefficient

- **End-to-End Pathloss.** It can be written as the sum of each segment's contribution, i.e. $b_1 + b_2 + n_1 \log_{10}(d_1) + n_2 \log_{10}(d_2)$, where $d = d_1 + d_2$. If the transparent relay is placed exactly midway between transmitter and receiver and both relaying segments exhibit the same pathloss behavior, this expression simplifies to $2b + 2n \log_{10}(d/2)$. The end-to-end pathloss hence experiences a change in parameters, i.e.

$$L(d) = b' + n' \log_{10}(d) \quad (24)$$

where $b' = 2b - 2n \log_{10} 2$ and $n' = 2n$. This leads to an increased pathloss slope and shift as already observed in the previous figure .

– Increased Pathloss [2/2] –

- **Example Pathloss Calculation.** To quantify this loss for an arbitrary number of relaying segments, let us e.g. assume a system with the source and destination separated by $d = 500$ m and relays placed at equidistance between them so that N relay segments occur. Then, with the model of [2], we have $b = -62.01$ dB and $n = 5.86$ leading to $b' = -62.01 \cdot N - 5.86 \cdot \log_{10} N$ dB and $n = 5.86 \cdot N$.
- **General Trends.** These losses diminish with variable amplification factor but are generally very large.

Relay Segments	1	2	3	4	5	6	7	8	9	10
Relative Gain [%]	0	-50	-66	-75	-80	-83	-86	-87	-89	-90

Table 3: Absolute and relative pathloss losses with relays placed between source and destination separated by 500 m caused by the non-linear propagation model.

– Aggregate Shadowing Powerlosses [1/2] –

- **Increase of Shadowing Variations.** In the case of transparent relays with independent shadowing channels in each relaying segment, the aggregated shadowing still obeys a Gaussian distribution in decibels, however, with a changed standard deviation w.r.t. a direct link. Using (21), the effective end-to-end shadowing standard deviation with N transparent relaying segments and a fixed amplification factor is given as

$$\sigma_{e2e,dB} = \sqrt{N} \sigma_{dB}.$$

- **More Realistic Model.** Using a more sophisticated model, such as given in [2], the aggregated end-to-end shadowing standard deviation for N equally long relaying segments can be calculated in decibel as follows:

$$\sigma_{e2e,dB} = \sqrt{N} \cdot S_s \cdot \left(1 - e^{-\frac{d/N - d_0}{D_s}} \right), \quad (25)$$

where S_s , d_0 and D_s are some model specific constants and d is the distance between source and destination.

– Aggregate Shadowing Powerlosses [2/2] –

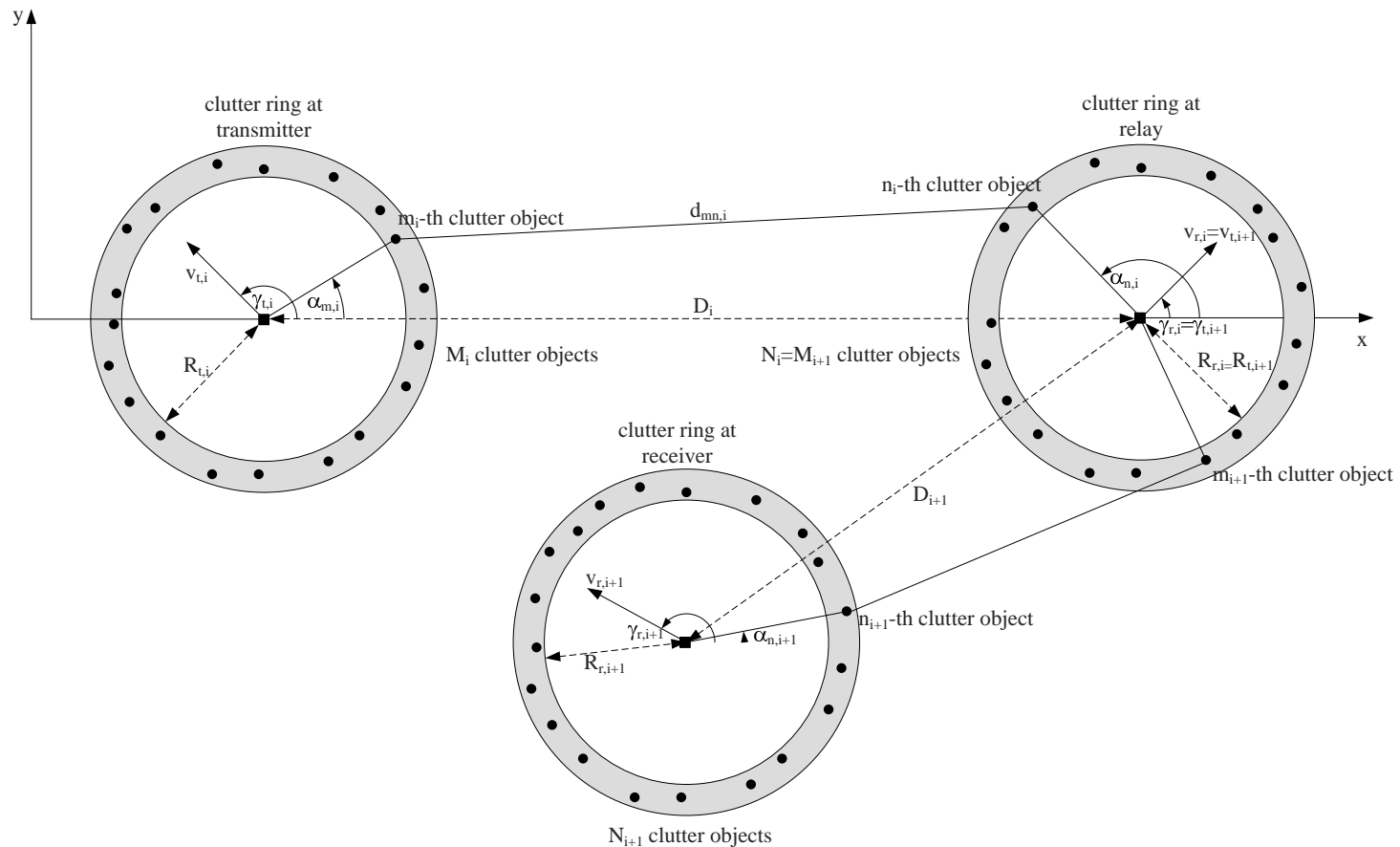
- **Example Model Realization.** The increase in shadowing standard deviation w.r.t. the case without relay in percent and in absolute dB values is summarized in Table 4, assuming $d = 500$ m, $S_s = 22.1$ dB, $d_0 = 10$ m and $D_s = 53$ m.
- **General Trends.** These losses are generally not negligible and further aggravate above discussed pathlosses. It is interesting to observe however that with above model, the shadowing losses start to diminish after around 5 relays and even turn into gains beyond 20 relays (not shown). This is due to a strong decrease of the shadowing standard deviation at very short distances.

Relay Segments	1	2	3	4	5	6	7	8	9	10
Relative Gain [%]	0	-29	-39	-44	-45	-46	-45	-44	-42	-40
Absolute Gain [dB]	0	-9	-14	-17	-18	-18	-18	-17	-16	-15

Table 4: Absolute and relative aggregate shadowing losses with relays placed between source and destination separated by 500 m caused by the non-linear behavior of the shadow standard deviation.

– Geometrical Model –

- Geometrical Model.** Following the approach as for the regenerative channel, this geometrical model is based on the same assumptions.



– Baseband Double-Bounced Model –

- **Baseband Model.** The baseband narrowband channel realization can be written as a superposition of any LOS, SBT, SBR and DB components.
- **Double Bounced (BD) Component.** Dealing here only with the double bounced component, it can be written as [6]:

$$h(t) = \prod_{i=1}^N h_i = \prod_{i=1}^N h_i^{\text{DB}} \quad (27)$$

$$= \prod_{i=1}^N \lim_{M_i, N_i \rightarrow \infty} \sum_{m_i=1}^{M_i} \sum_{n_i=1}^{N_i} \frac{1}{\sqrt{M_i N_i}} \cdot e^{j(2\pi(f_{m,i} + f_{n,i})t - kd_{mn,i} + \phi_{m,i} + \phi_{n,i})} \quad (28)$$

where i relates to the relaying segment and generally the same notation as for the regenerative channel has been used.

– Constant Amplification Factor–

- Cascaded Rayleigh Fading.** The double-Rayleigh channel results from the product of two complex Gaussian processes, i.e. $h = h_1 \cdot h_2$, the amplitude/envelope of which is $a = |h| = |h_1| \cdot |h_2| = a_1 \cdot a_2$ and the gain/power of which is $g = |h|^2 = |h_1|^2 \cdot |h_2|^2 = g_1 \cdot g_2$.
- Resultant PDF.** Using the rule for the PDF transformations of products of random variables, one easily establishes that the resultant PDF is given as:

$$p_g(g) = \int_0^\infty \frac{1}{A^2\xi} \cdot p_{g_1}(\xi) \cdot p_{g_2}\left(\frac{g}{A^2\xi}\right) d\xi \quad (29a)$$

$$= \int_0^\infty \frac{1}{A^2\xi} \cdot \frac{1}{\bar{g}_1} \exp\left(-\frac{\xi}{\bar{g}_1}\right) \cdot \frac{1}{\bar{g}_2} \exp\left(-\frac{g}{\bar{g}_2 A^2\xi}\right) d\xi \quad (29b)$$

$$= \frac{1}{A^2} \frac{2}{\bar{g}_1 \cdot \bar{g}_2} \cdot K_0\left(2\sqrt{\frac{1}{A^2} \frac{g}{\bar{g}_1 \cdot \bar{g}_2}}\right), \quad (29c)$$

where $K_0(\cdot)$ is the zeroth order modified Bessel function of the second kind.

– Variable Amplification Factor–

- **Transposition of Problem.** The power of the end-to-end transparent relay channel with variable amplification i.e.

$$g = \frac{P_2}{P_1} \cdot \frac{g_1 g_2}{g_1 + \sigma_1^2 / P_1} \quad (30)$$

is in structure the same as the end-to-end SNR in transparent relay channels with constant amplification This allows one to reuse prior tools and results.

- **Resultant PDF.** The PDF of the channel power e.g. is given as:

$$p_g(g) = \frac{2P_1}{P_2 \bar{g}_2} e^{-\frac{P_1 g}{P_2 \bar{g}_2}} \quad (31a)$$

$$\times \left(\sqrt{\frac{\sigma_1^2 g}{P_2 \bar{g}_1 \bar{g}_2}} K_1 \left[2 \sqrt{\frac{\sigma_1^2 g}{P_2 \bar{g}_1 \bar{g}_2}} \right] + \frac{\sigma_1^2}{P_1 \bar{g}_1} K_0 \left[2 \sqrt{\frac{\sigma_1^2 g}{P_2 \bar{g}_1 \bar{g}_2}} \right] \right) .$$

– ACF for Constant Amplification –

- **Cascaded Channel.** The first to report on the ACF of the transparent relaying channel was [10], which used the fact that the channel is of the form $h = h_1 h_2$ where h_1 and h_2 are respectively the channels of the first and second relaying segments.
- **Resultant ACF.** Assuming a constant amplification factor A , the normalized ACF can be calculated as [10]:

$$R(\Delta t) = \mathbb{E} \{h(t + \Delta t) \cdot h^*(t)\} \quad (32a)$$

$$= \mathbb{E} \{h_1(t + \Delta t)h_1^*(t)h_2(t + \Delta t)h_2^*(t)\} \quad (32b)$$

$$= R_1(\Delta t) \cdot R_2(\Delta t) \quad (32c)$$

$$= \prod_{i=1}^2 J_0 \left(2\pi \hat{f}_{t,i} \Delta t \right) \cdot J_0 \left(2\pi \hat{f}_{r,i} \Delta t \right). \quad (32d)$$

– ACF for Variable Amplification –

- **Approximation.** With variable amplification and a high operational SNR allows the end-to-end channel to be approximated by $h(t) \approx \sqrt{P_2/P_1} \exp[j\theta_1(t)] \cdot h_2(t)$.
- **Resultant ACF.** The normalized ACF can be calculated as [10]:

$$R(\Delta t) \approx \mathbb{E} \{ \exp[j\theta_1(t + \Delta t)] \exp[-j\theta_1(t)] h_2(t + \Delta t) h_2^*(t) \} \quad (33a)$$

$$= J_0 \left(2\pi \hat{f}_{t,1} \Delta t \right) \left[1 - J_0^2 \left(2\pi \hat{f}_{t,1} \Delta t \right) \right] \quad (33b)$$

$$\times {}_2F_1 \left(\frac{3}{2}, \frac{3}{2}, 2, J_0^2 \left(2\pi \hat{f}_{t,1} \Delta t \right) \right)$$

$$J_0 \left(2\pi \hat{f}_{r,1} \Delta t \right) \left[1 - J_0^2 \left(2\pi \hat{f}_{r,1} \Delta t \right) \right]$$

$$\times {}_2F_1 \left(\frac{3}{2}, \frac{3}{2}, 2, J_0^2 \left(2\pi \hat{f}_{r,1} \Delta t \right) \right)$$

$$\times J_0 \left(2\pi \hat{f}_{t,2} \Delta t \right) \cdot J_0 \left(2\pi \hat{f}_{r,2} \Delta t \right) .$$

PART 5

TRANSPARENT PHY LAYER

– Preliminary Note –

- Analysing the PHY layer performance of a wireless system is vital in understanding, optimising and synthesising system parameters.
- There are several hundred highly complex contributions on transparent PHY layer analysis and design available today, which requires us to concentrate on a very few of them.
- For this reason, we proceed with the following topics:
 1. discussion on optimum relay function;
 2. performance analysis of canonical topologies;
 3. space-time trellis transceiver design.

5.1 Optimal Relay Function

– Optimal Relay Function [1/2] –

- [71] and [72] questioned the optimality of transparent and regenerative relaying functions.
- They have derived different optimum functions for different underlying assumptions;
e.g. assuming BPSK modulation and a memoryless relay channel, the SNR-optimum $f(r)$ is:

$$f(x + n_1) = f(r) = \sqrt{\frac{P_r}{E \{ \tanh^2(\sqrt{P_s} r) \}}} \cdot \tanh(\sqrt{P_s} r), \quad (31)$$

where P_s and P_r are the source and relay powers, respectively.

- These results are a starter only, as they do not include the wireless fading and shadowing channel.



Figure 32: Finding the optimum relaying function $f(r)$.

– Optimal Relay Function [2/2] –

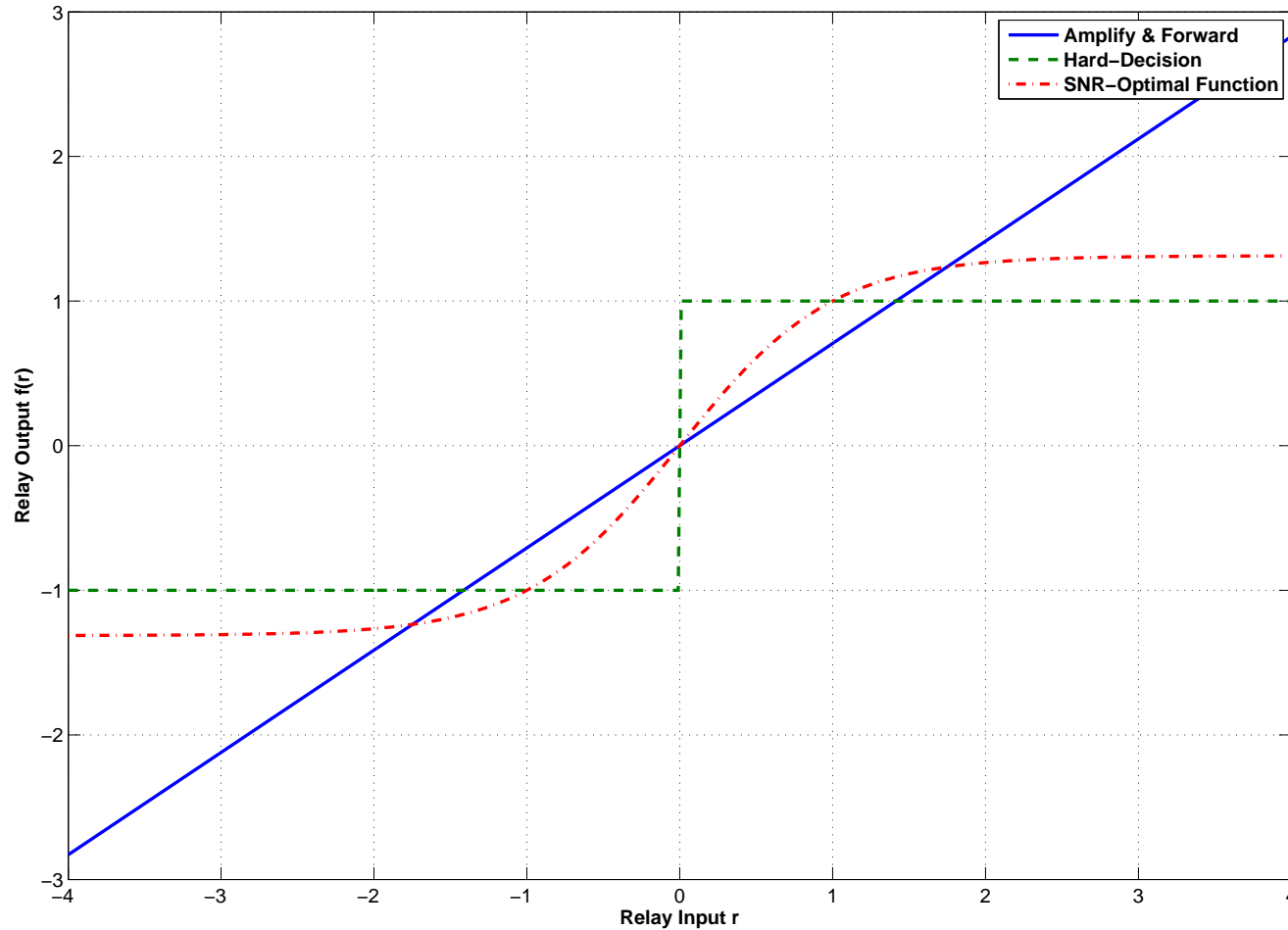
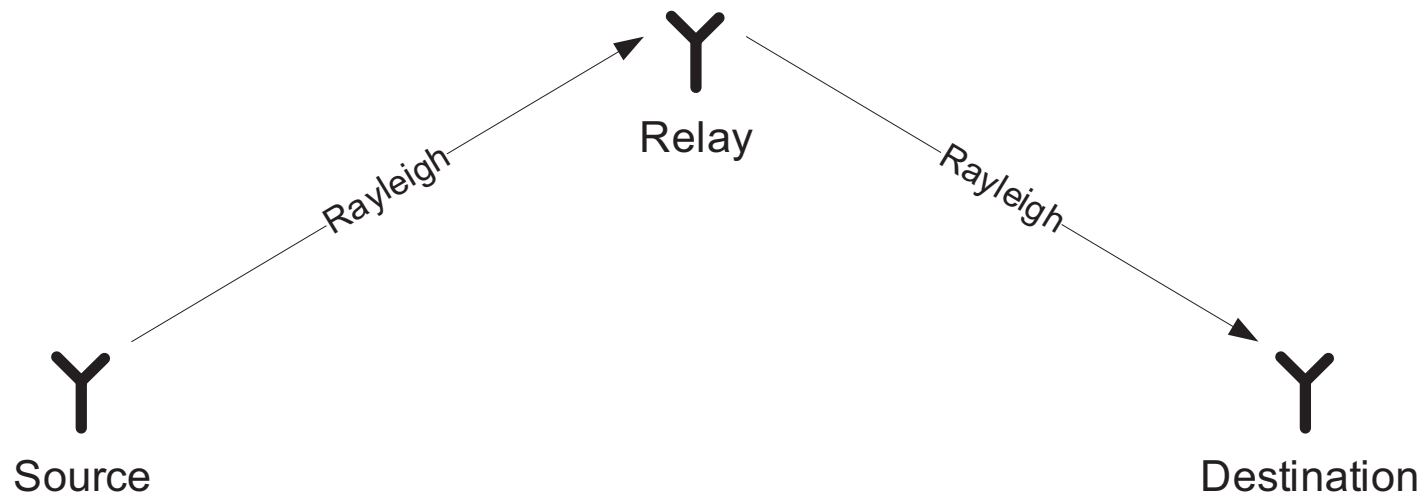


Figure 33: Finding the optimum SNR-maximising relaying function $f(r)$.

5.2 Performance Analysis

– Performance: Topology I [1/3] –

- We will follow [46] and assume the following:
 - 2-hop relay;
 - single relay;
 - fixed gain relay
 - Rayleigh fading channels;
 - no source-destination link;
- Derived results for MGF are in closed-form; however, most error rates remain in integral form.



– Performance: Topology I [2/3] –

- According to [46], the end-to-end SNR at the receiver with fixed gain A and partial CSI at the relay can be written as

$$\gamma = \frac{\gamma_1 \gamma_2}{C + \gamma_2}, \quad (32)$$

where $\gamma_i = P_i h_i^2 / N$, P_i is the transmission power, h_i is the Rayleigh fading channel, N the noise power, $C = \bar{\gamma}_1 [e^{1/\bar{\gamma}_1} E_1(1/\bar{\gamma}_1)]^{-1}$, $E_1(x)$ is the exponential integral function and $\bar{\gamma} = P_i E\{h_i^2\} / N$.

- This facilitates the MGF to be calculated, from which the performance of many coherent and differential modulation schemes can be derived in closed form:

$$M(s) = \frac{1}{\bar{\gamma}_1 s + 1} + \frac{C \bar{\gamma}_1 s e^{C/\bar{\gamma}_2 (\bar{\gamma}_1 s + 1)}}{\bar{\gamma}_2 (\bar{\gamma}_1 s + 1)^2} E_1 \left(\frac{C}{\bar{\gamma}_2 (\bar{\gamma}_1 s + 1)^2} \right). \quad (33)$$

- For instance, the BER of binary DPSK is

$$P_b(E) = \frac{1}{2} M(1). \quad (34)$$

– Performance: Topology I [3/3] –

- To derive (33), one would typically go via the outage probability, i.e.

$$P_{out} = P[\gamma < \gamma_{th}] = \int_0^{\infty} P\left[\frac{\gamma_1 \gamma_2}{\gamma_2 + C} < \gamma_{th} | \gamma_2\right] p_{\gamma_2}(\gamma_2) d\gamma_2 \quad (35)$$

$$= \int_0^{\infty} \frac{1}{\bar{\gamma}_2} \left[1 - e^{-(\gamma_{th}/\bar{\gamma}_1)(1+C/\gamma_2)}\right] e^{-\gamma_2/\bar{\gamma}_2} d\gamma_2 \quad (36)$$

$$= 1 - 2\sqrt{\frac{C\gamma_{th}}{\bar{\gamma}_1\bar{\gamma}_2}} e^{-\gamma_{th}/\bar{\gamma}_1} K_1\left(2\sqrt{\frac{C\gamma_{th}}{\bar{\gamma}_1\bar{\gamma}_2}}\right). \quad (37)$$

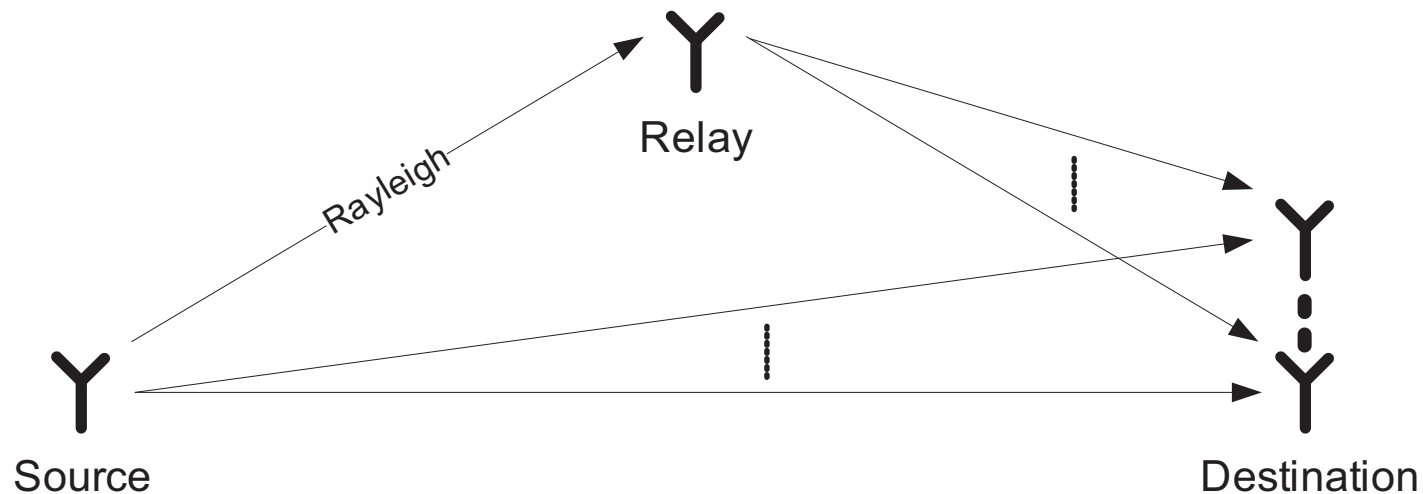
- By taking the derivative w.r.t. γ_{th} and replacing γ_{th} by γ , we obtain the pdf of γ as

$$p_{\gamma}(\gamma) = \frac{2e^{-\gamma/\bar{\gamma}_1}}{\bar{\gamma}_1} \left[\sqrt{\frac{C\gamma}{\bar{\gamma}_1\bar{\gamma}_2}} K_1\left(2\sqrt{\frac{C\gamma}{\bar{\gamma}_1\bar{\gamma}_2}}\right) + \frac{C}{\bar{\gamma}_2} K_0\left(2\sqrt{\frac{C\gamma}{\bar{\gamma}_1\bar{\gamma}_2}}\right) \right]. \quad (38)$$

- The MGF is finally found by evaluating $M(s) = \int_0^{\infty} p_{\gamma}(\gamma) e^{-s\gamma} d\gamma$.

– Performance: Topology II [1/3] –

- We will follow [73] and assume the following:
 - 2-hop relay with single relay;
 - fixed & variable relaying gains;
 - Rayleigh fading channels throughout;
 - $N > 1$ receiver antennas at destination;
 - M-PSK SER with MRC at destination.
- Closed-form results are asymptotic and only hold for high SNRs.



– Performance: Topology II [2/3] –

- Assuming $P_1 = P_2$ and **constant amplification** using (25), we get for the M-PSK

$$\begin{aligned}
 P_s(E) &= \frac{1}{\pi} \int_0^{\pi(M-1)/M} \frac{(-\xi)^{N-1} e^{\xi} \Gamma(0, \xi) - \sum_{j=1}^{N-1} (j-1)! (-\xi)^{N-1-j}}{\Gamma(N) (1 + 1/\xi)^N 1/\xi} d\theta \\
 &\leq \frac{M-1}{M} \frac{\Gamma(N-1)}{\Gamma(N)} \left(\frac{P_1}{2N} \right)^{-(N+1)}, \tag{39}
 \end{aligned}$$

where $\Gamma(x)$ is the Gamma function, $\Gamma(\cdot, \cdot)$ is the upper incomplete Gamma function, and $\xi = \sin^2 \theta / (\sin^2(\pi/M) P_1 / N)$. Diversity order is hence 'only' $N + 1$.

- Assuming $P_1 = P_2$ and **variable amplification** using (26), we get for the M-PSK

$$\begin{aligned}
 P_s(E) &= \frac{1}{\pi} \int_0^{\pi(M-1)/M} \left(1 + \frac{\sin^2(\pi/M) P_1}{\sin^2 \theta N} \right)^{-2N} d\theta \\
 &\leq \frac{M-1}{M} \left(\frac{P_1}{2N} \right)^{-2N}, \tag{40}
 \end{aligned}$$

where above integral is actually solvable in closed form. Full diversity order of $2N$ is achieved.

– Performance: Topology II [3/3] –

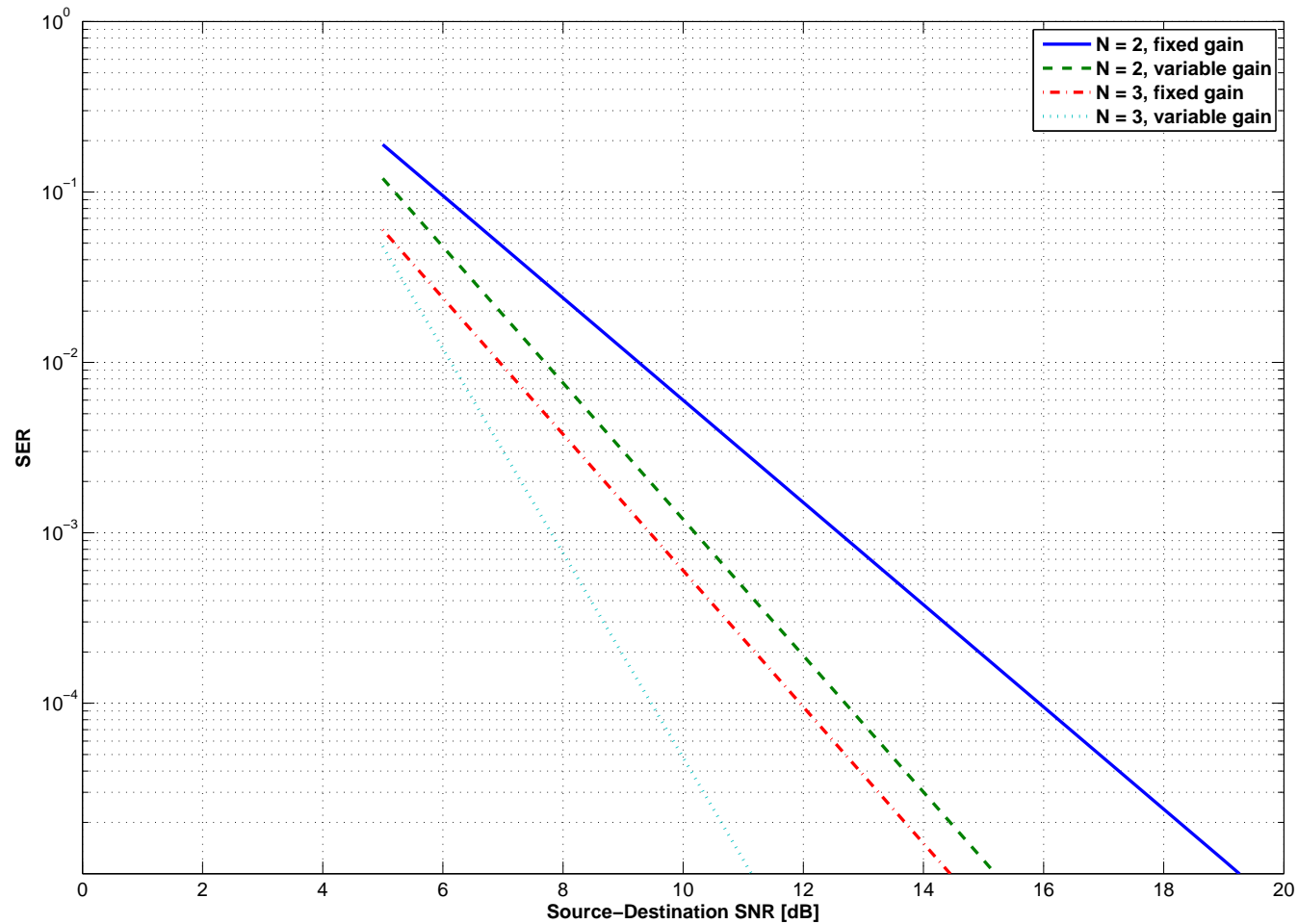
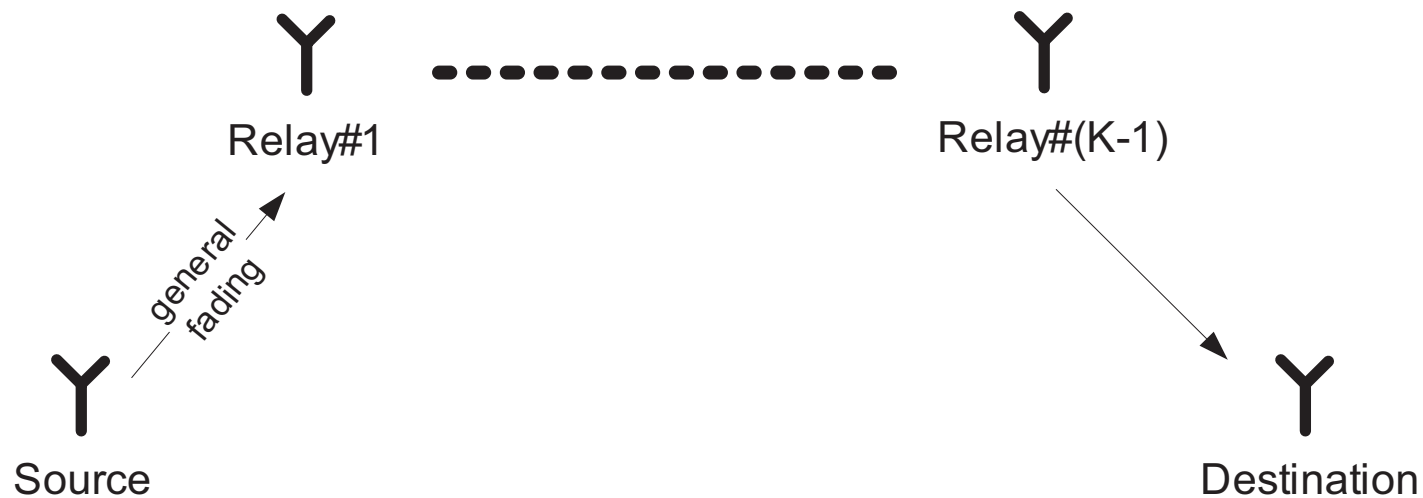


Figure 34: Upper bound to the SER of 4-PSK for different N and relay strategies.

– Performance: Topology IV [1/3] –

- We will follow [75] and assume the following:
 - K-hop relay;
 - fixed relaying gains;
 - partial CSI is available;
 - Rice & Nakagami fading channels;
- Derivation of optimum fixed relaying gains; derivation of fairly good upper bounds on the end-to-end SNR.



– Performance: Topology IV [2/3] –

- According to [75], the end-to-end SNR with MRC at the destination using a fixed gain,

$A_k = \sqrt{1/(C_k N)}$ can be written as

$$\frac{1}{\gamma} = \frac{1}{\gamma_1} + \frac{C_1}{\gamma_1 \gamma_2} + \dots + \frac{C_1 \dots C_{K-1}}{\gamma_1 \dots \gamma_K} = \frac{1}{K} \mathcal{H}, \quad (44)$$

where \mathcal{H} is the harmonic mean, i.e. $\mathcal{H} = \left[1/K \sum_{k=0}^K (\prod_{j=1}^k \gamma_j / C_{j-1})^{-1} \right]^{-1}$.

- Above SNR is intractable; however, using the fact that the harmonic mean can be upper bounded by the geometric mean, i.e. $\mathcal{H} \leq \mathcal{G} = \sqrt[K]{\prod_{k=1}^K (\prod_{j=1}^k \gamma_j / C_{j-1})}$, allowing γ to be upper bounded as

$$\gamma \leq \gamma_U = \mathcal{Z} \cdot \left[\prod_{k=1}^K \gamma_k^{(K+1-k)/K} \right] \quad (45)$$

where $\mathcal{Z} = \left[\frac{1}{N} \prod_{k=1}^K C_k^{-(K-k)/K} \right]$.

– Performance: Topology IV [3/3] –

- The optimum gains A_k can now be derived for Nakagami- m channels as:

$$A_k = \sqrt{\frac{e^{\lambda_k} \lambda_k^{m_k} \Gamma(1 - m_k, \lambda_k)}{N_k}}, \quad (46)$$

where $\lambda_k = m_k / \bar{\gamma}_k$.

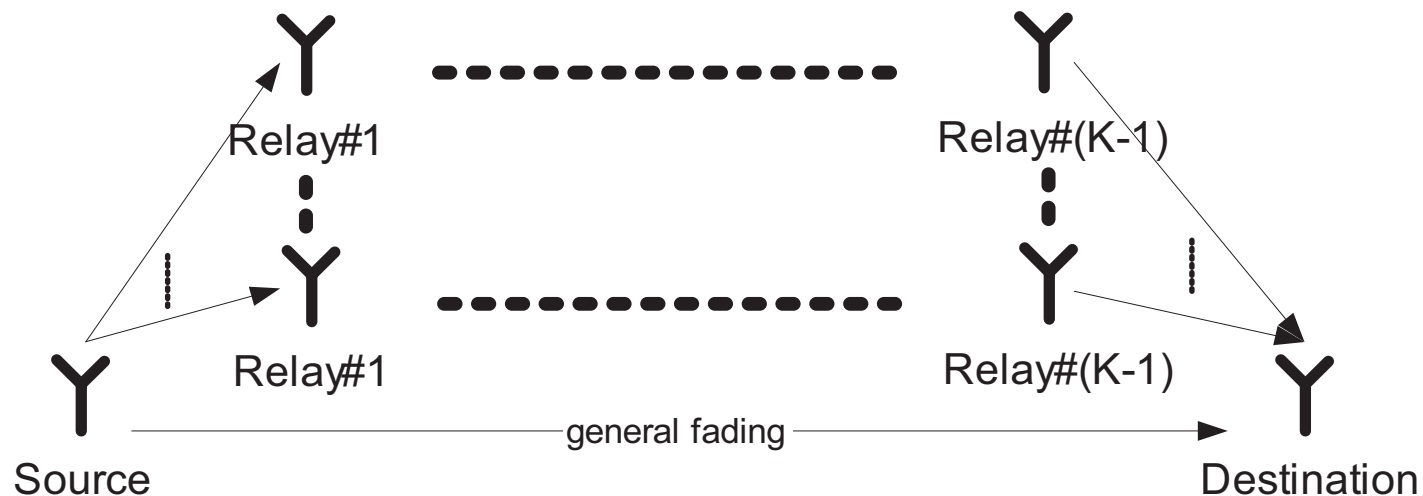
- This allows the n -th statistical moment to be computed as:

$$E\{\gamma_U^n\} = \mathcal{Z}^n \prod_{k=1}^K \left[\left(\frac{\bar{\gamma}_k}{m_k} \right)^{\frac{n(K-k+1)/K}{K}} \frac{\Gamma\left(m_k + \frac{n(K-k+1)/K}{K}\right)}{\Gamma(m_k)} \right]. \quad (47)$$

- Using these moments, error rates and outages can be calculated either in closed form or approximated by a converging series of moments.

– Performance: Topology V [1/2] –

- We will follow [76] and assume the following:
 - general multi-stage, multi-branch relay topology with variable relaying gains;
 - derivations are applicable to any fading channel;
 - MRC combining at destination.
- Noise in relays has been neglected to facilitate closed-forms. Asymptotically tight SERs are derived using a McLaurin expansion of the channel's pdf around zero.



– Performance: Topology V [2/2] –

- According to [76], the end-to-end SNR with MRC at the destination using a variable gain and neglecting noise can be written as

$$\gamma \approx \frac{\gamma_1 \gamma_2}{\gamma_1 + \gamma_2} + \gamma_0. \quad (48)$$

- The SER can be calculated as $P_s(E) = \int_0^\infty Q(k\gamma) pdf_\gamma(\gamma) d\gamma$, where k depends on the modulation scheme, $Q(x)$ is the Marcum Q-function and $pdf_\gamma(\gamma)$ is the channel's pdf.
- [76] has observed that $Q(k\gamma)$ drops rapidly to zero for increasing γ , hence giving little contributions to the integral. The main contribution comes from the region close to zero, in which a McLaurin series expansion is applicable, i.e. $p_\gamma(\gamma) = a\gamma^t + o(\gamma)$, leading to

$$P_s(E) \rightarrow \frac{2^t a \Gamma(t + 3/2)}{\sqrt{\pi}(t + 1)} (k\bar{\gamma})^{-(t+1)}. \quad (49)$$

- a depends on the channel; for instance, for a Rician- K channel, the SER can be bounded as

$$P_s(E) \rightarrow \frac{3(K + 1)^2}{4k^2} \left(\frac{1}{\bar{\gamma}_1} + \frac{1}{\bar{\gamma}_2} \right) \frac{1}{\bar{\gamma}_0}. \quad (50)$$

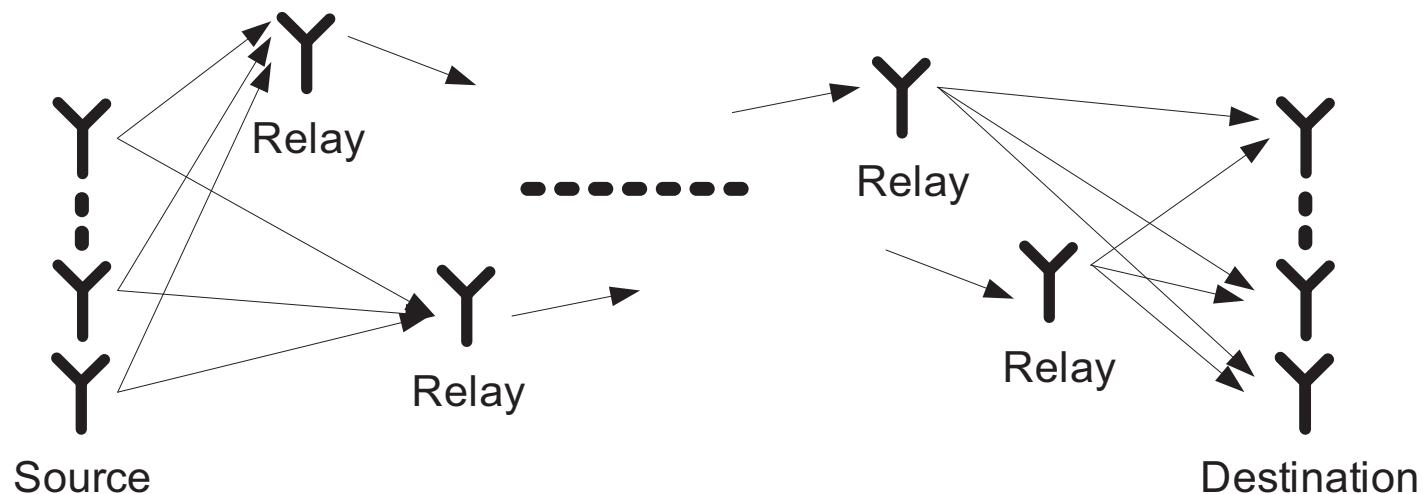
5.3 Space-Time Transceiver Design

– Transceiver Design: General –

- There is no time to discuss the numerous contributions which have recently emerged dealing with the transceiver design of transparent relaying schemes; however, some are listed below.
- [77] proposes a noise reduction scheme at the transparent relay, which is only applicable to binary modulations.
- [78] proposes a unitary precoder for the cooperative system achieving full diversity. For 4-QAM, they arrive at a closed-form optimum precoder, greatly improving performance.
- [79] proposes a lattice-coded cooperation scheme which generalises prior non-orthogonal amplify and forward protocols, while keeping the decoding complexity relatively low.
- [80] proposes novel STBCs based on the nonvanishing determinant criterion and is shown to achieve the optimal diversitymultiplexing trade-off of the channel.
- [81] propose equalization methods for cooperative STBC diversity schemes over frequency-selective fading channels.

– Transceiver Design: STTC [1/4] –

- [82] and later [83] have investigated the code design requirements for transparent space-time trellis codes (STTCs).
- By using prior analysis from [23] and [84], we wanted to derive design criteria for STTCs over below example topology.
- We assumed n transmit and m receive antennas and arbitrary channel fading statistics.



– Transceiver Design: STTC [2/4] –

- **Rank & Determinant Criterion** ($m \times n \leq 3$): The average error probability of that sequence \mathbf{e} is received if \mathbf{c} had been sent is:

$$\begin{aligned} \langle P(\mathbf{c} \rightarrow e) \rangle &\leq \mathbb{E}_{(\beta_{1,1}, \dots, \beta_{n,m})} \{ P(\mathbf{c} \rightarrow e | (\beta_{1,1}, \dots, \beta_{n,m})) \} \\ &= \int_{\beta \in \mathcal{R}^{n \times m}} d\beta \cdot p(\beta) \prod_{j=1}^m \prod_{i=1}^n e^{-\frac{1}{4} \frac{E_s}{N_0} \cdot \lambda_i |\beta_{i,j}|^2}, \end{aligned} \quad (51)$$

where E_s the symbol energy and N_0 the noise spectral density; m, n the number of receive and transmit antennas, respectively; and λ_i the i^{th} eigenvalue of the distance matrix

$\mathbf{A}(\mathbf{c}, e) = \mathbf{B}(\mathbf{c}, e)\mathbf{B}^H(\mathbf{c}, e)$, where \mathbf{B}^H denotes the Hermitian of \mathbf{B} . The difference matrix \mathbf{B} for codewords of length l is given as [23]:

$$\mathbf{B}(\mathbf{c}, e) = \begin{pmatrix} e_1^1 - c_1^1 & \cdots & e_l^1 - c_l^1 \\ \vdots & \ddots & \vdots \\ e_1^n - c_1^n & \cdots & e_l^n - c_l^n \end{pmatrix} \quad (52)$$

– Transceiver Design: STTC [3/4] –

- Furthermore, in (51), $p(\beta)$ is the probability distribution of the $n \times m$ dimensional random vector $\beta = (\beta_{1,1}, \dots, \beta_{n,m})$. For arbitrary channel realisations, this can be upper-bounded by

$$\langle P(\mathbf{c} \rightarrow e) \rangle \leq \prod_{j=1}^m \prod_{i=1}^n \left[\int_{\beta_{i,j}} p(\beta_{i,j}) \cdot e^{-\frac{1}{4} \frac{E_s}{N_0} \cdot \lambda_i |\beta_{i,j}|^2} d\beta_{i,j} \right].$$

- Defining $g(\beta_{i,j}, \lambda_i) = e^{-\frac{1}{4} \frac{E_s}{N_0} \cdot \lambda_i |\beta_{i,j}|^2}$, $x = \beta_{i,j}$ and using Schwarz' integral inequality, it can be shown that

$$\begin{aligned} \langle P(\mathbf{c} \rightarrow e) \rangle &\leq \prod_{j=1}^m \prod_{i=1}^n \left[\left(\frac{1}{\frac{2}{\pi} \frac{E_s}{N_0}} \right)^{\frac{1}{4}} \cdot \left(\frac{1}{\lambda_i} \right)^{\frac{1}{4}} \right] \\ &= \left(\prod_{i=1}^n \lambda_i \right)^{-\frac{m}{4}} \cdot \left(\frac{2}{\pi} \frac{E_s}{N_0} \right)^{-\frac{mr}{4}}. \end{aligned} \tag{53}$$

- Therefore, the minimum determinant of all codeword difference matrices needs to be maximised. The determinant criterion hence constitutes a sufficient upper bound for channels with any pdf.

– Transceiver Design: STTC [4/4] –

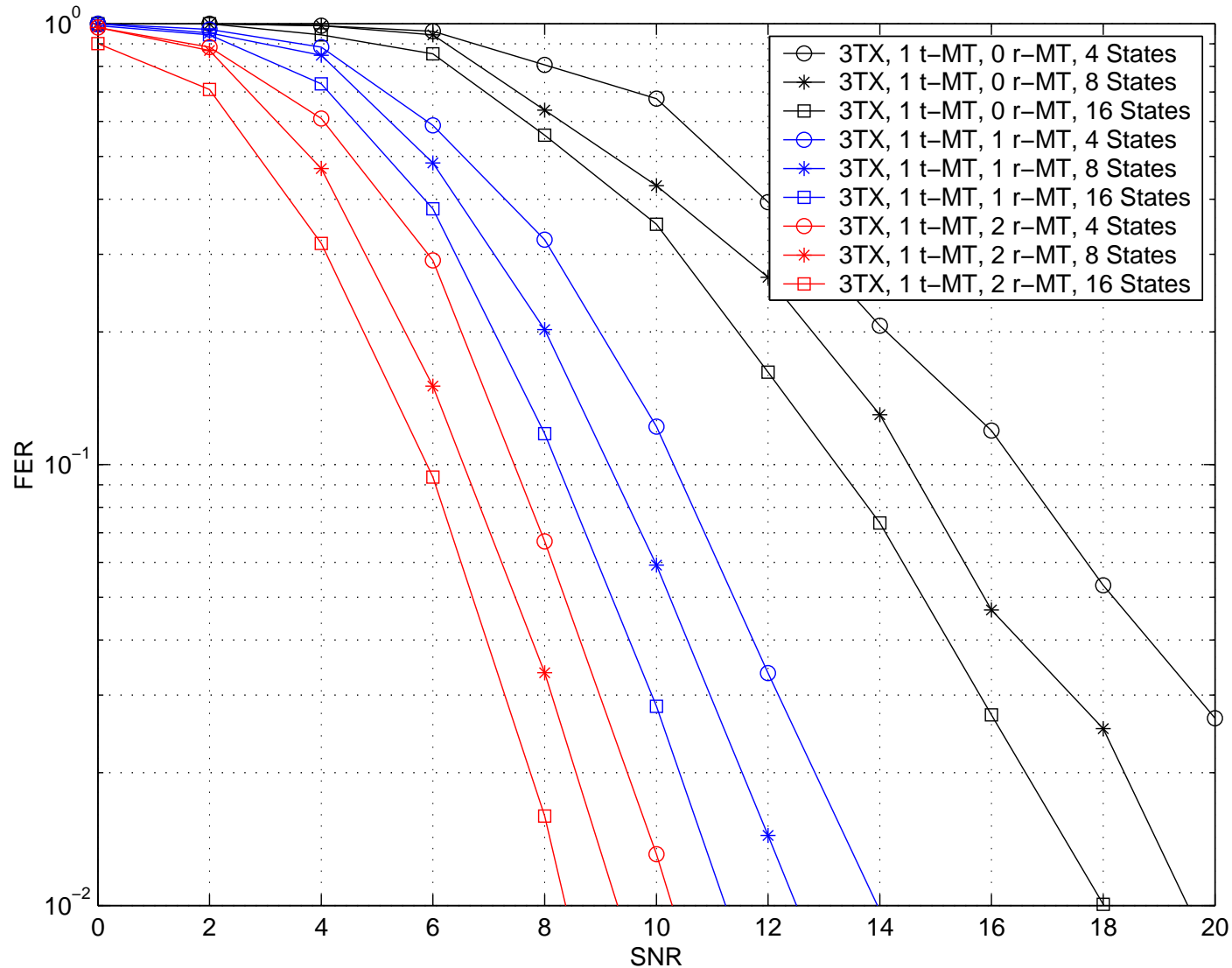


Figure 36: FER versus SNR for STTCs over transparent relays: 3 TX, 1 t-MT, a varying number of r-MTs and STTC states.

PART 6
REGENERATIVE PHY LAYER

– Preliminary Note –

- Analysing the PHY layer performance of a wireless system is vital in understanding, optimising and synthesising system parameters.
- There are several hundred highly complex contributions on regenerative PHY layer analysis and design available today, which requires us to concentrate on a very few of them.
- For this reason, we proceed with the following topics:
 1. Distributed Space-Time Block Codes;
 2. Estimate and Forward Protocols;
 3. Decode and Forward Protocols;
 4. Asynchronous Protocols.

6.1 Distributed STBCs

– System Model –

- **Transmitter:**

- number of distributed transmit antennas: t
- transmitted space-time block codeword: $\mathbf{x} \in \mathbb{C}^{t \times 1}$
- transmit power constraint: $\text{tr}\left(\mathbb{E}\{\mathbf{x}\mathbf{x}^H\}\right) \leq S$

- **Channel:**

- channel from transmitter $i \in (1, t)$ to receiver $j \in (1, r)$: $h_{i,j}$
- fading realisations of $h_{i,j}$: frequency-flat & uncorrelated
- grouping of sub-channel gains $h_{i,j}$: \mathbf{H}

- **Receiver:**

- received signal: $\mathbf{y} = \mathbf{H}\mathbf{x} + \mathbf{n}$
- r –dimensional noise vector \mathbf{n} has variance N per entry

- **Cooperative Link:**

- assumed to be error-free (!)

– Exact STBC Error Probabilities [1/4] –

- Following [86], we will consider distributed cooperative STBCs of arbitrary rate R .
- Furthermore, the sub-channel realisation $h_{i,j}$ obey Nakagami fading with fading parameter f ; the sub-channels may have different gains, thereby reflecting a possibly distributed deployment.
- We define $u \triangleq t \cdot r$, $\gamma_i \triangleq \mathbb{E} \{h_i h_i^*\}$ and assume $\sum_{i=1}^u \gamma_i = u$.

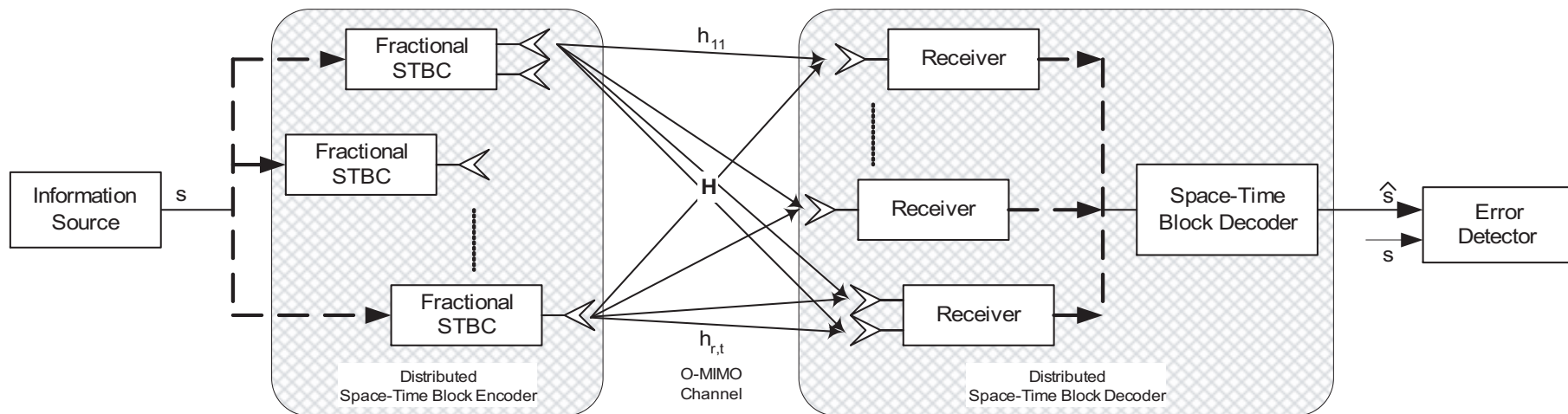


Figure 37: Distributed Space-Time Block Code transceiver system.

– Exact STBC Error Probabilities [2/4] –

Let's define

$$P_{\text{PSK}}(\alpha, u, M) \triangleq \frac{1}{(1 + \alpha)^u} \left[\frac{1}{2\sqrt{\pi}} \frac{\Gamma(u + 1/2)}{\Gamma(u + 1)} {}_2F_1 \left(u, 1/2; u + 1; (1 + \alpha)^{-1} \right) \right. \\ \left. + \frac{\sqrt{1 - g_{\text{PSK}}}}{\pi} F_1 \left(1/2, u, 1/2 - u; 3/2; \frac{1 - g_{\text{PSK}}}{1 + \alpha}, 1 - g_{\text{PSK}} \right) \right] \quad (54)$$

$$P_{\text{QAM}}(\alpha, u, M) \triangleq \frac{1}{(1 + \alpha)^u} \frac{2q}{\sqrt{\pi}} \frac{\Gamma(u + 1/2)}{\Gamma(u + 1)} {}_2F_1 \left(u, 1/2; u + 1; (1 + \alpha)^{-1} \right) \quad (55) \\ - \frac{1}{(1 + 2\alpha)^u} \frac{2q^2}{\pi(2u + 1)} F_1 \left(1, u, 1; u + 3/2; \frac{1 + \alpha}{1 + 2\alpha}, 1/2 \right)$$

where $\Gamma(x)$ is the complete Gamma function, ${}_2F_1(a, b; c; x)$ is the Gauss hypergeometric function with 2 parameters of type 1 and 1 parameter of type 2 [87] (§9.14.1)), and $F_1(a, b, b'; c; x, y)$ is the Appell hypergeometric function of two variables [87] (§9.180.1). Furthermore, α is a parameter, M is the modulation order, $g_{\text{PSK}} \triangleq \sin^2(\pi/M)$, $g_{\text{QAM}} \triangleq 3/2/(M - 1)$, $q \triangleq 1 - 1/\sqrt{M}$.

– Exact STBC Error Probabilities [3/4] –

- Based on the analysis of [88] & [86], the symbol error rate (SER) of M-QAM and M-PSK STBC systems operating over a Nakagami fading channel with different sub-channel gains $\gamma_{i \in (1,u)}$ and different fading factors $f_{i \in (1,u)}$ can be derived in closed form as

$$P_s(e) = \sum_{i=1}^u \sum_{j=1}^{f_i} K_{i,j} \cdot P_{\text{PSK/QAM}} \left(\frac{1}{R} \frac{\gamma_i}{f_i t} \frac{S}{N}, j, M \right) \quad (56)$$

where

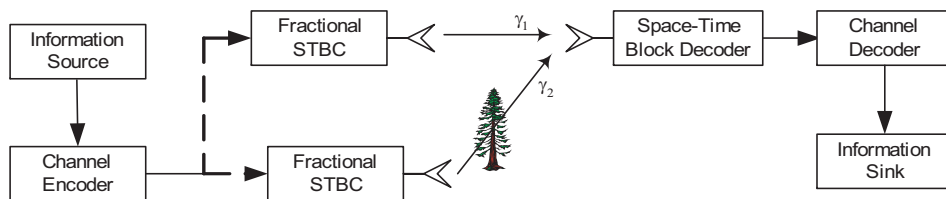
$$K_{i,j} = \frac{1}{(f_i - j)! \left(-\frac{1}{R} \frac{\gamma_i}{f_i t} \frac{S}{N} \right)^{f_i - j}} \frac{\partial^{f_i - j}}{\partial s^{f_i - j}} \left[\prod_{\substack{i'=1, \\ i' \neq i}}^u \frac{1}{\left(1 - \frac{1}{R} \frac{\gamma_{i'}}{f_{i'} t} \frac{S}{N} \cdot s \right)^{f_{i'}}} \right]_{s = \left(\frac{1}{R} \frac{\gamma_i}{f_i t} \frac{S}{N} \right)^{-1}}$$

- For memoryless fading channels, the bit error rate (BER) and frame error rate (FER) for frames of D symbols are respectively well approximated by

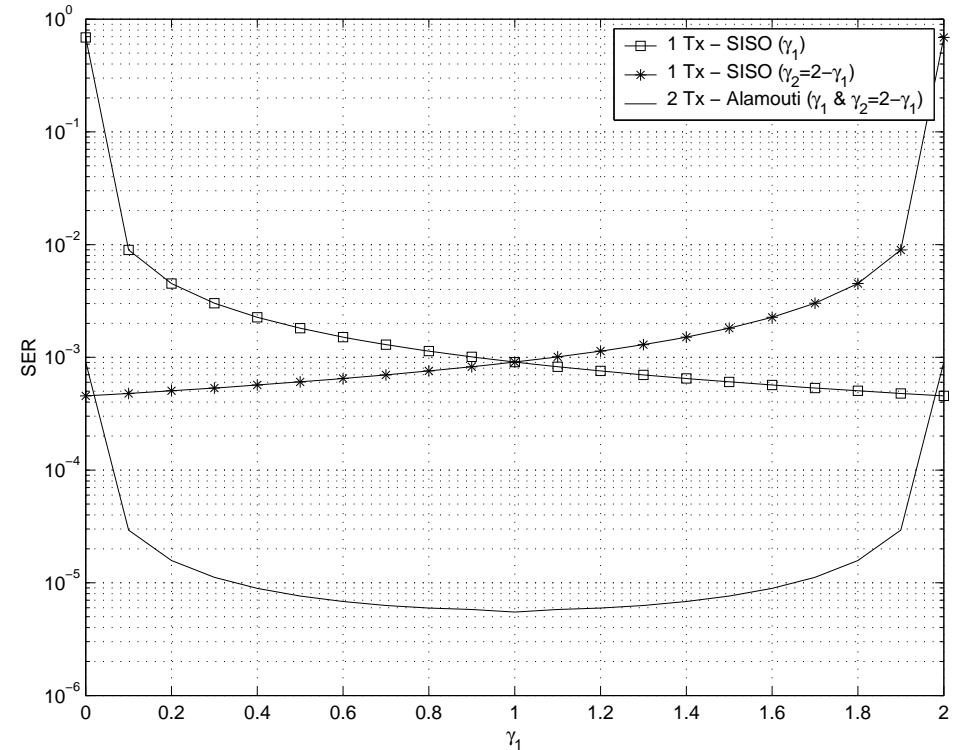
$$P_b(e) \approx \frac{P_s(e)}{\log_2(M)} \quad \text{and} \quad P_f(e) \approx 1 - (1 - P_s(e))^D \quad (57)$$

– Exact STBC Error Probabilities [4/4] –

Error rate performance of distributed STBC scheme exhibits a high stability:



(a) Distributed Alamouti scheme with unequal sub-channel gains due to different pathloss & shadowing.



(b) SER versus the normalised power γ_1 in the first link for a distributed Alamouti system operating at 2 bits/s/Hz; SNR=30dB.

Figure 38: Topology and performance of distributed Alamouti scheme.

6.2 Estimate & Forward Protocols

– Considered Topology –

Following [86], the aim is to analyse the end-to-end error rate for the below general topology assuming the estimate & forward protocol:

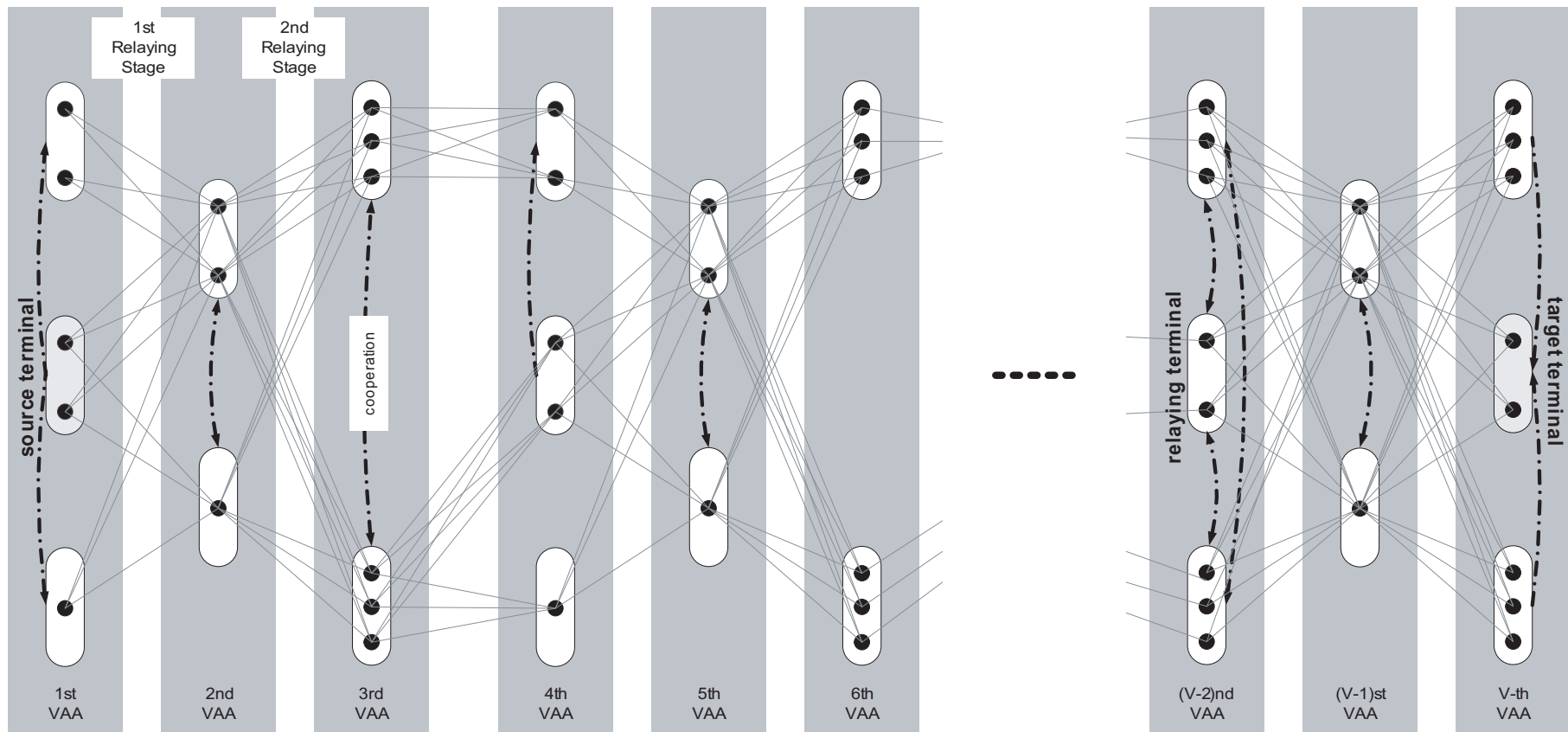


Figure 39: Distributed-MIMO multi-stage relaying topology.

– End-to-End Error Rate [1/4] –

- We assume first no cooperation and unequal-power Rayleigh fading channels.
- To obtain the exact end-to-end BER is not trivial, as an error occurring in one node may or may not be corrected by a parallel node.
- This creates dependencies between the error events at each stage in dependency of:
 - the modulation scheme used,
 - the prevailing channel statistics,
 - the average channel attenuations,
 - as well as the deployed STBC.
- The fairly complex interdependencies call for suitable simplifications, where we will weigh the strength of a channel with a given error probability against the strength of the other channels.
- Subsequent explanations relate to Figure 40.

– End-to-End Error Rate [2/4] –

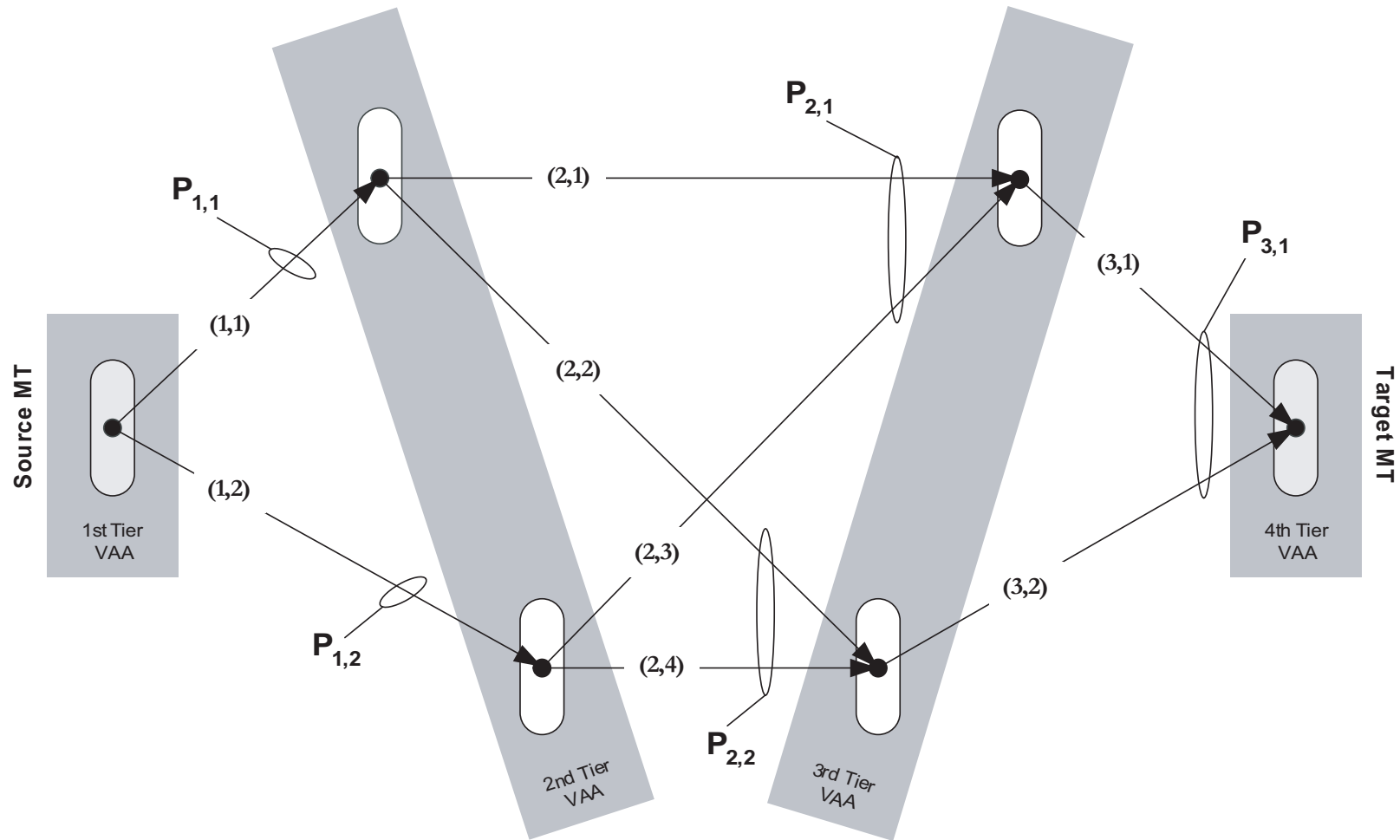


Figure 40: 3-stage distributed O-MIMO communication system without cooperation.

– End-to-End Error Rate [3/4] –

- We assume that the system operates at low error rates which causes only one error event at a time in the entire network.
- Let us assume that an error occurs in link (1,1); however, (1,2) is error free. Then the probability that the error propagates further is related to the strengths of channels (2,1) and (2,3).
- It is intuitive and hence conjectured here that the probability that such error propagates is proportional to the strength of the STBC branch it departs from, here (2,1) for one of two MISO channels, and (2,2) for the other one.
- Therefore, the probability that an error which occurred in link (1,1) with probability $P_{1,1}$ propagates through the O-MISO channel spanned by (2,1) and (2,3) is approximated as $P_{1,1} \cdot \gamma_{2,1} / (\gamma_{2,1} + \gamma_{2,3})$, where the strength of the erroneous channel (2,1) is normalised by the total strength of both sub-channels.
- To capture the probability that such an error propagates until the t-MT, all possible paths in the network have to be found and the original probability of error weighed with the ratios between the respective path gains.

– End-to-End Error Rate [4/4] –

- Taking the previously said into account and assuming that at high SNRs only one such error will occur at any link, the end-to-end BER for the network depicted in Figure 40 can be expressed as

$$\begin{aligned}
 P_{b,e2e}(e) \approx & \left[P_{1,1}(e) \left(\frac{\gamma_{2,1}}{\gamma_{2,1} + \gamma_{2,3}} \frac{\gamma_{3,1}}{\gamma_{3,1} + \gamma_{3,2}} + \frac{\gamma_{2,2}}{\gamma_{2,2} + \gamma_{2,4}} \frac{\gamma_{3,2}}{\gamma_{3,1} + \gamma_{3,2}} \right) + \right. \\
 & \left. P_{1,2}(e) \left(\frac{\gamma_{2,4}}{\gamma_{2,2} + \gamma_{2,4}} \frac{\gamma_{3,2}}{\gamma_{3,1} + \gamma_{3,2}} + \frac{\gamma_{2,3}}{\gamma_{2,1} + \gamma_{2,3}} \frac{\gamma_{3,1}}{\gamma_{3,1} + \gamma_{3,2}} \right) \right] + \\
 & \left[P_{2,1}(e) \left(\frac{\gamma_{3,1}}{\gamma_{3,1} + \gamma_{3,2}} \right) + P_{2,2}(e) \left(\frac{\gamma_{3,2}}{\gamma_{3,1} + \gamma_{3,2}} \right) \right] + \left[P_{3,1}(e) \right]
 \end{aligned}$$

- This can be simplified to

$$\begin{aligned}
 P_{b,e2e}(e) \approx & \left[\xi_{1,1} P_{1,1}(e) + \xi_{1,2} P_{1,2}(e) \right] + \\
 & \left[\xi_{2,1} P_{2,1}(e) + \xi_{2,2} P_{2,2}(e) \right] + \left[\xi_{3,1} P_{3,1}(e) \right]
 \end{aligned}$$

where $\xi_{v,i}$ is the probability that an error occurring in link (v, i) will propagate to the t-MT.

– Clustering –

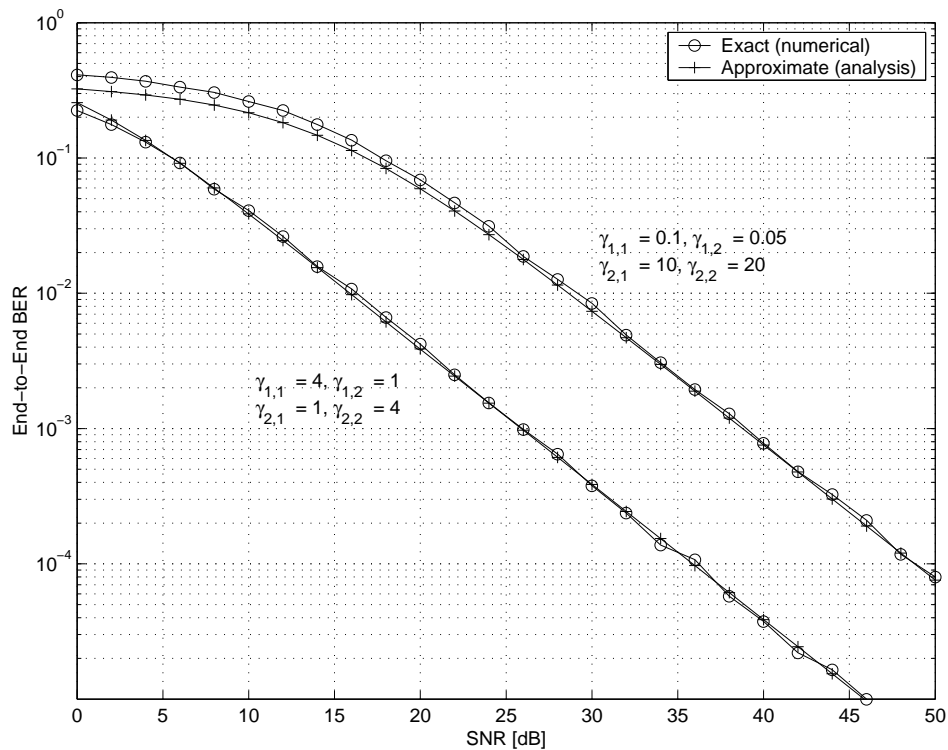
- This is easily generalised to networks of any size and any form of partial cooperation.
- To this end, remember that there are $Q_{v \in (1, K)}$ cooperative clusters at the v^{th} stage, each of which will yield an error probability of $P_{v \in (1, K), i \in (1, Q_v)}$.
- The end-to-end BER is hence approximated as

$$P_{b,e2e}(e) \approx \sum_{v=1}^K \sum_{i=1}^{Q_v} \xi_{v,i} P_{v,i}(e) \quad (58)$$

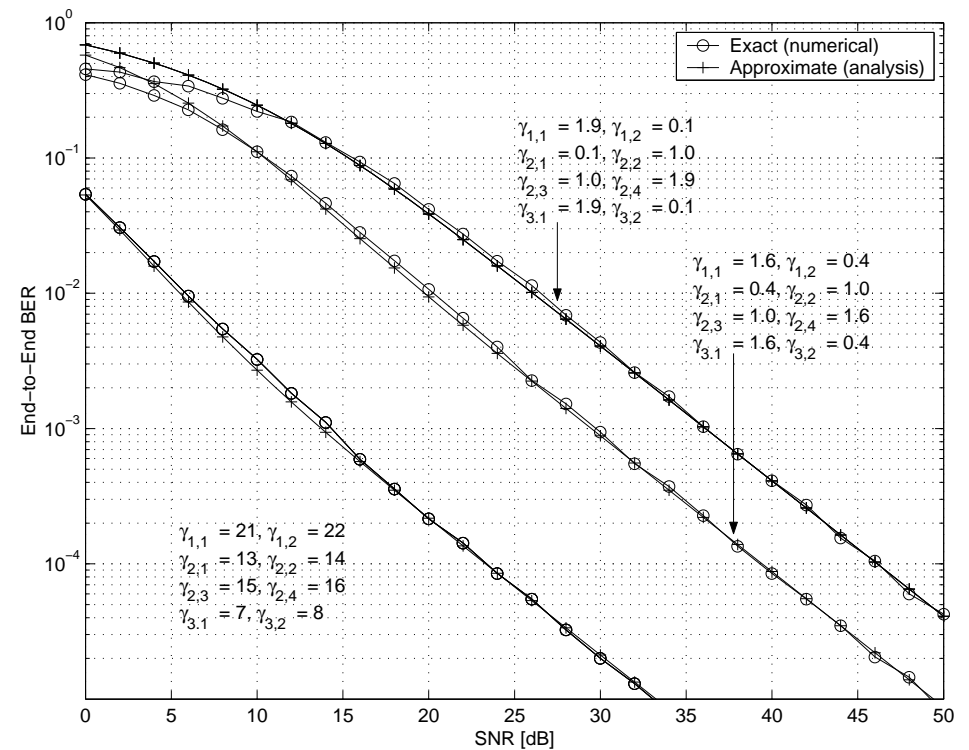
where the probabilities $\xi_{v,i}$ are easily found from the specific network topology.

- The BERs $P_{v,i}(e)$ can be found from the previously derived SERs with an appropriate number of transmit and receive antennas per cluster, as well as prevailing channel conditions.
- The proposed approximation holds with high precision, as demonstrated by means of the following performance graphs.

– Performance –



(a) Numerically obtained and derived end-to-end BER versus the SNR in the first link for a two-stage network without cooperation.



(b) Numerically obtained and derived end-to-end BER versus the SNR in the first link for a three-stage network without cooperation.

Figure 41: End-to-end BER of various 2- & 3-stage relaying topologies.

– Throughput Maximisation –

- In [86], the end-to-end throughput-maximising optimised fractional power and optimised fractional frame duration have been obtained as

$$\alpha'_v = \frac{\prod_{w=1, w \neq v}^K R_w \cdot \log_2(M_w)}{\sum_{k=1}^K \prod_{w=1, w \neq k}^K R_w \cdot \log_2(M_w)} \quad (59)$$

$$\beta'_v = \left[\sum_{w=1}^K \alpha'_w \sqrt{\frac{\sum_{i=1}^{Q_v} \sum_{j \in i} \xi_{v,i}^{-1} K_{v,i,j}^{-1} A_v^{-1} B_{v,i,j}}{\sum_{i=1}^{Q_w} \sum_{j \in i} \xi_{w,i}^{-1} K_{w,i,j}^{-1} A_w^{-1} B_{w,i,j}}} \right]^{-1} \quad (60)$$

where the notation $j \in i$ represents the j^{th} sub-channel belonging to the i^{th} cluster, Furthermore, $K_{v,i,j} = \prod_{j' \in i, j' \neq j} \frac{\gamma_{v,j}}{\gamma_{v,j} - \gamma_{v,j'}}$ and

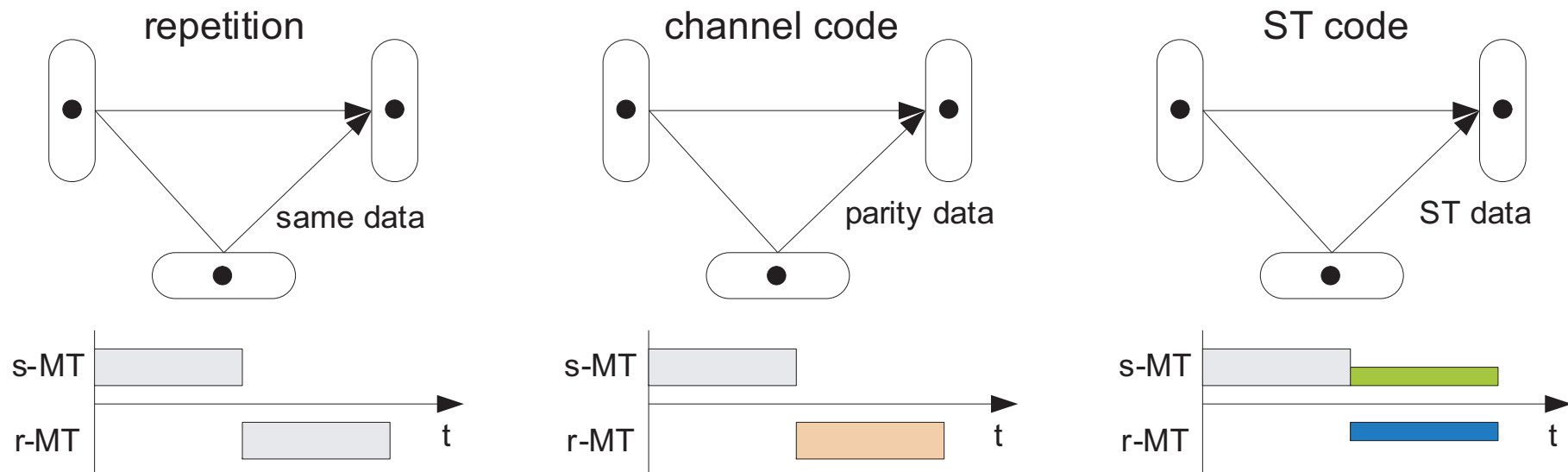
$$A_v = \begin{cases} \frac{M_v - 1}{M_v \log_2(M_v)} & \text{for M-PSK} \\ \frac{2q_v}{\log_2(M_v)} & \text{for M-QAM} \end{cases} \quad B_{v,i,j} = \begin{cases} \frac{g_{\text{PSK},v}}{R_v} \frac{\gamma_{v,j \in i}}{t_v} \frac{S}{N} & \text{for M-PSK} \\ \frac{g_{\text{QAM},v}}{R_v} \frac{\gamma_{v,j \in i}}{t_v} \frac{S}{N} & \text{for M-QAM} \end{cases}$$

6.3 Decode & Forward Protocols

– Decode & Forward Methods –

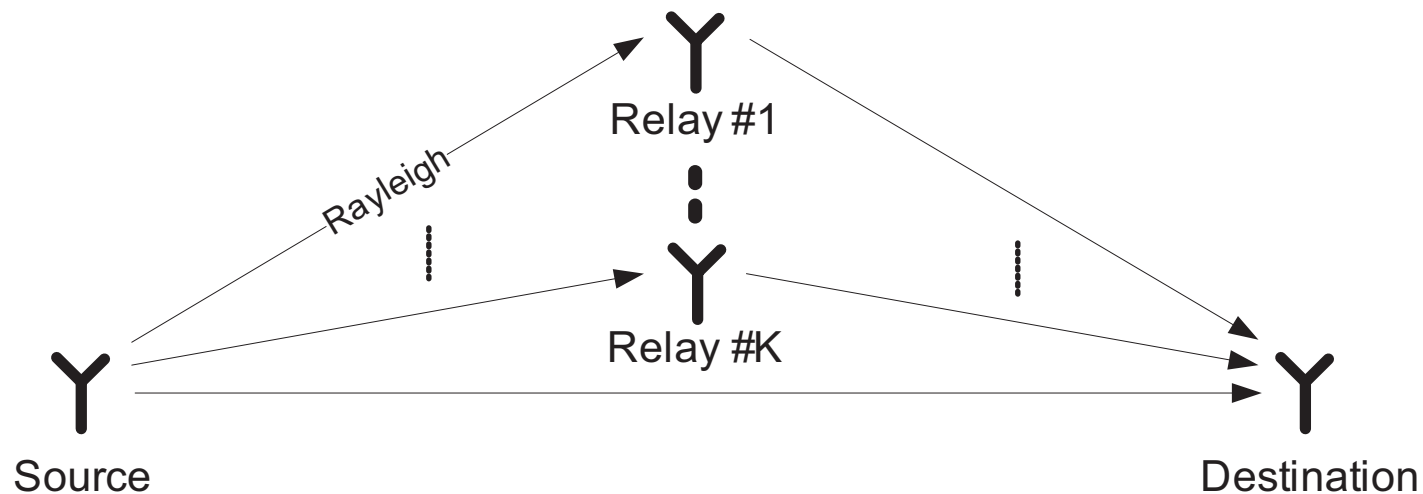
- The most tractable DF methods are:
 - repetition based (repeat codeword during relaying)
 - channel code based (relay parity information)
 - space-time code based (construct ST codeword or multiplex)

Supportive Case:



– Channel Coded: Topology –

- We will follow [89] and assume the following:
 - 2-hop relay;
 - K relay stations;
 - variable relaying gains;
 - Rayleigh fading channels throughout;
 - BPSK, channel coder, MRC at destination.
- Optimised power allocation at source and relays; pertinent to realistic systems.



– Channel Coded: System Model –

- Source first broadcasts $s(t)$ to both the destination and relays at time t .
- Upon receiving signals from the source, each relay decodes the received signal, re-encodes it and transmits it as $x_{r,k}(t)$
- The power of source and relays are constrained, where
 - P is the overall power;
 - $\alpha_0 \cdot P$ is the power allocated to the source;
 - $\alpha_{r,k} \cdot P$ is the power allocated to the k –th relay;
 - $\alpha_0 + \sum_{k=1}^K \alpha_{r,k} = 1$.
- The respective fading channel powers are:
 - γ_0 is the average fading channel power between source and destination;
 - $\gamma_{1,k}$ is average fading channel power between source and k –th relay;
 - $\gamma_{2,k}$ is average fading channel power between k –th relay and source;

– Channel Coded: Approximate DF Model [1/4] –

- We define:
 - $SNR_{in,1,k}$ the input SNR at the decoder of the k –th relay;
 - $SNR_{out,1,k}$ the output SNR of the decoder of the k –th relay;
- Relationship between these SNRs for DF is $SNR_{out,1,k} = f(SNR_{in,1,k})$.
- For convolutional codes, the above relationship can be upper-bounded at high SNR by [90]:

$$SNR_{out,1,k} \leq SNR_{in,1,k} \cdot R \cdot d_{free}, \quad (61)$$

where R is the channel code rate and d_{free} its free distance.

- For other types of block and channel codes as well as tighter bounds, one can use the theory invoked in [91].

– Channel Coded: Approximate DF Model [2/4] –

- Soft-output at the decoder k at time-sample moment i for BPSK modulation can be modelled as

$$\tilde{s}_k(i) = s_k(i) (1 - \tilde{n}_k(i)), \quad (62)$$

where $s_k(i)$ is the exact transmitted symbol.

- Furthermore, $\tilde{n}_k(i)$ is an equivalent noise with mean $\mu_{\tilde{n},k}$ and variance $\sigma_{\tilde{n},k}^2$, which can be calculated as [92]

$$\mu_{\tilde{n},k} = \frac{1}{l} \sum_{i=1}^l |\tilde{s}_k(i) - s_k(i)|, \quad (63)$$

$$\sigma_{\tilde{n},k}^2 = \frac{1}{l} \sum_{i=1}^l (\tilde{s}_k(i) - s_k(i) - \mu_{\tilde{n},k})^2, \quad (64)$$

where l is the code sequence length.

– Channel Coded: Approximate DF Model [3/4] –

- The signals transmitted from the k –th relay is hence given as

$$x_{r,k}(i) = \beta_k \tilde{s}_k(i), \quad (65)$$

where β_k is a normalisation factor calculated from the transmit power constraint at the relay as

$$\beta_k^2 \left((1 - \mu_{\tilde{n},k})^2 + \sigma_{\tilde{n},k}^2 \right) \leq \alpha_{r,k} \cdot P. \quad (66)$$

- After some manipulations, one can calculate the end-to-end SNR at the destination [89]:

$$\gamma \leq \left(\gamma_0 + \sum_{k=1}^K \frac{\gamma_{1,k} \gamma_{2,k} \alpha_{r,k} R d_{free}}{\gamma_{2,k} \alpha_{r,k} + \gamma_{1,k} \alpha_{r,k} R d_{free} + N_0/P} \right) \frac{\alpha_0 \cdot P}{N_0}, \quad (67)$$

where N_0 is the noise power spectral density.

– Channel Coded: Approximate DF Model [4/4] –

- From this, we can finally calculate the optimum distributed power allocation coefficients for source and relays:

$$\alpha_0^{opt} = \frac{8\gamma_0^2 + Rd_{free} \sum_{k=1}^K \gamma_{1,k} \gamma_{2,k} \pm 8\gamma_0 \sqrt{\gamma_0^2 + \frac{1}{4}Rd_{free} \sum_{k=1}^K \gamma_{1,k} \gamma_{2,k}}}{8\gamma_0^2 + 2Rd_{free} \sum_{k=1}^K \gamma_{1,k} \gamma_{2,k} \pm 8\gamma_0 \sqrt{\gamma_0^2 + \frac{1}{4}Rd_{free} \sum_{k=1}^K \gamma_{1,k} \gamma_{2,k}}}$$

and

$$\alpha_{r,k}^{opt} = \frac{Rd_{free} \gamma_{1,k} \gamma_{2,k}}{8\gamma_0^2 + 2Rd_{free} \sum_{k=1}^K \gamma_{1,k} \gamma_{2,k} \pm 8\gamma_0 \sqrt{\gamma_0^2 + \frac{1}{4}Rd_{free} \sum_{k=1}^K \gamma_{1,k} \gamma_{2,k}}}.$$

- It can be observed that the power allocation factor for k –th relaying node is proportional to the channel and coding gain of the k -th relay link.
- The power gains w.r.t. equal power allocation for different channel configurations are shown in the subsequent slide.

– Channel Coded: Power Gains –

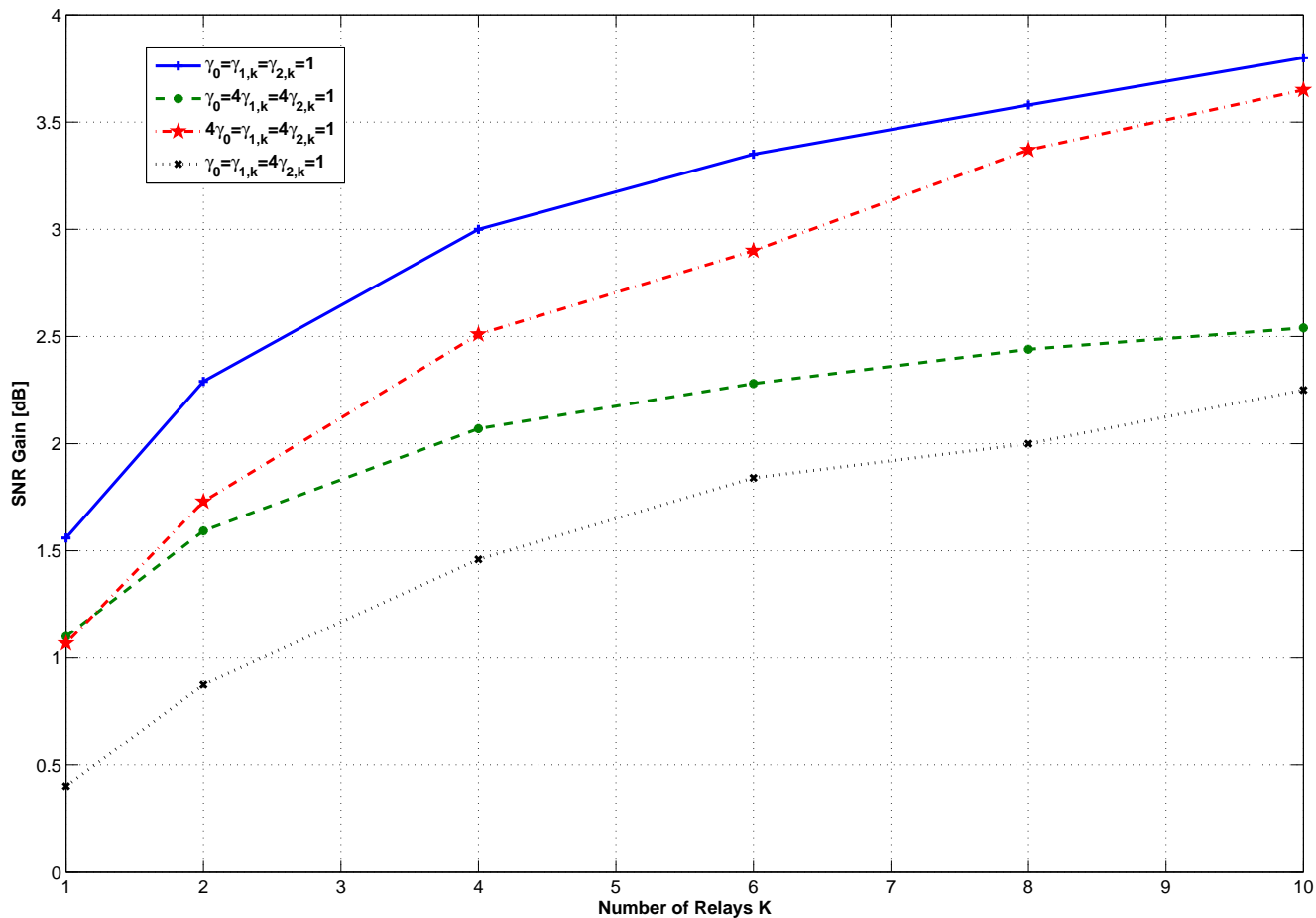
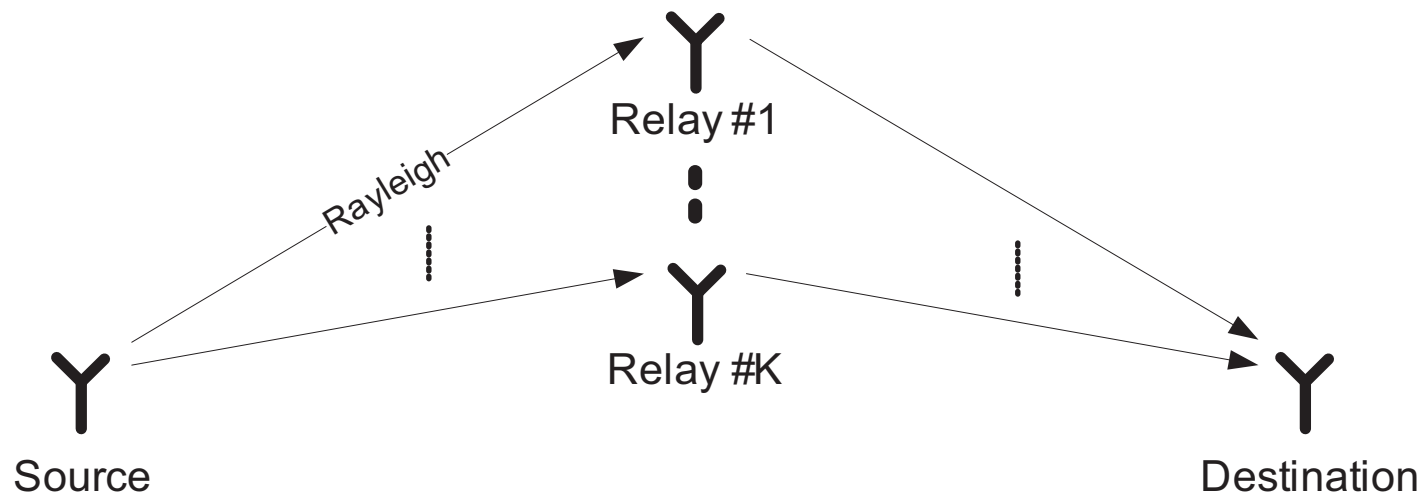


Figure 42: Power gains can be achieved by using prior theory, where this gain will monotonically increase as the number of relays increases.

– Space-Time Coded: Code Design [1/4] –

- We will follow [103] and assume the following:
 - two-hop relay system with K relaying nodes;
 - Rayleigh fading channel;
 - relay only re-transmits if received correctly;
 - MLSE detector at destination.
- Upper bound to the pairwise error probability (PEP) has been derived.



– Space-Time Coded: Code Design [2/4] –

- According to [103], the received sequence vector at the destination is

$$\mathbf{y}_d = \sqrt{P_2} \mathbf{X} \mathbf{D}_I \mathbf{h} + \mathbf{n}, \quad (68)$$

where \mathbf{X} is the space-time code sequence, \mathbf{n} the noise, \mathbf{h} the channel vector from the relays to the destination, and $\mathbf{D}_I = \text{diag}(I_1, \dots, I_K)$ the relay state matrix.

- $I_k = 1$ with probability $(1 - P_k)^L$ if relay decoded information successfully from source and $I_k = 0$ otherwise with probability $1 - (1 - P_k)^L$, where L is the frame length and for M-QAM

$$P_k \leq \frac{2Ng(2)}{bP_1 \overline{|h_{1,k}|^2}}, \quad (69)$$

where $b = 3/(M - 1)$, $g(2) = 4Y/\pi \int_0^{\pi/2} \sin^2 \theta d\theta - 4Y^2/\pi \int_0^{\pi/4} \sin^2 \theta d\theta$ and $Y = 1 - 1/\sqrt{M}$. I_k is hence Bernoulli distributed.

- We will subsequently assume that all channel realisations are symmetric, i.e.

$$\overline{|h_{1,k}|^2} = \overline{|h_{1,K}|^2} \text{ and } P_k = P_K.$$

– Space-Time Coded: Code Design [3/4] –

- Maximum likelihood decoding is applied, where the PEP can be bounded by:

$$\begin{aligned}
 Pr(\mathbf{X}_1 \rightarrow \mathbf{X}_2 | \mathbf{I}, \mathbf{h}) &= Pr \left(\| \mathbf{y} - \sqrt{P_2} \mathbf{X}_1 \mathbf{D}_\mathbf{I} \mathbf{h} \|^2 > \| \mathbf{y} - \sqrt{P_2} \mathbf{X}_2 \mathbf{D}_\mathbf{I} \mathbf{h} \|^2 | \mathbf{I}, \mathbf{h}, \mathbf{X}_1 \right) \\
 &\leq \sum_{k=0}^K (1 - L \cdot P_K)^k (L \cdot P_K)^{K-k} \cdot \Omega(P_2/N)
 \end{aligned} \tag{70}$$

where

$$\Omega(x) = \sum_{\mathbf{I}: n_\mathbf{I}=k} \frac{\binom{2k-1}{k-1}}{x^k \prod_{i=1}^k \lambda_i^\mathbf{I}}. \tag{71}$$

Here, $n_\mathbf{I}$ is the number of active relays (assuming that the space-time codeword is full-rank) and $\lambda_i^\mathbf{I}$ are the nonzero eigenvalues of sent signal matrix corresponding to state \mathbf{I} .

- Above equation allows us to gain insights into the design criteria of the space-time code word.

– Space-Time Coded: Code Design [4/4] –

- Following [103] and assuming α to be the fractional power of the first stage, we rewrite the PEP as

$$Pr(\mathbf{X}_1 \rightarrow \mathbf{X}_2 | \mathbf{I}, \mathbf{h}) \leq SNR^{-K} \sum_{k=0}^K \left(\frac{2Lg(2)}{b\alpha|h_{1,K}|^2} \right)^{K-k} \cdot \Omega(1 - \alpha) \quad (72)$$

- The **diversity gain** is given as

$$D = \lim_{SNR \rightarrow \infty} -\log(PEP) / \log(SNR) = K, \quad (73)$$

which indicates that any full-rank MIMO code will achieve full diversity if used for the decode and forward space-time protocol.

- The **coding gain** is given as

$$C = 1 / \sqrt[n]{\sum_{k=0}^K \left(\frac{2Lg(2)}{ba_1|h_{1,K}|^2} \right)^{K-k} \cdot \Omega(1 - \alpha)} \quad (74)$$

which indicates that – among all determinant-maximising space-time codes – special decode and forward space-time codes need to be constructed to maximise coding gain.

6.4 Asynchronous Protocols

– Synchronisation Methods –

- Of major concern for distributed relaying networks is how to maintain synchronisation between cooperative nodes and nodes belonging to the same relaying stage, whether cooperating or not.
- Several approaches are possible, some of which are dealt with subsequently:
 - **Natural Synchronisation:** Assuming that terminals belonging to the same relaying hop require the same processing time, i.e. reception, decoding, re-encoding, transmission, then path differences leading to relative delays less than the symbol duration are acceptable.
 - **Extended Cyclic Prefix:** As long as the cooperative scheme uses OFDM and the CP is longer than the channel's power delay profile plus the maximum expected asynchronism, ISI is mitigated inherently. In addition, Cyclic Delay Diversity can be used!
 - **Asynchronous STC:** It is also possible to design space-time coding schemes which are robust to asynchronisms, however, mostly at the cost of a loss in spectral efficiency and/or performance.

– Natural Synchronisation [1/3] –

We will estimate the allowed spatial separation between relaying terminals belonging to the same relaying stage for the best and worst case, so that natural synchronisation is still possible:

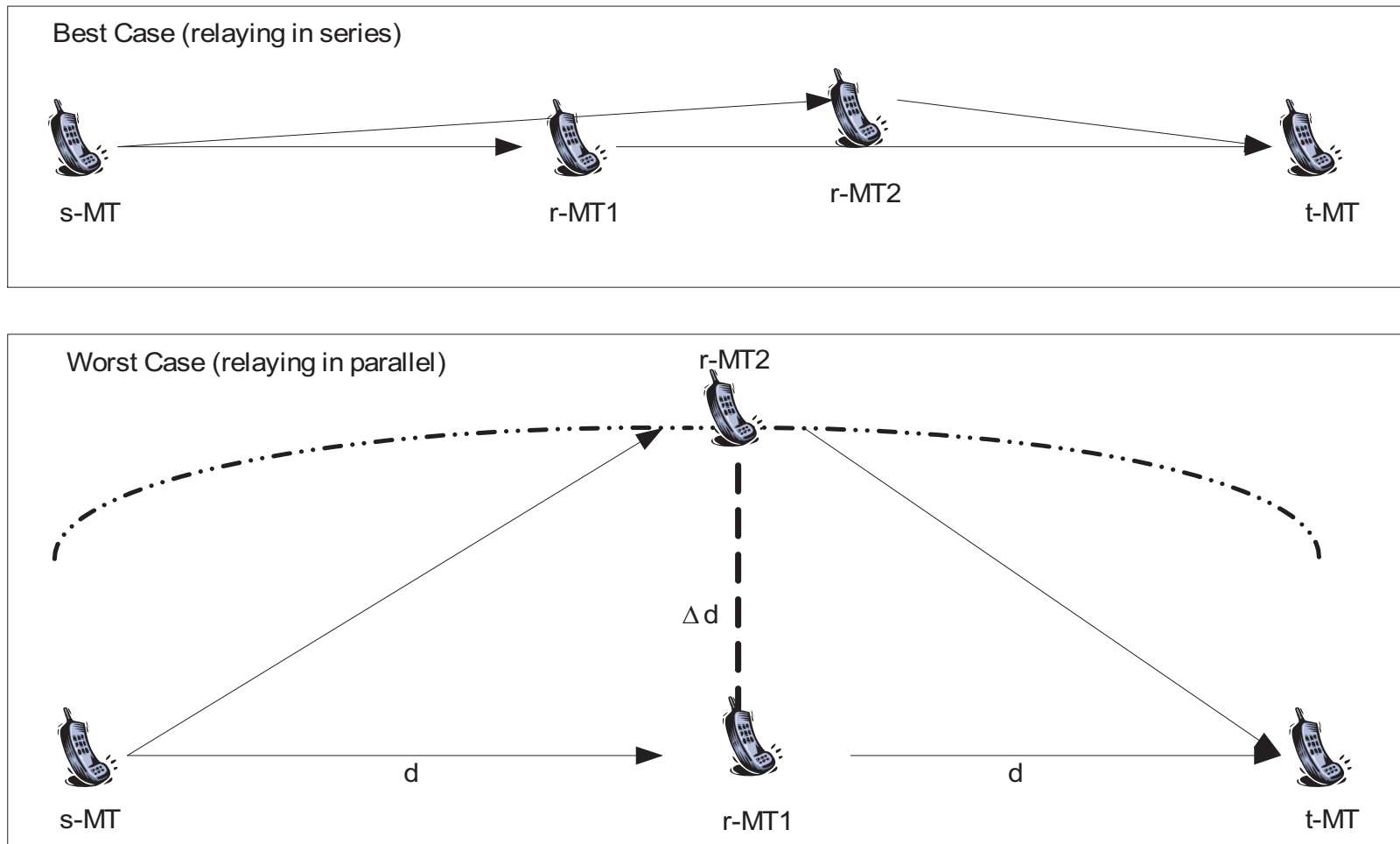


Figure 45: Best and worst case for natural synchronisation between terminals.

– Natural Synchronisation [2/3] –

- The time synchronisation error ought to be below sampling rate ΔT , which allows an optical path difference of $\Delta T \cdot c$, where $c \approx 3 \cdot 10^8$ m/s is the speed of light.
- Assuming equal processing time in each r-MT, the topological distribution has to obey:

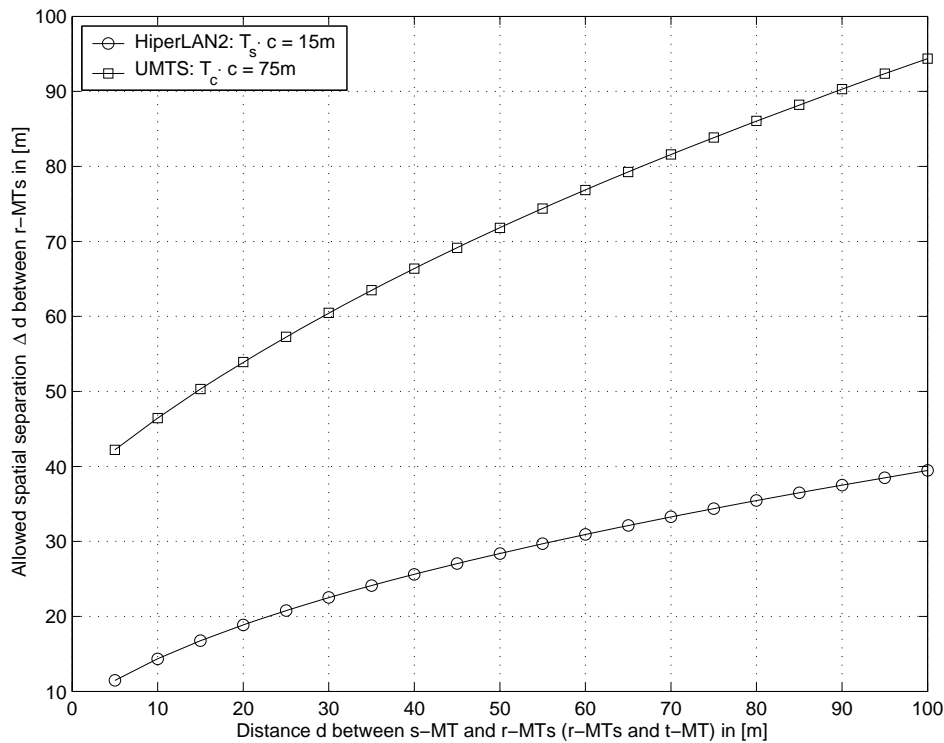
$$\left| (d_{s \rightarrow r_2} + d_{r_2 \rightarrow t}) - (d_{s \rightarrow r_1} + d_{r_1 \rightarrow t}) \right| \leq \Delta T \cdot c \quad (78)$$

- For the best case, i.e. both r-MTs are on the line between s-MT and t-MT, they can be separated by any distance because $|(d_{s \rightarrow r_2} + d_{r_2 \rightarrow t}) - (d_{s \rightarrow r_1} + d_{r_1 \rightarrow t})| = 0$.
- For the worst case, i.e. one r-MT lies on the line between s-MT and t-MT and the other r-MT is on the ellipse with the s-MT and t-MT in its foci. For simplicity, we assume that the first r-MT is exactly in the middle between s-MT and t-MT and the second r-MT is perpendicular. For this case, the allowed spatial separation between both r-MTs is easily obtained as:

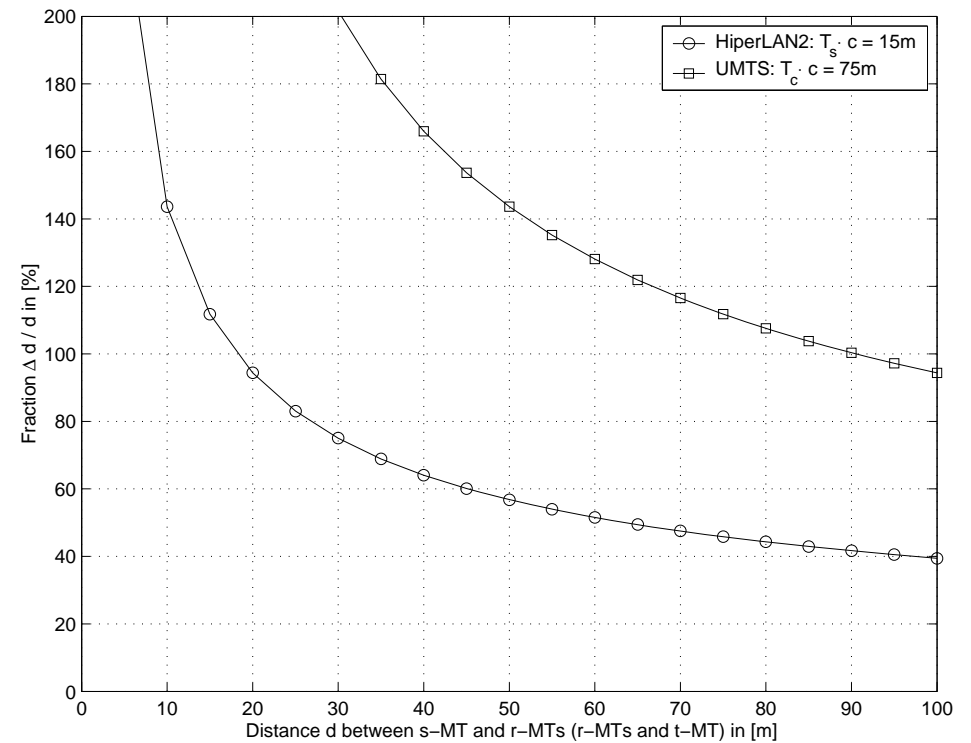
$$\Delta d \leq \sqrt{\left(\frac{\Delta T \cdot c}{2d} + 1 \right)^2 - 1} \quad (79)$$

where d is the distance between the t-MT (s-MT) and the first r-MT.

– Natural Synchronisation [3/3] –



(a) Allowed spatial separation between r-MTs for WLAN and UMTS according to the topology in Figure 45.



(b) Fraction of the allowed spatial separation between r-MTs w.r.t. the absolute distance between s-MT and r-MT for WLAN and UMTS according to the topology in Figure 45.

Figure 46: Study of allowed spatial separation for natural synchronisation.

– CDD/OFDM Inherent Synchronisation [1/2] –

- Cyclic delay diversity (CDD) is the application of delay diversity (DD) to OFDM; DD has been pioneered by A. Wittneben in 1993 and CDD by Armin Dammann and Stefan Kaiser in 2001.
- It is a transmit diversity scheme, where the same signal stream is transmitted from each available antenna with a controlled mutual timing offset.
- This makes the channel more frequency selective and hence yields a performance gain when detected with MLSE or MMSE equaliser.
- Furthermore, CDD has the following properties:
 - The optimum delays between the transmit antennas depend on the modulation scheme (and fading channel).
 - There is no modification required to the receiving side.
 - Although the deployment of MLSE and MMSE is possible without an outer channel code, this will rarely be the case.
 - A delay spread of less than the cyclic prefix length is tolerated, which makes it very attractive for distributed deployment with loose synchronisation.

– CDD/OFDM Inherent Synchronisation [2/2] –

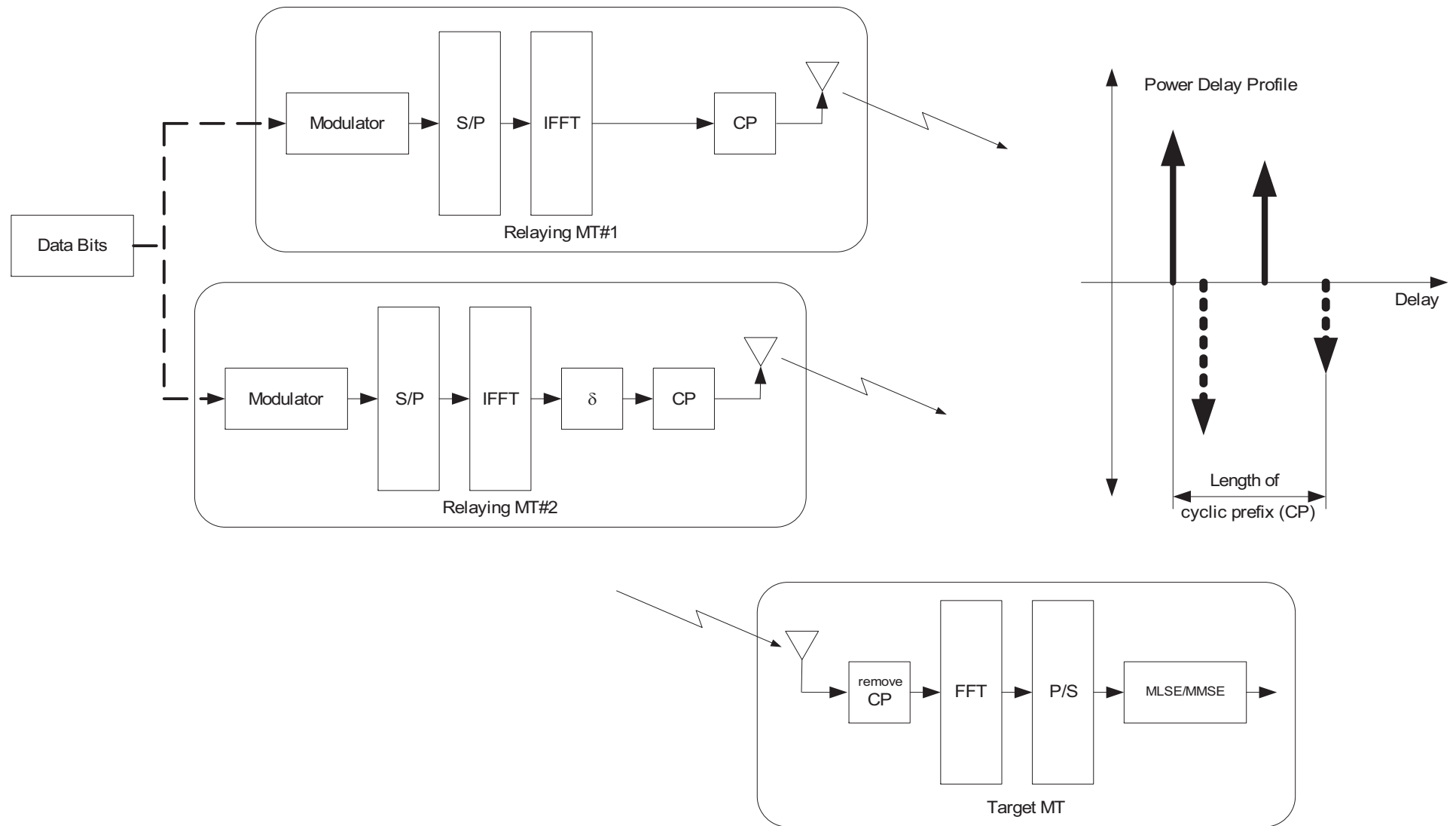
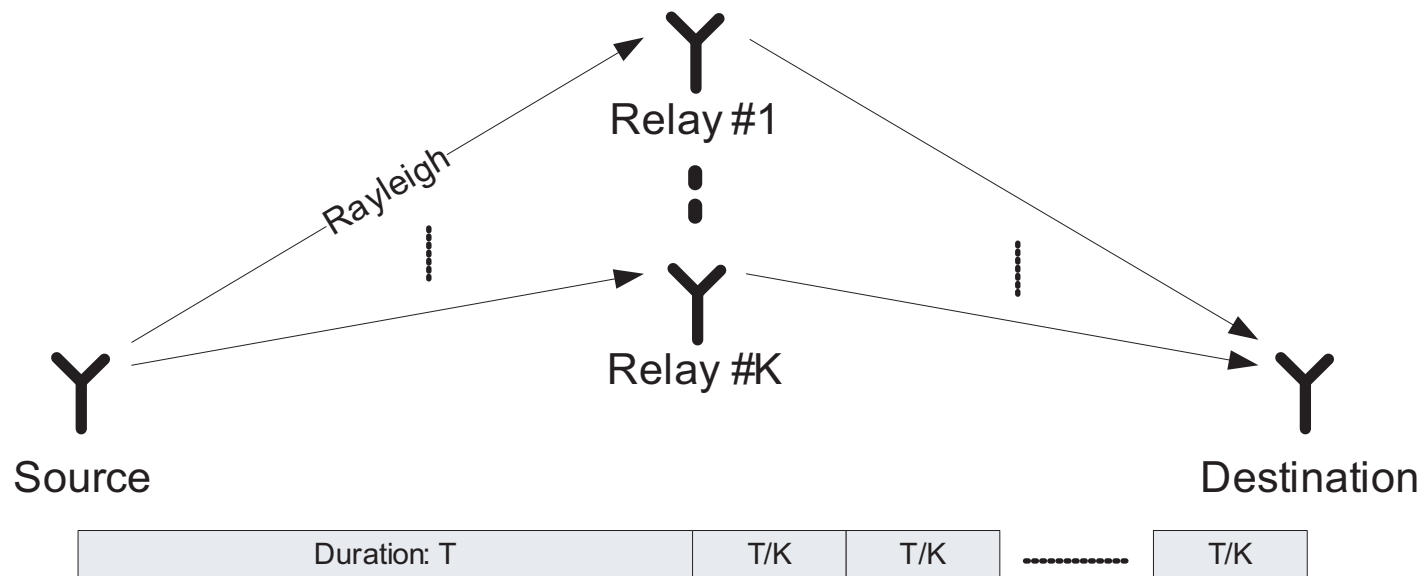


Figure 47: Cyclic delay diversity transmitter and receiver.

– Asynchronous Space-Time Code Design [1/4] –

- Various Asynchronous space-time code designs have been proposed in recent years, most notably [105]–[115] and also [103].
- We will concentrate on [103] according to below topology, where we assume Rayleigh channels and orthogonal and hence loosely synchronised relay frames. This greatly facilitates asynchronous communication.



– Asynchronous Space-Time Code Design [2/4] –

- According to [103], the received sequence vector at the k –th relay is

$$\mathbf{y}_k = \sqrt{P_1} h_{1,k} \mathbf{s} + \mathbf{n}_{r,k}, \quad (80)$$

where \mathbf{s} is the source symbol sequence, $\mathbf{n}_{r,k}$ the noise at the relay and $h_{1,k}$ the channel from source to relay.

- It is assumed that the k –th relay performs a 'sequence-contraction' by means of a linear transformation \mathbf{t}_k , i.e. $\mathbf{t}_k \mathbf{y}_k$, where necessarily $L = K$.
- For subsequent analysis, a codeword vector \mathbf{x} is defined as

$$\mathbf{x} = [\mathbf{t}_1^T, \dots, \mathbf{t}_K^T]^T \mathbf{s} = \mathbf{T} \mathbf{s} \quad \text{and} \quad \mathbf{X} = \text{diag}(\mathbf{x}), \quad (81)$$

where \mathbf{T} is a $K \times K$ linear transformation matrix.

- From above, $x_k = \mathbf{t}_k \mathbf{s}$ and x_{mk} is the k –th element of the \mathbf{x}_m codeword.

– Asynchronous Space-Time Code Design [3/4] –

- Using a maximum likelihood decoder, the PEP can be upper bounded by:

$$PEP = Pr(\mathbf{X}_m \rightarrow \mathbf{X}_j) \quad (82)$$

$$\leq N^K \frac{\prod_{k=1, x_{mk} \neq x_{jk}}^K \left(\frac{1}{P_1 |h_{1,k}|^2} + \frac{1}{P_2 |h_{2,k}|^2} \right)}{\prod_{k=1, x_{mk} \neq x_{jk}}^K \frac{|x_{mk} - x_{jk}|^2}{4}}. \quad (83)$$

- The **diversity gain** is hence given as

$$D = \lim_{SNR \rightarrow \infty} -\log(PEP) / \log(SNR) = \min_{m \neq j} \text{rank}(\mathbf{X}_m - \mathbf{X}_j), \quad (84)$$

which indicates that the difference matrix $\mathbf{x}_m - \mathbf{x}_j$ should be full-rank for any codeword \mathbf{x} .

- The **coding gain** is given as

$$C = \sqrt[K]{\prod_{k=1}^K |x_{mk} - x_{jk}|^2}, \quad (85)$$

which requires the minimum product distance to be maximized.

– Asynchronous Space-Time Code Design [4/4] –

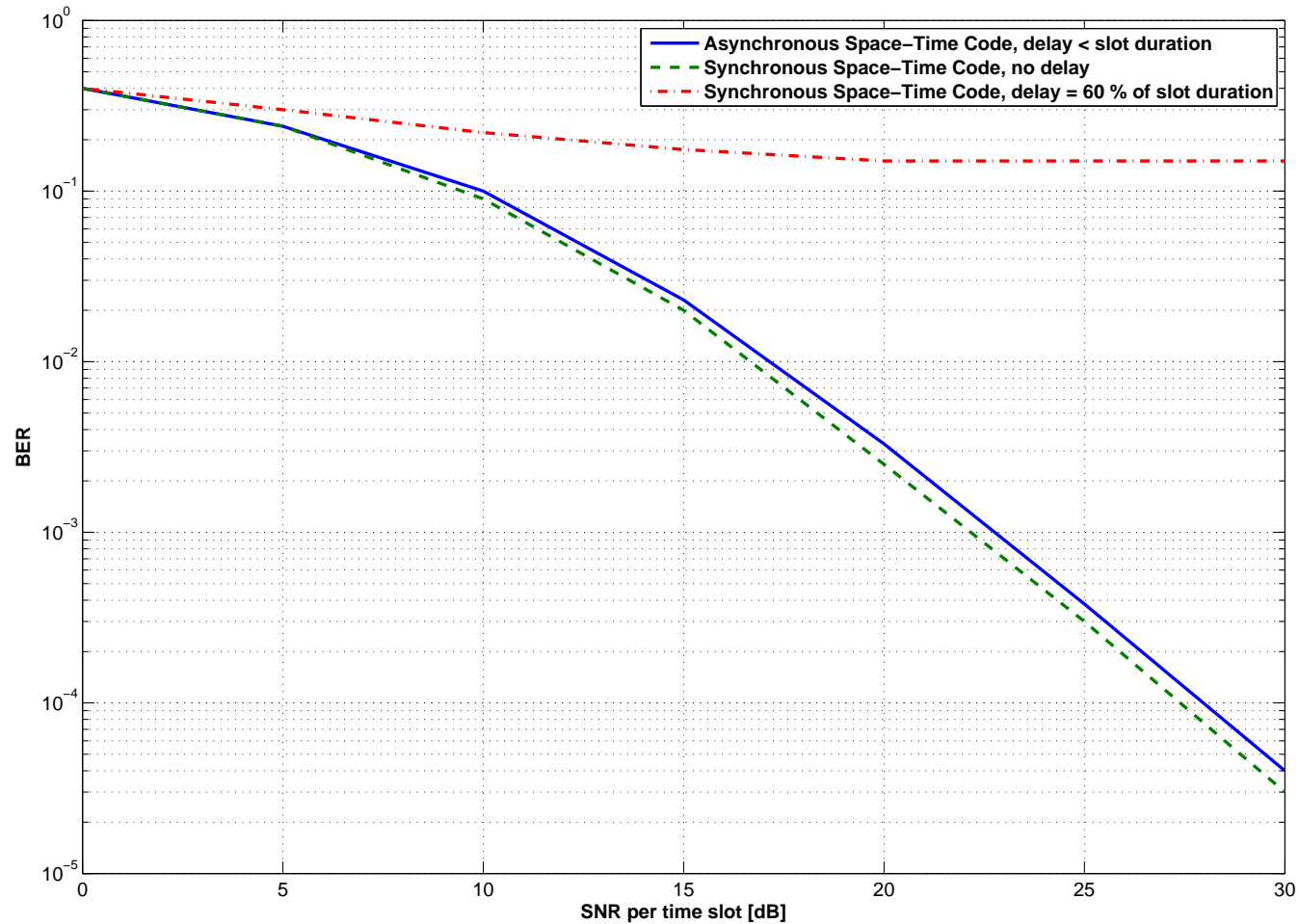


Figure 48: BER for two relays using optimum Vandermonde matrices \mathbf{T} for constructing \mathbf{x} [103].

PART 7

MAC & X-Layer Design

– Preliminary Note –

- The MAC layer is central to the throughput and delay of a wireless system.
- There are dozens contributions available today, which is why we only concentrate on some basic MAC and cross-layer design issues.
- We proceed with the following topic:
 1. cooperative-diversity slotted ALOHA MAC with routing protocol;
 2. throughput of cooperative PHY-optimized CSMA/CA based MACs;
- These are contributions which we found very interesting but have no time to dwell on:
 - Selection diversity including fading and capture effects: [116];
 - Cooperative schemes based on RTS/CTS protocols: [119]–[129].

– MAC is Centre of Gravity! –

The MAC decides upon:

- transmit power levels → error rates, interference behaviour
- frame lengths → throughput, interference behaviour
- scheduling timings → delay, interference behaviour
- IP packet 'buffering' → QoS

	CSMA-type MAC (conventional)	Reservation-type MAC (distr. & coop.)	Hybrid MAC
Control Signalling	synchr/hop reserv/etc.	not useful	?
Data Traffic	bursty data	'regularized' data	?

7.2 CSMA-Type PHY/MAC Optimisation

– Approach for CSMA-type MAC [1/3] –

We are interested in a **general mathematical framework** which quantifies:

- **throughput** (for bursty data)
- **delay** (for signalling and bursty data)

in dependency of

- node density, distribution & traffic
- transmission & interference radii
- pathloss/shadowing/fading models

which allows us to

- characterise performance of CSMA/4W-HS/SW-ARQ/etc protocols
- **synthesise an optimum MAC**

– Approach for CSMA-type MAC [2/3] –

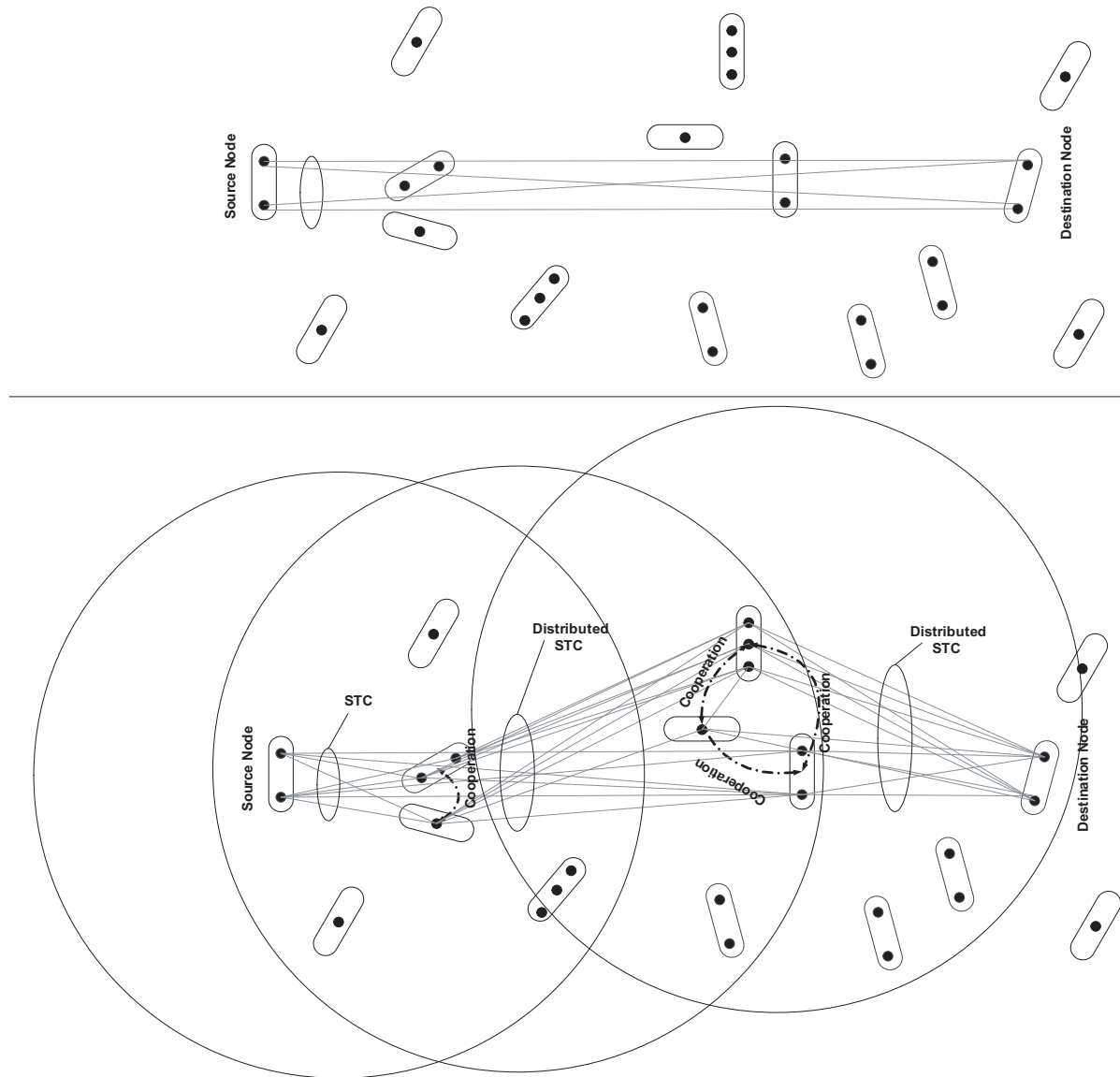


Figure 50: Multi-hop CSMA/CA scenario with two different transmit power levels (coverage areas).

– Approach for CSMA-type MAC [3/3] –

low modulation index (BPSK)	high modulation index (64QAM)
→ low error rate (low prob. of loss)	→ high error rate (high prob. of loss)
→ long packets (high prob. of collision)	→ short packets (low prob. of collision)
with channel code	without channel code
→ low error rate (low prob. of loss)	→ high error rate (high prob. of loss)
→ long packets (high prob. of collision)	→ short packets (low prob. of collision)

Can we capture this trade-off analytically?

– CSMA-type PHY/MAC Optimisation [1/6] –

'1': normalised packet length

D : delay period

a : slot duration ($=\log_2(M)/N_b$)

T : transmission period

p : persistency factor

B : busy period

P_f : frame error probability

I : idle period

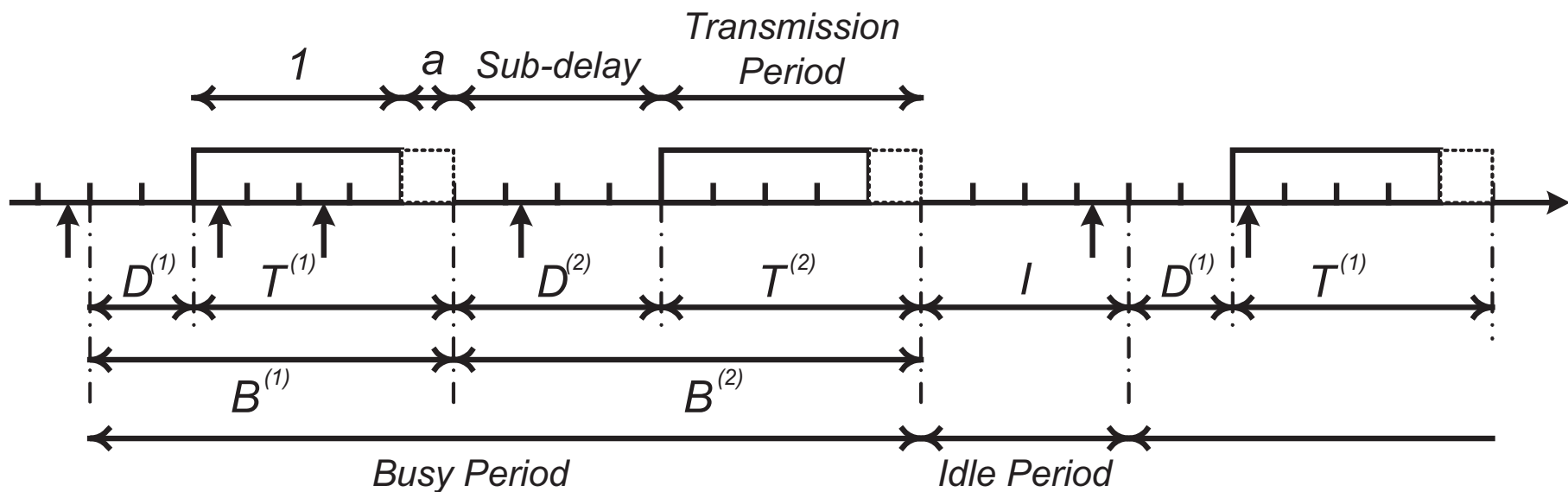


Figure 51: Time sequence of events for basic p -persistent CSMA/CA.

– CSMA-type PHY/MAC Optimisation [2/6] –

The useful average end-to-end network throughput can be derived as

$$\bar{S} = B \times \frac{1}{\bar{N}} \times \frac{\bar{U}}{\bar{B} + \bar{I} + \bar{C}} \quad (86)$$

where

- B is the number of bits per packet;
- \bar{N} is the average number of hops from source to destination;
- \bar{U} is the average useful transmission time;
- \bar{B} is the average busy time;
- \bar{I} is the average idle time;
- \bar{C} is the average cooperation time;

– CSMA-type PHY/MAC Optimisation [3/6] –

- We can derive the average idle period \bar{I} to be

$$\bar{I} = \frac{a}{1 - (1 - g)^{M_t}} \quad (87)$$

- We can derive the average busy period \bar{B} to be

$$\bar{B} = E[D^{(1)}] + (\bar{J} - 1)E[D^{(2)}] + \bar{J}(1 + a) \quad (88)$$

where the average number of busy sub-periods is given as

$$\bar{J} = \frac{N}{(1 - g)^{(1+1/a)(M_t-1)}} \quad (89)$$

and

$$E[D^{(j)}] = \begin{cases} d(1) & j = 1 \\ d(1 + 1/a) & j = 2, 3, \dots \end{cases} \quad (90)$$

where

– CSMA-type PHY/MAC Optimisation [4/6] –

$$\begin{aligned}
 d(X) &= \frac{a}{N - (1 - g)^{X(M_t - 1)}} & (91) \\
 &\cdot \sum_{k=1}^{\infty} \left\{ N(1 - p)^k - p \left[\frac{(1 - p)^k - (1 - g)^k}{p - g} \right] \right\} \\
 &\cdot \left\{ (1 - p)^k - p(1 - g)^X \left[\frac{(1 - p)^k - (1 - g)^k}{p - g} \right] \right\}^{M_t - 1} \\
 &- \frac{a(1 - g)^{X(M_t - 1)}}{N - (1 - g)^{X(M_t - 1)}} \sum_{k=1}^{\infty} \left[\frac{p(1 - g)^k - g(1 - p)^k}{p - g} \right]^{M_t}
 \end{aligned}$$

- Similarly, we can derive the average useful period \bar{U} to be

$$E[U^{(j)}] = \begin{cases} u(1) & j = 1 \\ u(1 + 1/a) & j = 2, 3, \dots \end{cases} \quad (92)$$

where

– CSMA-type PHY/MAC Optimisation [5/6] –

$$\begin{aligned}
 u(X) = & \frac{p \cdot (1 - P_f)}{N - (1 - g)^{X(M_t-1)}} \sum_{k=0}^{\infty} \left\{ (1 - p)^{k+1} \right. & (93) \\
 & \left. - p(1 - g)^X \left[\frac{(1 - p)^{k+1} - (1 - g)^{k+1}}{p - g} \right] \right\}^{M_t-2} \\
 & \cdot \left\{ (1 - g)^k (1 - p)^k [N(1 - g)^X - 1] \right. \\
 & \left. + M_t \left\{ (1 - p)^k - (1 - g)^X \left[\frac{p(1 - p)^k - g(1 - g)^k}{p - g} \right] \right\} \right. \\
 & \left. \cdot \left\{ N(1 - p)^{k+1} - p \left[\frac{(1 - p)^{k+1} - (1 - g)^{k+1}}{p - g} \right] \right\} \right\} \\
 & - \frac{M_t g p (1 - g)^{X(M_t-1)}}{N - (1 - g)^{X(M_t-1)}} \sum_{k=1}^{\infty} \left[\frac{p(1 - g)^{k+1} - g(1 - p)^{k+1}}{p - g} \right]^{M_t-1} \\
 & \cdot \left[\frac{(1 - g)^k - (1 - p)^k}{p - g} \right]
 \end{aligned}$$

– CSMA-type PHY/MAC Optimisation [6/6] –

- The average cooperation time \bar{C} is easily calculated as:

$$\bar{C} = \frac{\bar{U} \cdot N_c}{\alpha}, \quad (94)$$

where

- \bar{U} is the average useful transmission time;
 - N_c is the number of cooperating links per relaying stage;
 - α is the strength of the cooperative data-pipe w.r.t. the relaying pipe.
- Here, we assumed that a reservation based MAC protocol is used per cooperative stage.
 - For the design and analysis of a CSMA-based MAC at the cooperative stage, please, consult [130].

– Performance: Transmission Range [1/6] –

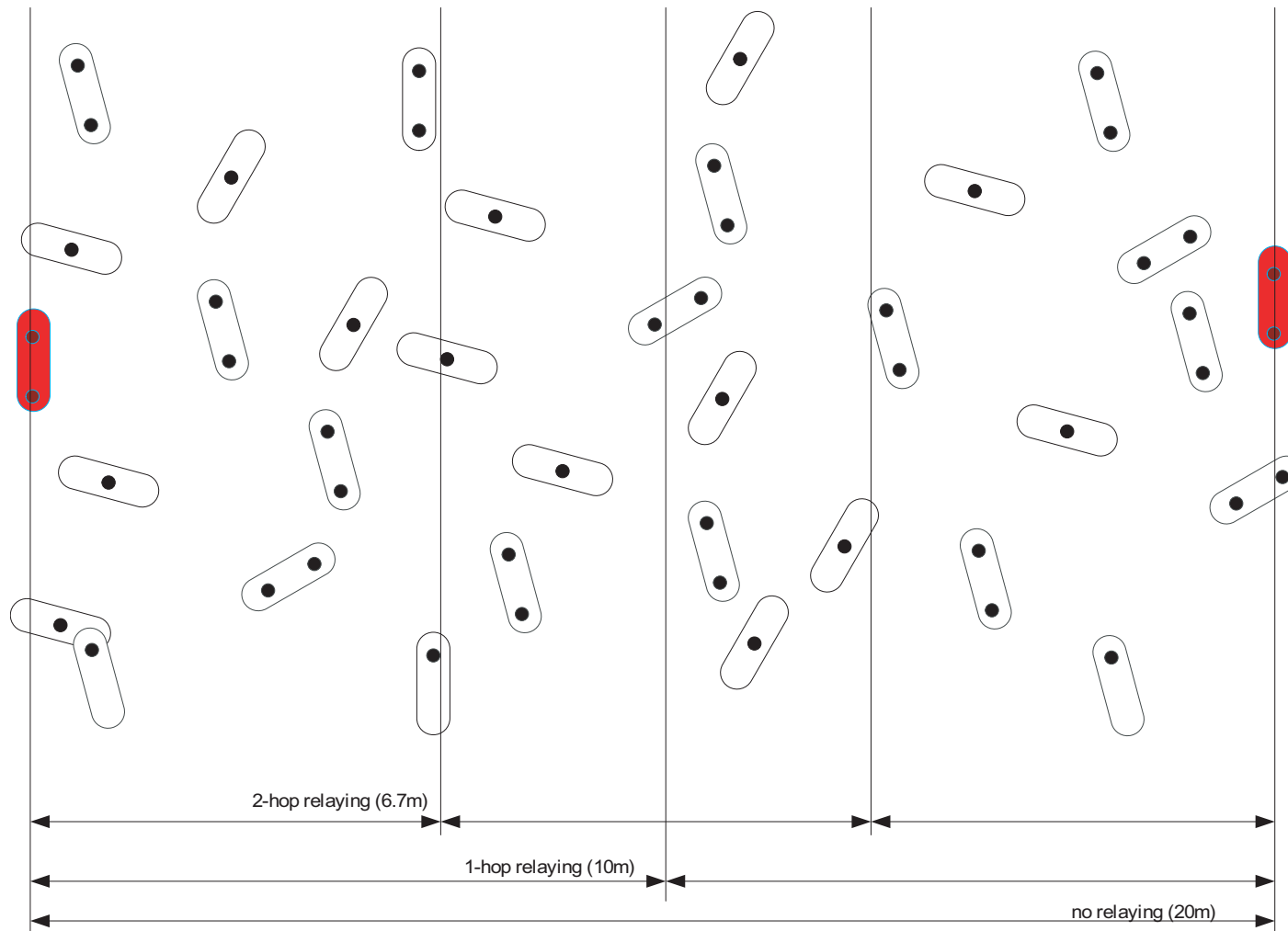


Figure 52: We have choice of a single hop, dual hop, triple hop, etc.

– Performance: Transmission Range [2/6] –

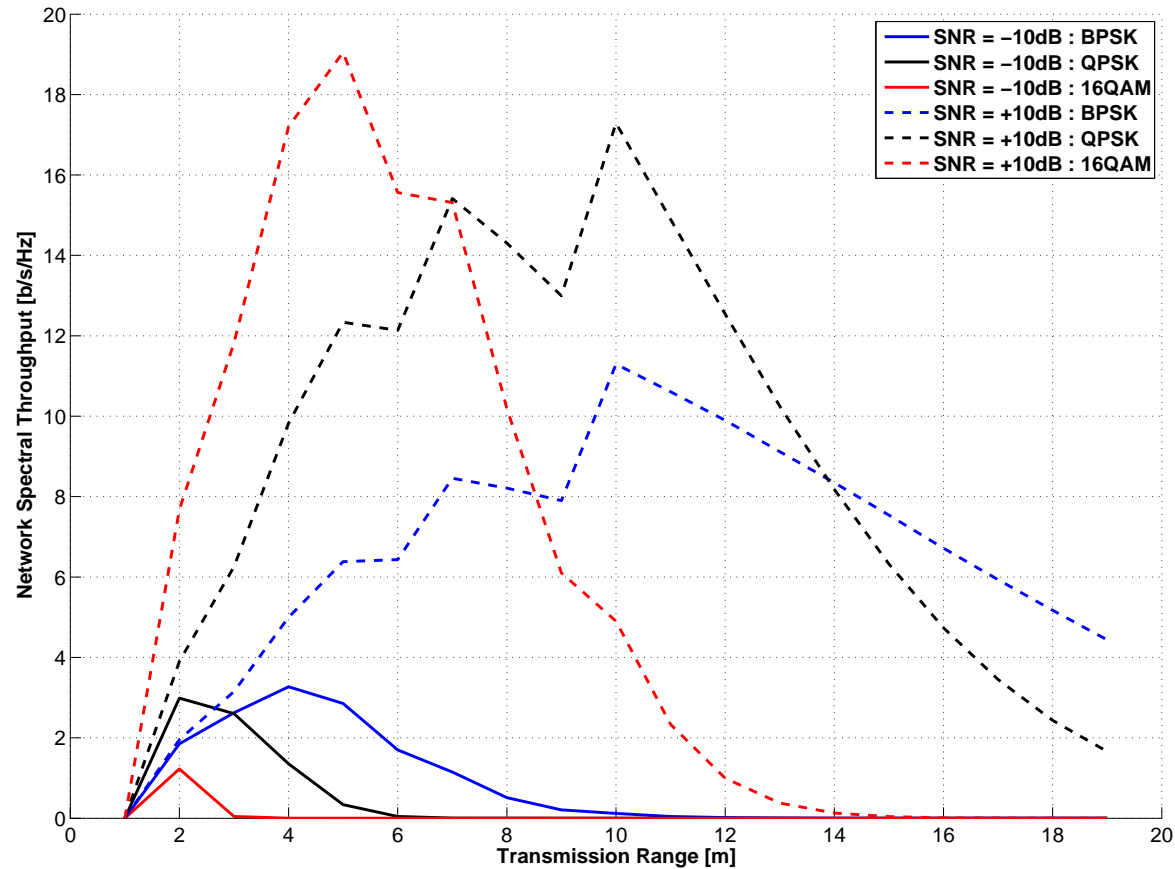


Figure 53: Assumptions: -30dB/dec pathloss, $p = 3\%$, $g = 0.5\%$, $a = 0.01$, $B = 30 \cdot \log_2(M)$, one antenna per node, no cooperation (just relaying).

– Performance: Cooperation [3/6] –

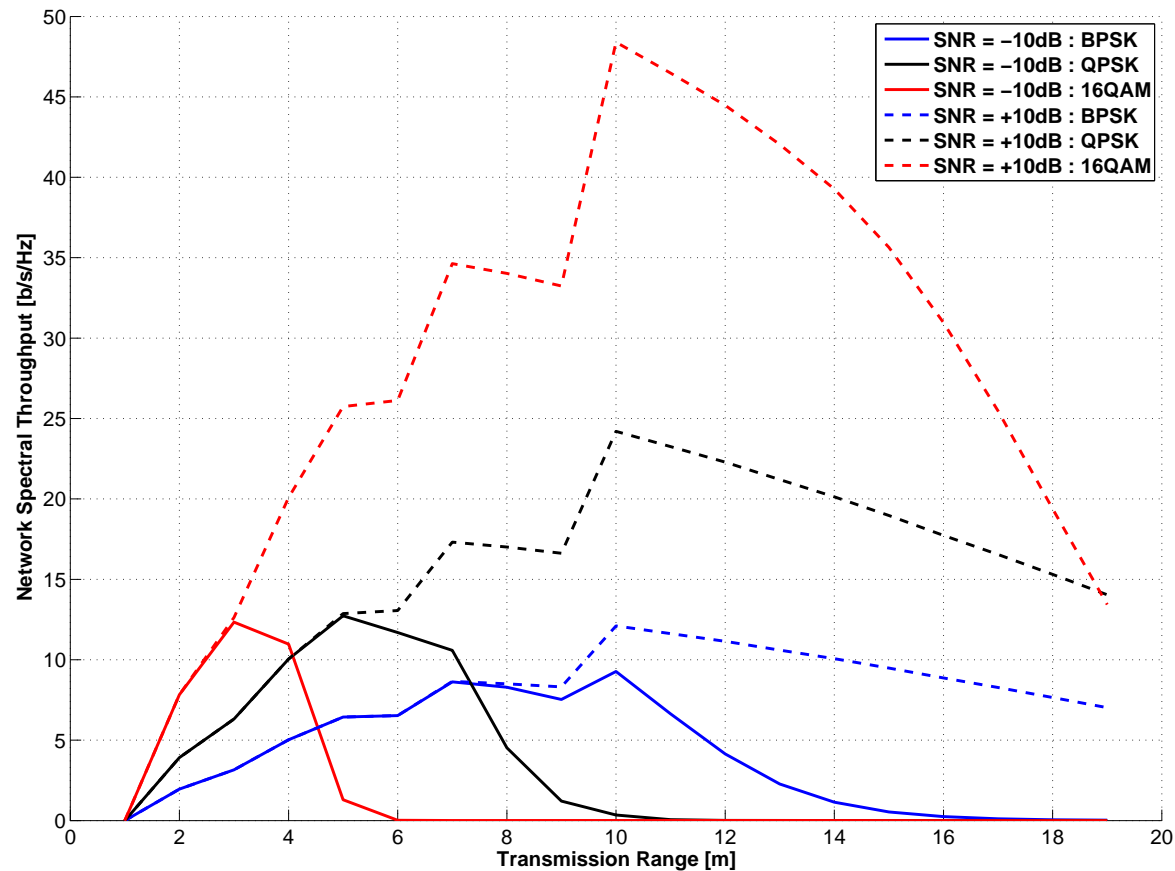


Figure 54: Assumptions: -30dB/dec pathloss, $p = 3\%$, $g = 0.5\%$, $a = 0.01$, $B = 30 \cdot \log_2(M)$, one antenna per node, three nodes cooperate, $\alpha \rightarrow \infty$.

– Performance: Cooperation Pipe [4/6] –

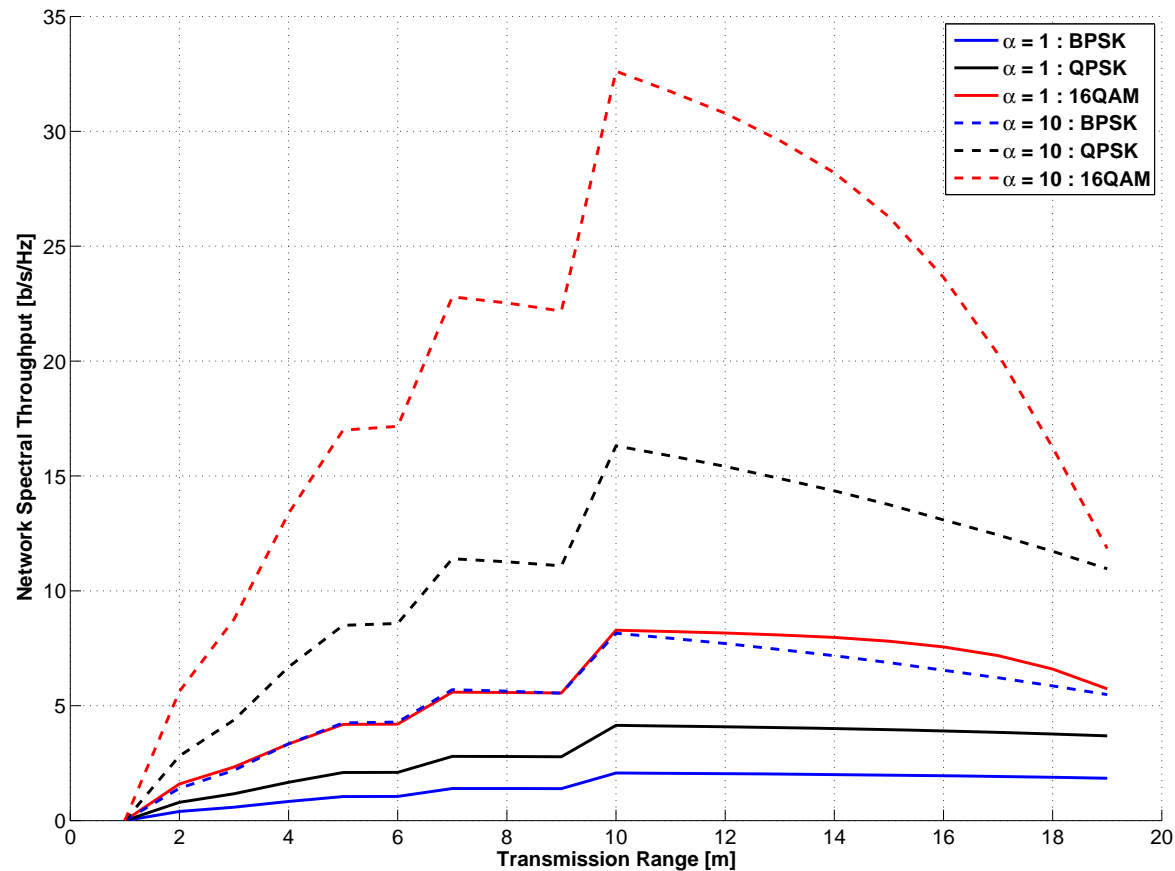


Figure 55: Assumptions: -30dB/dec pathloss, $p = 3\%$, $g = 0.5\%$, $a = 0.01$, $B = 30 \cdot \log_2(M)$, one antenna per node, three nodes cooperate, $\text{SNR} = 10\text{dB}$.

– Performance: Channel Code [5/6] –

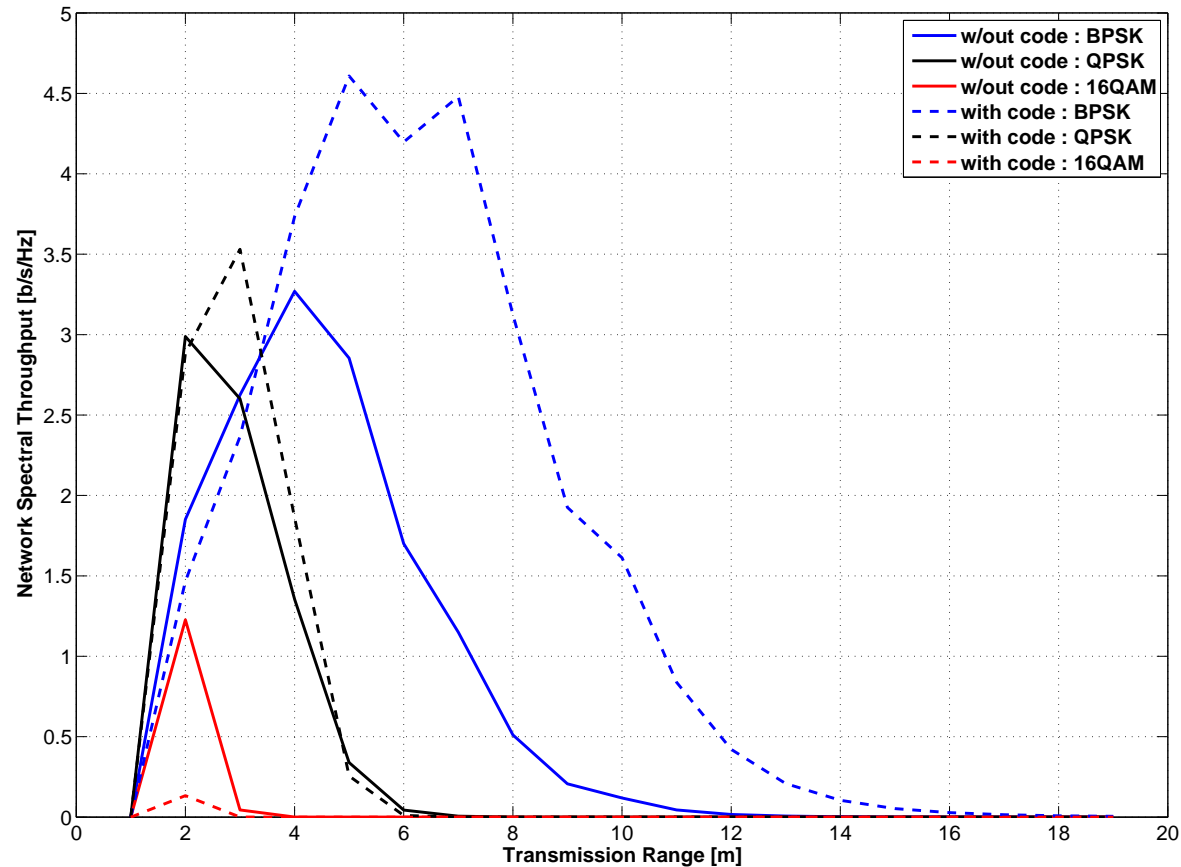


Figure 56: Assumptions: -30dB/dec pathloss, $p = 3\%$, $g = 0.5\%$, $a = 0.01$, $B = 30 \cdot \log_2(M)$, one antenna per node, no cooperation, $\text{SNR} = -10\text{dB}$.

– Performance: Channel Code [6/6] –

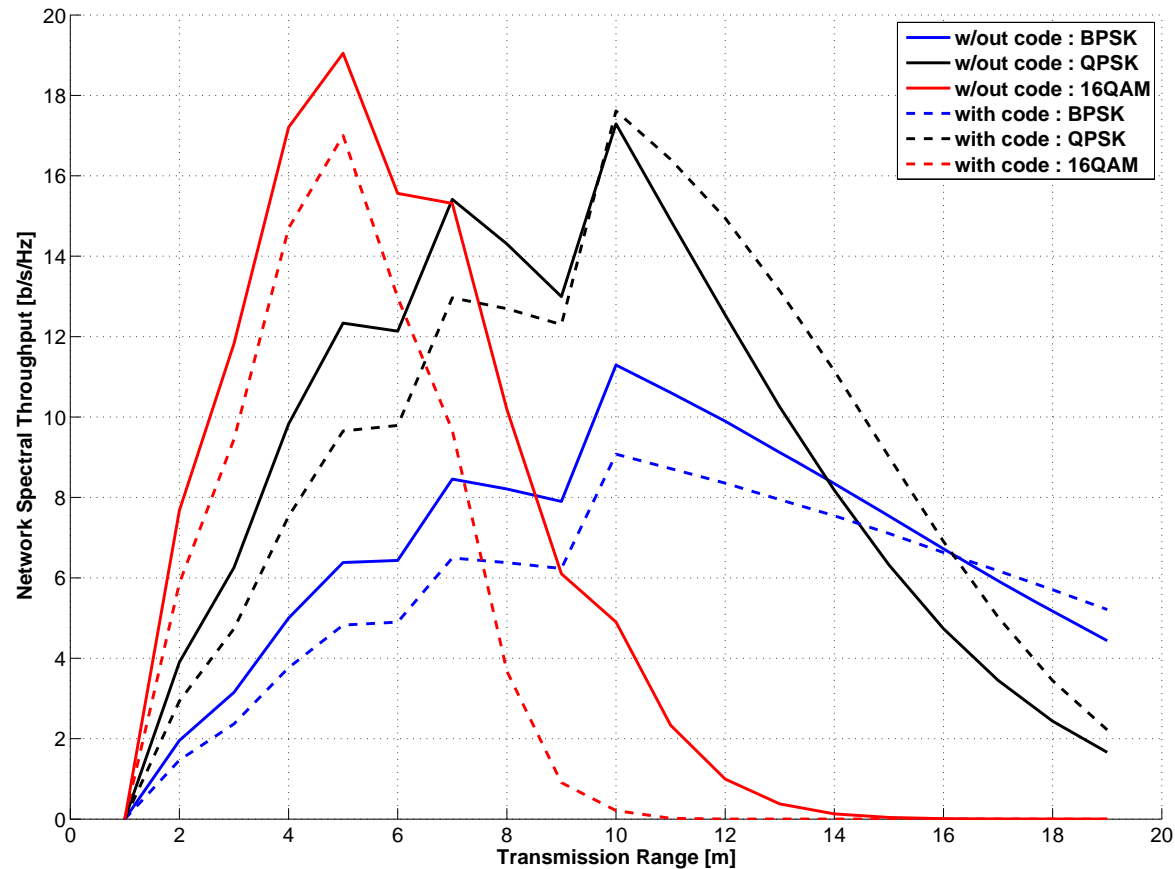


Figure 57: Assumptions: -30dB/dec pathloss, $p = 3\%$, $g = 0.5\%$, $a = 0.01$, $B = 30 \cdot \log_2(M)$, one antenna per node, no cooperation, SNR= +10dB.

PART 9
THE ROAD AHEAD

– Only Some Thoughts –

- Capacity and algorithmic PHY layer designs are fairly well explored; despite numerous unsolved problems, novel contributions are likely to be incremental.
- RF, MAC, routing protocols, cross-layer design and roll-outs are areas which are still in their infancy; there is hence a lot of room for innovative contributions.
- What we may need today in these type of networks are entirely novel approaches for system analysis, such as from physics or biology.
- A personal answer to the question posed at the beginning:
 - **Ripe:** Technology (already available for a long time since there is no magic);
 - **Hype:** Expectations (inflated research body on this subject).

We need commercially viable products if cooperative systems do not want to fall for the same fate as traditional ad hoc networks, which have been researched for several decades without any tangible product on the civil market today.

– Credits –

The following people's input (text, figures, research results) have been used with thanks throughout this presentation:

- Dr Athanasios Gkelias, Imperial College, UK
- Dr Yonghui Li, University of Sydney, Australia
- Thomas Watteyne, France Telecom R&D, France
- Timus Bogdan, KTH, Sweden
- Roger B. Marks, Mitsuo Nohara, Jose Puthenkulam, Mike Hart, all involved in IEEE 802.16j.